

Unraveling Novel Roles of Xanthine Oxidase in Sickle Cell Disease

by

Heidi Marie Schmidt

BSE, Case Western Reserve University, 2017

Submitted to the Graduate Faculty of the
School of Medicine in partial fulfillment
of the requirements for the degree of
Doctor of Philosophy

University of Pittsburgh

2022

UNIVERSITY OF PITTSBURGH

SCHOOL OF MEDICINE

This dissertation was presented

by

Heidi Marie Schmidt

It was defended on

December 7, 2021

and approved by

Dr. Patrick Pagano, Professor of Medicine, Department of Pharmacology & Chemical Biology

Dr. Bruce Freeman, Irwin Fridovich Distinguished Professor and Chair, Department of
Pharmacology & Chemical Biology

Dr. Francisco Schopfer, Associate Professor, Department of Pharmacology & Chemical Biology

Dr. Edwin Jackson, Professor of Medicine, Department of Pharmacology & Chemical Biology

Dr. Donna Stolz, Associate Professor, Department of Cell Biology

Dr. Eric Kelley, Associate Professor, Department of Physiology and Pharmacology (West
Virginia University)

Dissertation Director: Dr. Adam Straub, Associate Professor of Medicine, Department of
Pharmacology & Chemical Biology

Copyright © by Heidi Marie Schmidt

2022

Unraveling Novel Roles of Xanthine Oxidase in Sickle Cell Disease

Heidi Marie Schmidt, PhD

University of Pittsburgh, 2022

Hemolysis, the release of hemoglobin and heme from red blood cells, is a defining characteristic of hemolytic diseases such as sickle cell disease (SCD); however, the mechanisms that enable the organism to cope with excessive hemoglobin and heme when canonical mediators are depleted remain poorly understood. Xanthine oxidase (XO) is one enzyme that has been reported to have elevated activity in SCD. XO oxidizes hypoxanthine to xanthine and xanthine to uric acid as part of purine degradation. A byproduct of these reactions is the production of $O_2^{\cdot-}$ or H_2O_2 . Increased production of oxidants by elevated XO activity has been thought to cause endothelial damage. We hypothesized that XO could have condition dependent dichotomous functions in SCD where under basal XO function endothelial damage results from increased oxidant production and under heme overload conditions XO regulates a secondary mechanism of heme scavenging and degradation. To test this hypothesis, we treated bone marrow transplanted sickle mice with the XO inhibitor febuxostat for 10 weeks. Treated mice had less hemolysis and improved pulmonary vascular function, identifying XO as a key driver of hemolysis during basal SCD conditions. Next, we studied the role of XO during heme crisis by injecting bone marrow transplanted sickle mice with hemin. Mice lacking hepatic XO had reduced 24-hour survival indicating, for the first time, a protective mechanism for XO. We found that XO is released in response to free heme in a toll like receptor 4-dependent manner to increase circulating levels of XO. Subsequent studies revealed that XO can bind free heme and facilitate degradation to prevent platelet activation and aggregation. Based on these findings, we hypothesize that XO activity is

elevated in SCD in anticipation of a heme crisis event. XO activity could create a microenvironment on the endothelial surface designed to specifically protect the endothelium by binding free heme, inducing a heme splitting reaction, and chelating the free iron released with uric acid. However, the protective functions during a crisis could come at a cost over time, as elevated XO activity at baseline could elicit chronic endothelial cell damage and exacerbate hemolysis in hemolytic diseases.

Table of Contents

Preface.....	xiv
1.0 Introduction.....	1
1.1 Sickle Cell Disease	1
1.2 The Impact of Xanthine Oxidase (XO) on Hemolytic Diseases.....	4
1.2.1 Summary.....	4
1.2.2 Introduction.....	5
1.2.3 Xanthine Oxidase	9
1.2.4 XOR Regulation	9
1.2.5 XOR-Endothelial Interaction.....	11
1.2.6 Therapeutic Inhibitors of XO	11
1.2.7 XOR, ROS, and Hemolytic Diseases	13
1.2.8 Summary and Conclusions.....	17
1.2.9 Acknowledgements.....	17
1.3 Summary and Hypotheses	18
2.0 Xanthine Oxidase Drives Hemolysis and Vascular Malfunction in Sickle Cell	
Disease	20
2.1 Summary	21
2.2 Introduction	22
2.3 Materials and Methods	24
2.3.1 Animals	24
2.3.2 Bone Marrow Transplanted Chimeric Mice	25

2.3.3 Echocardiogram	27
2.3.4 Closed Chest Right Ventricle (RV) Micro-Catheterization	27
2.3.5 Pulmonary, Mesenteric, and Thoracodorsal (TDA) Ex-Vivo Two-Pin Wire Myography.....	28
2.3.6 Blood Collection and Hematologic Phenotyping.....	29
2.3.7 XO Activity	30
2.3.8 Coumarin Boronic Acid (CBA) Assay	30
2.3.9 Trichrome Staining	31
2.3.10 Statistics	31
2.4 Results.....	32
2.4.1 Febuxostat Treatment Significantly Decreases Plasma and Tissue XO Activity	32
2.4.2 XO Inhibition Decreased Hemolysis in Chimeric Sickle Mice.....	38
2.4.3 XO Inhibition Improves Pulmonary Vasoreactivity in Chimeric Sickle Mice	45
2.4.4 Improvements in Pulmonary Vasoreactivity Did Not Manifest into Cardiac Changes	49
2.4.5 Hepatic XO is Not the Driver of Hemolysis in Chimeric Sickle Mice	56
2.5 Discussion	65
2.6 Acknowledgements	69
2.7 Sources of Funding	69
3.0 Xanthine Oxidase Binds and Degrades Heme During Hemolytic Crisis in Sickle Cell Disease	70

3.1 Summary	70
3.2 Introduction	73
3.3 Materials and Methods	75
3.3.1 Animals	75
3.3.2 Bone Marrow Transplanted Chimeric Mice	76
3.3.3 Hemin Challenge and Hematologic Phenotyping	77
3.3.4 Primary Murine Hepatocyte Isolation and Culture	78
3.3.5 AML12 Cell Culture Conditions and Treatment.....	78
3.3.6 XO Activity	79
3.3.7 XOR Protein Quantification	79
3.3.8 XOR RNA Quantification	80
3.3.9 Molecular Modeling of XO and Heme	80
3.3.10 Heme Binding Dot Blot.....	81
3.3.11 Platelet Activation	81
3.3.12 Platelet Aggregation.....	82
3.3.13 Generation of Oxyhemoglobin	83
3.3.14 XO/OxyHb UV-VIS	83
3.3.15 Electron Paramagnetic Resonance (EPR) Spectroscopy	83
3.3.16 Nitric Oxide (NO) Consumption Assay.....	84
3.3.17 Statistics	85
3.4 Results.....	86
3.4.1 XO is released into circulation in response to heme crisis	86
3.4.2 Hepatic XO release occurs through heme-TLR4 signaling.....	90

3.4.3 Hepatocyte-specific XDH knockout accelerates death in response to heme challenge.....	94
3.4.4 XO binds free heme and protects against platelet activation and aggregation	97
3.4.5 XO activity facilitates hemoglobin degradation	102
3.5 Discussion	105
3.6 Acknowledgements	111
4.0 General Conclusions and Future Directions	112
4.1 The Dual Functions of XO in Sickle Cell Disease	112
4.2 Is the role of XO condition and compartment specific?	113
4.3 Does GAG composition mediate the role of XO activity in SCD?	115
4.4 What mechanisms regulate hepatic XO release?	116
4.5 Are XO allelic variants disease modifiers in SCD?	117
4.6 Final Conclusions.....	118
Bibliography	119

List of Tables

Table I. Febuxostat treatment significantly decreased uric acid concentration and XO activity in plasma and tissues of AA control mice at 10 weeks post-initiation of treatment with effects on plasma detected as early as 3 weeks.....	37
Table II. Febuxostat treatment significantly decreased uric acid concentration and XO activity in plasma and tissues of SS sickle mice at 10 weeks post-initiation of treatment with effects on plasma detected as early as 3 weeks.	38
Table III. Blood cell indices for Townes AA bone marrow transplanted mice at 0, 3, 6, and 10 weeks of drinking normal water (AA) or febuxostat treated water (AA + Febux).	41
Table IV. Blood cell indices for Townes SS bone marrow transplanted mice at 0, 3, 6, and 10 weeks of drinking normal water (SS) or febuxostat treated water (SS + Febux).	42
Table V. Closed chest right heart catheterization indices for Townes AA, AA+febuxostat, SS, SS+febuxostat, Xdh^{fl/fl}, and HXdh^{-/-} chimeras ten weeks post-engraftment.....	52
Table VI. Right ventricle echocardiogram indices for Townes AA, AA+febuxostat, SS, SS+febuxostat, Xdh^{fl/fl}, and HXdh^{-/-} chimeras ten weeks post-engraftment.....	54
Table VII. Left ventricle echocardiogram indices for Townes AA, AA+febuxostat, SS, SS+febuxostat, Xdh^{fl/fl}, and HXdh^{-/-} chimeras ten weeks post-engraftment.....	55
Table VIII. Hepatocyte-specific XO knockout significantly decreased uric acid concentration and XO activity in plasma and liver tissue of HXdh^{-/-} mice at 10 weeks post-engraftment with effects on plasma detected as early as 3 weeks.	62

Table IX. Blood cell indices for Townes SS bone marrow transplanted Xdh^{fl/fl} and HXdh^{-/-} chimeras at weeks 0, 3, 6, and 10 weeks post-engraftment. 63

Table X. Blood cell indices for Townes AA bone marrow transplanted mice at baseline and 24 hours post-heme challenge. 89

Table XI. Hemin injection significantly increased uric acid concentration and XO activity in plasma of SS sickle mice compared to AA control mice 24 hours post-hemin challenge of treatment. 89

Table XII. Hepatocyte specific XO knockout decreased liver XO activity without impacting lung or kidney XO activity. 96

List of Figures

Figure 1. Hemolysis releases free heme and induces inflammation.	8
Figure 2. XO binds GAGs and produces ROS at the endothelial surface	16
Figure 3. XO is a key driver of hemolysis in SCD.....	22
Figure 4. Febuxostat treatment inhibits XO activity in chimeric sickle cell disease mice. ..	35
Figure 5. Characterization of chimeric SCD mouse model treated with febuxostat.	36
Figure 6. XO inhibition improves hematologic parameters.....	40
Figure 7. XO inhibition decreases hemolysis.....	43
Figure 8. Evaluation of hemolysis in AA and SS mice treated with febuxostat.	44
Figure 9. XO inhibition decreases constriction across multiple vascular beds but only improves dilation in pulmonary arteries.	46
Figure 10. Ex-vivo wire myography of AA mice treated with febuxostat.	48
Figure 11. XO inhibition did not affect pulmonary pressure or cardiac function.....	52
Figure 12. XO inhibition did not affect the cardiac fibrosis observed in SS sickle mice.....	53
Figure 13. Hepatocyte-specific XO knockout did not decrease hemolysis or alter pulmonary vasoreactivity.....	59
Figure 14. Characterization and evaluation of hemolysis in hepatocyte-specific XO KO mice.	60
Figure 15. Evaluation of vasoreactivity and cardiac function of HXdh^{-/-} mice.....	65
Figure 16. XO mediated hemoglobin degradation and iron chelation pathway.	72
Figure 17. WT SS mice have a significant increase in plasma XO activity in response to heme crisis.....	87

Figure 18. WT SS mice had a 75% survival rate following heme crisis.	88
Figure 19. Heme-TLR4 signaling releases XO from primary murine hepatocytes and AML12 cells.	93
Figure 20. Knockdown and pharmacological inhibition of TLR4 in AML12 cells.	94
Figure 21. Hepatocyte Specific XO Knockout Increases Death Following Heme Challenge	95
Figure 22. Bone Marrow Engraftment of Hepatocyte Specific XO Knockout Mice	96
Figure 23. XO binds hemin and prevents platelet activation and aggregation.	100
Figure 24. Hemin-XO binding is stronger than hemin-albumin interaction.	101
Figure 25. XO activity facilitates oxyhemoglobin degradation.	105

Preface

Dedication

I dedicate this work to my Gram and Nana, Penny Kaercher and Anna Marie Gire. For over 21 years you both have taught me the importance and value of education. I am lucky to have the opportunity to pursue my doctorate degree and incredibly grateful for the unwavering support you have given me over the years. You have inspired me to always keep learning.

With Love,

Your “Bubbly” Granddaughter/Sweet Pea

Acknowledgements

I am extremely grateful for the opportunity to pursue my PhD at the University of Pittsburgh in the Molecular Pharmacology Graduate Program and in the Vascular Medicine Institute. The support, mentorship, and friendship I have gained during this time has been invaluable.

A special thank you to my mentor, Dr. Adam Straub. From the very first time I met with you; it was obvious that you genuinely cared about my success. You encouraged me to pursue lofty goals and supported me every step of the way so that I could achieve them. I have learned so much from you and hope to one day be as great of a mentor to someone as you have been for me. I was lucky enough to have two amazing mentors and want to thank Dr. Eric Kelley for his support, guidance, and wealth of knowledge about XO. I could not have asked for a better mentoring team who taught me so much and always believed in me.

I would also like to thank my thesis committee: Drs. Patrick Pagano, Bruce Freeman, Francisco Schopfer, Edwin Jackson, and Donna Stolz. Your insightful comments helped to drive my project forward and you have shaped me into a better scientist.

Science truly is a group effort, and I could not have reached this point without the constant support of members from the Straub lab, past and present. Thank you to Dr. Katherine Wood for the help with bone marrow transplants and guidance as I learned about sickle cell disease. Thank you to Drs. Shuai Yuan, Joe Galley, and Oyin Dosunmu-Ogunbi for help with experiments and comradery in the lab. Thank you to Megan Miller for the constant support, help with trouble shooting experiments, and being someone I could always go to in the lab. Thank you to Scott Hahn for help with the countless hemin injections we did together. I learned so much from you and you always made being at work fun. Thank you to Dr. Brittany Durgin for being my unofficial mentor

in the lab. You were a constant support for me in the lab whether I need help with experiments, writing, or life. You are an amazing role model, mentor, and friend, and I am a better scientist because your support. Thank you to the more recent additions to the Straub lab: Stefanie Taicit, Robert Hall, and Mate Katonka. I wish you all the best of luck and hope you enjoy being a member of this lab as much as I did. Thank you to Sara Lewis from Dr. Eric Kelley's lab for running hundreds of samples for XO activity for me and Dr. Evan DeVallance for his collaboration and help in better understanding the mechanisms of hepatic XO release.

Thank you so much to my friends and family. I am so grateful to have so many amazing people in my life. One of the best things to come out of graduate school is the lifelong friendships I have made. Thank you to Nicole Kaminski, Sam Herron, Keaton Solo, Nicole Martucci, Bill Tennant, Nolan Carew, and so many more. Thank you to my new family, Mary and Bob Boyle (and everyone else), for always being interested in my work and cheering me on along the way. Thank you to my grandparents, Penny and Ray Kaercher and Anna Marie Gire, for teaching me the value of education. Thank you to my sister, Heather Schmidt, for always supporting me and making me smile. Thank you to my parents, Kristy and Vince Schmidt, none of this would be possible without you. I am lucky to have parents who I consider my best friends. I am proud to be your daughter and can't thank you enough for your constant support.

And finally, thank you to my husband, Calvin Boyle. You have celebrated every high and supported me through every low in graduate school. You always remind me to look on the positive side and help me to focus on what is important when I get caught up in the small details. Thank you for always being my rock and I can't wait to see where life takes us.

1.0 Introduction

Xanthine oxidase (XO) activity has been shown to be increased in several hemolytic conditions, including sickle cell disease (SCD)¹, malaria², and sepsis³; however, the role of XO during heme crisis has yet to be identified. Current dogma in the field has classified elevated XO activity as pathological, due to the increase in oxidant production, particularly in the vascular compartment⁴⁻⁹. We hypothesized that XO activity was elevated in hemolytic disease for a reason, and potentially has beneficial properties depending on the conditions. Therefore, we sought to explore the role of XO in SCD under both basal conditions and instances of severe hemolysis.

1.1 Sickle Cell Disease

SCD affects ~1 in 360 African Americans born each year¹⁰ and has an even larger impact in other parts of the world such as Sub-Saharan Africa where 230,000 newborns were diagnosed with SCD in 2010¹¹⁻¹³. This led the World Health Organization to classify SCD as a global health problem^{10,12}; however, therapeutic options remain limited and life expectancy of SCD patients is significantly reduced.

SCD is caused by a single point mutation in the beta chain of the hemoglobin gene that replaces a glutamic acid with a valine^{11,14}. Hemoglobin is a critical protein comprised of two alpha globin chains and two beta globin chains and is the protein found in red blood cells (RBCs) that delivers oxygen from the lungs throughout the rest of the body¹⁵. This amino acid substitution causes hemoglobin within RBCs to polymerize and take on their characteristic sickle shape,

resulting in several pathological implications^{11,16,17}. Healthy RBCs can flow through the vasculature and small capillaries with ease; however, sickle RBCs can stick to each other and the vessel wall resulting in blocked blood flow, vasoocclusive crises and RBC hemolysis^{16,18-20}. Ruptured RBCs release hemoglobin and heme into circulation which are key drivers of the vascular and pain complications associated with SCD^{11,18}.

Oxidants play an important role in the pathogenesis of SCD²¹. The combination of cell free hemoglobin and increase in reactive species from enzymes such as XO decrease the bioavailability of nitric oxide (NO)²². NO bioavailability is further decreased by catabolism of the nitric oxide synthase substrate arginine by plasma arginase²². NO is a crucial molecule for vasodilation and relaxes the smooth muscle surrounding blood vessels to allow for increased circulation²². Reduced NO bioavailability can lead to pulmonary hypertension¹⁶, leg ulceration, priapism, and stroke, while increased hemolysis leads to fewer RBCs in circulation which alters blood viscosity^{18,22}. This combined with trapping of sickle RBCs in narrow capillaries results in frequent vasoocclusions and can manifest as pain crisis, acute chest syndrome and osteonecrosis^{20,22}. These problems at the level of the RBCs and capillaries can ultimately cause major multi-organ complications and failure.

There is currently no cure for SCD; however, there are four Food and Drug Administration (FDA) approved treatments. For over 20 years hydroxyurea was the only FDA approved drug for the treatment of SCD. It was not until 2017 that L-glutamine was approved and Crizanlizumab and Voxelotor were most recently improved in 2019. Each of these drugs has a different mechanism of action. Hydroxyurea functions by increasing fetal hemoglobin levels^{16,19,23,24}. Fetal hemoglobin contains two alpha and two gamma hemoglobin chains, but levels only remain high for the first 2-4 months of life²⁵. Because fetal hemoglobin does not contain the mutant beta chain,

increasing fetal hemoglobin in sickle patients can alleviate some of their symptoms²⁵. L-glutamine is given to increase the amount of free glutamine in the blood to generate antioxidant molecules that can help neutralize the oxidative stress that occurs in sickle RBCs^{19,26}. Crizanlizumab is a monoclonal antibody that binds p-selectin on the surface of activated endothelial cells and platelets²⁷. In doing so, it prevents sickled RBCs from binding to the surface and therefore helps to prevent vasoocclusive crises by keeping the vessels clear²⁷. Lastly, Voxelotor prevents hemoglobin polymerization by increasing hemoglobin's affinity for oxygen^{28,29}. Oxygenated hemoglobin cannot polymerize and therefore the drug decreases the proportion of sickled RBCs in circulation^{28,29}. Despite the recent advancements in therapeutic options, the molecular drivers of hemolysis in SCD remain poorly understood and there are currently no small molecule drugs designed specifically to inhibit hemolysis in SCD patients.

One enzyme that has been shown to have elevated activity in SCD is XO. Dr. Bruce Freeman's group reported that plasma XO activity is increased in both human patients and in the Townes mouse model of SCD¹. This increase in plasma XO activity was paired with a subsequent decrease in liver XO activity and increase in aortic XO activity¹. They also looked at the localization of XO within the aorta and liver and found that the SCD mice had an increase in XO expression along the vessel wall of the aorta and a decrease in XO expression surrounding the central vein within the liver¹. Finally, western blot analysis demonstrated an increase in plasma and a decrease in liver XO protein levels in the sickle mice¹. While this paper was important in showing increased plasma expression and activity of XO in SCD, it did not describe the function or role of XO in SCD.

1.2 The Impact of Xanthine Oxidase (XO) on Hemolytic Diseases

Heidi M. Schmidt^{1,2}, Eric E. Kelley³, and Adam C. Straub^{1,2}

¹Pittsburgh Heart, Lung, Blood and Vascular Medicine Institute,

²Department of Pharmacology and Chemical Biology, University of Pittsburgh, Pittsburgh,
Pennsylvania,

³Department of Physiology and Pharmacology, West Virginia University, School of Medicine,
Morgantown, West Virginia

Copyright Redox Biology, 2019

1.2.1 Summary

Hemolytic diseases are associated with elevated levels of circulating free heme that can mediate endothelial dysfunction directly via redox reactions with biomolecules or indirectly by upregulating enzymatic sources of reactive species. A key enzymatic source of these reactive species is the purine catabolizing enzyme, xanthine oxidase (XO) as the oxidation of hypoxanthine to xanthine and subsequent oxidation of xanthine to uric acid generates superoxide ($O_2^{\cdot-}$) and hydrogen peroxide (H_2O_2). While XO has been studied for over 120 years, much remains unknown regarding specific mechanistic roles for this enzyme in pathologic processes. This gap in knowledge stems from several interrelated issues including: 1) lethality of global XO deletion and the absence of tissue-specific XO knockout models have coalesced to relegate proof-of-principle experimentation to pharmacology; 2) XO is mobile and thus when upregulated locally can be

secreted into the circulation and impact distal vascular beds by high-affinity association to the glycocalyx on the endothelium; and 3) endothelial-bound XO is significantly resistant (> 50%) to inhibition by allopurinol, the principle compound used for XO inhibition in the clinic as well as the laboratory. While it is known that circulating XO is elevated in hemolytic diseases including sickle cell, malaria, and sepsis, little is understood regarding its role in these pathologies. As such, the aim of this review is to define our current understanding regarding the effect of hemolysis (free heme) on circulating XO levels as well as the subsequent impact of XO-derived oxidants in hemolytic disease processes.

1.2.2 Introduction

Excess circulating free heme is associated with numerous hemolytic diseases including sickle cell disease (SCD), thalassemia, sepsis, cardiac bypass, and malaria^{2,3,30-32}. Oxidation of reduced heme ($\text{Fe}^{2+} \rightarrow \text{Fe}^{3+}$) can result in heme and hemoglobin (Hb) release from red blood cells (RBCs) into the circulation^{31,33}. Under normal physiologic conditions, heme and Hb are immediately scavenged and degraded in plasma or sequestered and transported to tissues such as the liver for degradation^{31,33}. However, under conditions of severe hemolysis, circulating heme reaches levels that saturate the scavenging and degradation pathways, resulting in significant extracellular levels of free heme that can initiate intravascular cell and tissue damage^{31,33}.

Under basal levels of hemolysis, Hb is bound by haptoglobin (Hp) and targeted to macrophages where the complex is taken up via endocytosis and degraded (Figure 1)³¹. Likewise, free heme in the plasma is either bound by hemopexin (Hx) or immediately degraded to iron, carbon monoxide and biliverdin by the enzyme heme oxygenase-1 (HO-1)³⁰. Hx targets heme primarily to the liver and spleen, allowing heme to be cleared through the endothelium,

endocytosed by hepatocytes, and degraded by cellular HO-1 or redistributed for heme iron recycling (Figure 1)^{31,33}. However, under conditions of severe hemolysis, Hx and HO-1 become saturated, resulting in oxidative damage to surrounding tissues due to a decrease in heme degradation and simultaneous increase in circulating free heme³¹. For example, reaction of free heme with O₂ can generate superoxide (O₂^{•-}), and subsequently elevate hydrogen peroxide (H₂O₂) levels via spontaneous or enzymatic dismutation as well as hydroxyl radical (HO[•]) levels by reaction of peroxide(s) with transition metals including heme-iron (Fe). Enhanced abundance of these reactive species mediate lipid, protein, and DNA oxidation resulting in cell and tissue damage, endothelial dysfunction, and loss of vascular homeostasis (Figure 1)^{30,34}. While the catalytically active Fe in heme as well as “free Fe” derived from heme is considered the seminal source of oxidants in hemolytic disease, subsequent contributions from alternative sources are significant to the progression of this inflammatory process. For example, free heme activates toll-like receptor 4 (TLR4) signaling, resulting in activation of pro-inflammatory pathways which include amplification of ROS levels from sources alternative to those generated via Fe-mediated reactions (Figure 1)^{31,35}.

In addition to hemolysis, reactive oxygen species (ROS) and reactive nitrogen species (RNS) (e.g., nitric oxide (•NO), nitrogen dioxide (•NO₂) and peroxynitrite (ONOO⁻)) are generated under numerous pathological conditions that often accompany hemolytic diseases (e.g., ischemia-reperfusion injury and chronic inflammation)³⁶⁻³⁸. The main pathways in which O₂^{•-} is generated include the mitochondrial electron transport chain, nicotinamide-adenine dinucleotide phosphate (NADPH) oxidases, uncoupled nitric oxide synthase (NOS), and xanthine oxidase (XO)³⁷. XO is one such mechanism that is noted to be upregulated in hemolytic disease¹. XO generates oxidants by shuttling electrons derived from purine oxidation to either univalently (O₂^{•-}) or divalently

(H₂O₂) reduce O₂^{•-}. This elevation of XO activity may result in increased formation of RNS via the diffusion-limited reaction between XO-derived O₂^{•-} with •NO to generate ONOO⁻³⁹; however, increased rates of O₂^{•-} formation from the other sources mentioned above may also contribute. The increased presence of ONOO⁻ may lead to alteration in cell signaling via post-translational modification of critical sulfhydryls on effector proteins, diminution of •NO-mediated vasodilatory action, and loss of endothelial barrier integrity via induction of membrane lipid peroxidation^{40,41}.

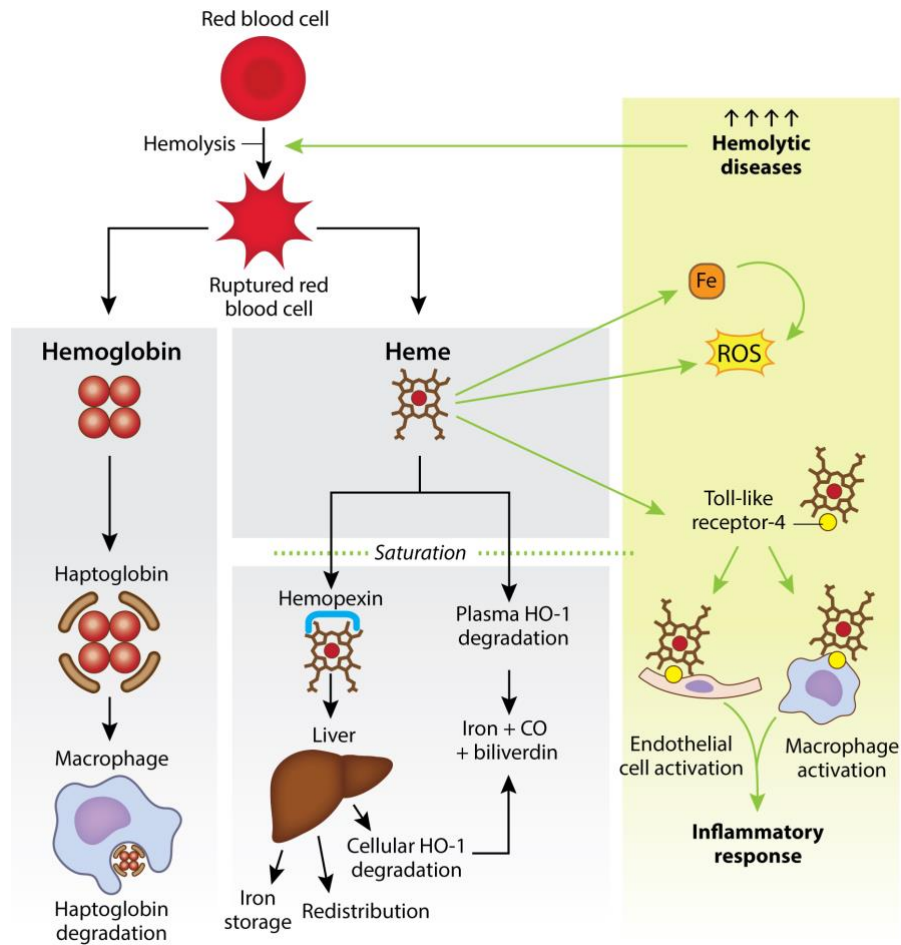


Figure 1. Hemolysis releases free heme and induces inflammation.

A red blood cell (RBC) undergoing hemolysis releases hemoglobin (Hb) and heme. Hb is bound by haptoglobin (Hp) and targeted to macrophages for degradation. Heme is either 1) bound by hemopexin (Hx) and targeted to the liver for iron storage, redistribution, or degradation by cellular heme oxygenase-1 (HO-1); or 2) degraded directly in the plasma by HO-1 into iron, carbon monoxide (CO) and biliverdin (gray panel). Hemolytic diseases cause elevated levels of hemolysis which saturate Hx and HO-1. When these pathways are saturated, heme activates toll-like receptor-4 (TLR4) triggering an immune response. Separately, heme can also generate reactive oxygen species (ROS) directly and indirectly through iron (green panel).

1.2.3 Xanthine Oxidase

Xanthine oxidoreductase (XOR) is a name commonly used to encompass two interconvertible forms of the same enzyme: dehydrogenase (XDH) and oxidase (XO)⁴². XOR is transcribed and translated as XDH, a ~300 kDa homodimer consisting of four redox centers in each subunit: one molybdenum cofactor (Mo-co), one flavin adenine dinucleotide (FAD) site, and two Fe₂S₂ sites⁴³. XDH catalyzes the oxidation of hypoxanthine to xanthine and xanthine to uric acid at the Mo-co site and electrons are shuttled via the two Fe₂S₂ clusters to the FAD site where NAD⁺ is reduced to NADH. XOR exists primarily as XDH intracellularly; yet, once in the extracellular space and circulation XO is the dominant isoform⁴³. The principle difference between XO and XDH is their oxidizing substrate affinity where XO demonstrates diminished affinity for NAD⁺ and over 11-fold increased affinity for O₂⁴⁴. As such, electrons derived from hypoxanthine and xanthine oxidation by XO are quickly accepted by O₂ to generate O₂^{•-} and H₂O₂¹. Della Corte and Stirpe made several important discoveries in the late 1960s and early 1970s showing that XOR is irreversibly or reversibly converted to XO via proteolysis or oxidation of cysteine residues, respectively⁴⁵⁻⁴⁷. As the crystal structure of bovine milk XDH was solved, the site of proteolysis was identified as following Lys551, and the sites of oxidation were identified as Cys535 and Cys592 with formation of a disulfide bridge⁴⁴.

1.2.4 XOR Regulation

While much is known regarding XOR biochemistry, transcriptional and translational regulation is much less understood. The human *xdh* gene is located on the p22 band of chromosome two and contains several possible binding sites for translational modification: four

CCAAT/enhancer binding sites, three IL-6 responsive elements, an NF- κ B site, and TNF α , interferon- γ , and interleukin-1 responsive units⁴⁸. XOR expression is reported to be controlled by a variety of factors including hormones, growth factors, and inflammatory cytokines; yet the most studied effector of XOR expression/activity is hypoxia^{49,50}. While many studies have described transcriptional and post-translational up-regulation of XOR by severe hypoxia⁵¹⁻⁵⁴, modest hypoxia (10% O₂) is also capable of inducing significant elevation of XOR expression, activity, export from endothelial cells, and XO-dependent ROS production⁵⁰. The described moderate hypoxic conditions are comparable to levels observed in congestive heart failure patients⁵⁰. Parks and Granger were the first to describe an elevation in purine catabolites under hypoxic conditions as they attributed the increased hypoxanthine observed during hypoxia to the breakdown of ATP→ADP→AMP→adenosine→inosine→hypoxanthine (purine degradation pathway)⁵⁵. This is crucial in terms of XO function as increased levels of hypoxanthine require increased XO activity for further oxidation to uric acid, all while generating O₂^{•-} and H₂O₂ as byproducts⁵⁵. It is important to note that elevated circulating free heme can induce RBC lysis resulting in release of ATP into the circulation⁵⁶⁻⁵⁸. This ATP is quickly catabolized to adenosine then to hypoxanthine creating a milieu similar to that described above for moderate hypoxia⁵⁶. Elevated levels of hypoxanthine may consequently trigger upregulation of XOR activity in addition to activating purine salvage via hypoxanthine-guanine phosphoribosyl transferase (HPGRT)⁵⁹. Interestingly, we have previously described upregulation of XOR via adenosine activation of adenosine A_{2B} receptors on endothelial cells⁵⁰. Therefore, the combination of increased adenosine and hypoxanthine levels could significantly amplify XOR activity and allied ROS generation during hemolytic crisis; a process already wrought with abundant oxidant generation attributable to heme itself.

1.2.5 XOR-Endothelial Interaction

A critical concept when considering the impact of XOR on disease processes in general and hemolytic disease specifically, is that XOR is mobile and has a high affinity ($K_d = 6$ nM) for glycosaminoglycans (GAGs) on the apical surface of the vascular endothelium^{60,61}. As such, XOR can be upregulated in one anatomic site (e.g., liver), exported to the circulation, bound to endothelial GAGs, and thus sequestered in vascular beds distal from the site of origin⁶⁰⁻⁶⁴. When coupled to the elevated circulating levels of hypoxanthine, it is in this setting that XO can critically contribute to oxidant-mediated vascular dysfunction⁵. Binding and immobilization of XOR on the vascular GAGs also has significant kinetic consequences including alteration in the relative amounts of $O_2^{\cdot-}$ and H_2O_2 produced as well as resistance to inhibition by pyrazolopyrimidine-based inhibitors (see Therapeutic Inhibitors of XO, below)⁶⁵⁻⁶⁷. In the aggregate, mobility and capacity to avidly associate to the endothelium in a manner that is resistant to inhibition affords XO the ability to critically contribute to loss of vascular homeostasis.

1.2.6 Therapeutic Inhibitors of XO

There are currently two XO inhibitors that are FDA approved for the treatment of gout: allopurinol and febuxostat⁶⁸. While allopurinol has been used in the clinic for over fifty years, febuxostat (Uloric[®]) was approved in 2009⁶⁸. Current reports suggest allopurinol may be the superior drug for diminishing uric acid levels to the extent that symptoms of gout are alleviated; however, febuxostat is a more potent XO inhibitor and may be more useful in treating diseases with elevated XO activity at the surface of endothelial cells⁶⁸. Allopurinol is a hypoxanthine mimetic that prevents oxidation of hypoxanthine and xanthine at the Mo-co site of XOR⁶⁹. XOR

oxidizes allopurinol, a suicide inhibitor, with the transfer of two electrons to form oxypurinol, the pharmacologically active form of the drug, which then competitively inhibits XO^{65,70}. Since the oxidation of allopurinol to oxypurinol results in reduction of XOR, O₂^{•-} and H₂O₂ are generated as unfortunate byproducts⁶⁵. In addition, GAG-immobilized XOR is resistant to inhibition by allo/oxypurinol. For example, concentrations (200–400 μM) of allo/oxypurinol, greater than the clinical working range (20–80 μM) are required to achieve 45–50% inhibition of XO⁶⁶. While allopurinol is effective at relieving symptoms of gout, it may be a poor choice for targeting endothelial-associated XO-derived ROS generation.

Febuxostat is reported to have a *K_i* some 6,000 times lower than allopurinol and does not react directly with the Mo-co site of XOR, but rather binds the pocket leading to the active site via electrostatic interaction thus blocking purine access. As such, it does not induce enzyme turn-over and unwanted production of O₂^{•-} and H₂O₂^{65,71,72}. This makes febuxostat an ideal pharmaceutical for pathologic conditions where O₂^{•-} and H₂O₂ generated by XO contribute to endothelial injury. The IC₅₀ of febuxostat (4.4 nM) did increase 2.5-fold when XO was bound by GAGs, but this is significantly lower than the 22-fold increase observed with allopurinol (64 μM)⁶⁵. Febuxostat completely inhibited O₂^{•-} formation at or below 50 nM, a concentration well below the clinical C_{max} (15 μM)⁶⁵.

Whereas both pyrazolopyrimidine-based inhibitors and febuxostat are effective in reducing uric acid levels and oxidant generation by inhibiting XO, they are not without shortcomings. For example, clinical administration of allopurinol: 1) is limited to significantly reduced dosing in patients with preexisting renal disease, 2) is known to mediate substantive hypersensitivity issues which also limits dosage and 3) effects alternative purine catabolic pathways^{41,73}. While febuxostat has demonstrated superior specificity and potency to allo/oxypurinol, it too has been associated

with negative clinical outcomes. For example, febuxostat administration has been associated with rhabdomyolysis in patients with chronic kidney disease (CKD)⁷⁴ and has been shown to be non-inferior to allopurinol regarding rates of adverse cardiovascular events where all-cause mortality and cardiovascular mortality were greater in febuxostat-treated patients than patients treated with allopurinol⁷⁵. When taken together, the issues related to currently available FDA-approved XO inhibition approaches may indeed limit the potential for their effective use in hemolytic disease, affirming the need for alternative approaches to alter XO activity.

1.2.7 XOR, ROS, and Hemolytic Diseases

Upregulation of XDH has been associated with hypoxia-induced vaso-occlusive crisis in SCD mice and humans^{1,76}. Aslan and colleagues demonstrated that ischemia/reperfusion injury in SCD mice resulted in release of XDH from the liver into the circulation, rapid conversion to XO via plasma proteases, immobilization on endothelial GAGs, and represented a major source of $O_2^{\cdot-}$ and H_2O_2 in the vascular compartment¹, as depicted in Fig. 2. In this setting, XO-derived oxidants can alter cell signaling processes as well as induce overt damage¹. For example, diminution in $^{\cdot}NO$ -mediated signaling (e.g., vasodilatory response) can result from the diffusion-limited reaction between XO-derived $O_2^{\cdot-}$ and $^{\cdot}NO$ to form $O=NOO^{\cdot}$. In addition, both XO-derived $O_2^{\cdot-}$ and H_2O_2 can mediate protein and lipid oxidation which can affect vascular homeostasis by also altering signaling pathways directly (e.g., oxidation of eNOS-associated BH4) or indirectly via disruption of cellular membrane integrity. Evidence for the contribution of XO to oxidant load is also revealed by substantively elevated circulating XO in SCD patients compared to healthy controls⁷⁶.

Hepatic ischemic injury and hypoxia, in mice and rats, also increase XDH release from the liver into the vasculature and induce rapid conversion of XDH to XO during reperfusion^{7,77}. Due

to the relatively high circulating half-life of XO, significant damage can be done to the endothelium due to XO-dependent oxidant generation⁷. Elevated XO levels were observed in diseases involving liver injury such as hepatitis, jaundice, and chronic renal failure (secondary effects on the liver)⁷. Of particular interest is that elevated levels of circulating XO are reported to positively associate with chronic liver disease (cirrhosis, chronic hepatitis and cholestatic disorders); yet, they do not correlate with indices of liver damage, suggesting a signaling event alternative to hepatocellular damage is operative, and thus may drive upregulation of XDH with subsequent release into the circulation⁷⁸. However, patients with virus-related cirrhosis demonstrated significantly enhanced levels of circulating XO that did positively correlate with the extent of liver damage as indicated by assessment of ALT leaving the field a bit unclear at present⁷⁹.

More specifically related to “hemolytic” disease are patients with malaria and/or sepsis. Asymptomatic malaria patients demonstrate a two-fold elevation in circulating XO levels compared to controls whereas patients hospitalized with severe malaria have plasma XO levels over 3.25-fold greater than asymptomatic individuals and thus 6.5- fold greater than controls². Similarly, upon diagnosis, sepsis patients who did not subsequently survive presented with significantly elevated plasma (2.2-fold) XO activity³. However, 24 h post diagnosis these non-survivors displayed less plasma XO activity than survivors; thus, indicating a temporal relationship regarding circulating XO activity and the severity of the disease as well as the overall outcome. Regardless of survival outcomes, plasma XO activity correlated positively with indices of oxidant stress including protein carbonylation and lipid peroxidation. This principle was also seen in a rodent model of experimental sepsis where treatment with allopurinol and/or metal chelation therapy with desferrioxamine significantly abrogated the abundance of biomolecular free radicals

indicating critical contributions from both XO and Fenton-type reactions stemming from RBC lysis⁸⁰.

While it is clear that there are contributory roles for XO in hemolytic disease, it is equally clear that the mechanisms underpinning specific signaling events leading to upregulation of XDH, triggers to release XDH into the circulation and the subsequent impact of circulating XO remain to be defined. For example, it has been suggested that TLR-4 signaling serves to elevate XOR levels⁸¹; yet, there are no reports revealing empirical evidence that this is the case. On the other hand, it has been reported that XO-derived ROS were essential for TLR4-induced NFAT5 (nuclear factor of activated T cells) activation of murine macrophages; again, leaving the field a bit unclear⁸². This gap in our current understanding of the linkage between heme overload and up-regulation of XDH affirms the need for further study.

Hx is a natural antioxidant that binds heme as it is released during hemolysis and targets the complex to the liver parenchymal cells for degradation and recycling of the Hx and iron⁸³. However, increased nitration of Hx during inflammation can diminish the protective antioxidant properties during heme toxicity⁸³. Erythrocytes undergo a significant amount of oxidative stress and ROS production and thus require a number of enzymatic and non-enzymatic antioxidants including superoxide dismutase (SOD), catalase (CAT), glutathione peroxidase (GPx), glutathione reductase (GR), glutathione (GSH) and vitamins E and C⁸⁴. SCD hemoglobin generates twice as much $O_2^{\cdot-}$, H_2O_2 and HO^{\cdot} compared to normal hemoglobin, and thus have increased antioxidant function often resulting in antioxidant deficiencies⁸⁴. Antioxidant therapeutic approaches are being examined as an option for treating SCD because they can be administered at low cost through food and can be administered in combination with hydroxyurea to decrease oxidative stress⁸⁵.

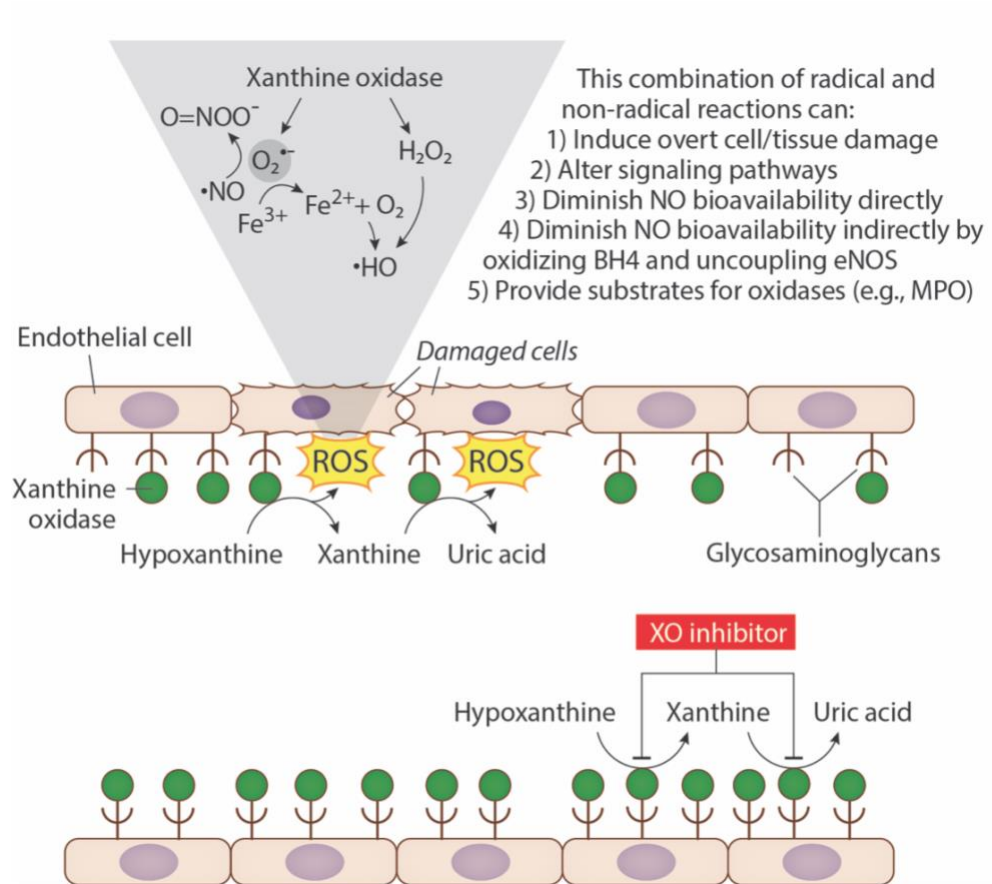


Figure 2. XO binds GAGs and produces ROS at the endothelial surface

Xanthine oxidase (XO) released from the liver can bind to the surface of endothelial cells via interactions with glycosaminoglycans (GAGs). As hypoxanthine is converted to xanthine, and xanthine to uric acid by XO, reactive oxygen species (ROS) are generated at the surface of endothelial cells. XO produces either $O_2^{\bullet-}$ or H_2O_2 which can lead to production of $ONOO^-$ or $\bullet HO$ (top). Treatment with an XO inhibitor such as febuxostat inhibits XO and blocks the conversion of hypoxanthine to xanthine and xanthine to uric acid preventing ROS production and damage at the endothelial cell surface (bottom).

1.2.8 Summary and Conclusions

The high levels of hemolysis associated with hemolytic diseases, cause a saturation of protective pathways resulting in an increase in $O_2^{\cdot-}$, H_2O_2 and $\cdot HO$ generation and activation of inflammatory pathways^{31,35}. XO is one mechanism of ROS generation that has been observed in elevated circulating levels in murine models of hemolytic disease and clinically. Circulating XO can significantly contribute to the oxidant load in the vascular compartment by binding to the endothelial glycocalyx^{60,61}. In this setting XO is resistant to inhibition by clinically applicable concentrations of allo/oxypurinol and thus may serve to amplify the oxidant load derived from heme-related reactions and thus exacerbate an existing oxidant assault. However, the signaling events that link elevation in heme concentration and upregulation/export of cellular XDH are not defined. Further exploration of these signaling events will provide a clearer understanding of the role of XOR in hemolytic disease and likely improve clinical practices and outcomes.

1.2.9 Acknowledgements

Funds were provided by National Institutes of Health Grants R01 HL 133864 and R01 HL 128304 (ACS), P01 AG043376 and P20 GM109098 (EEK), American Heart Association (AHA) Grant-in-Aid 16GRNT27250146 (ACS) and Bayer Pharma Sponsored Research Grant (ACS). Additionally, other support was provided by the Institute for Transfusion Medicine and the Hemophilia Center of Western Pennsylvania (ACS). Graphical design was provided by Anita Impagliazzo.

1.3 Summary and Hypotheses

While it has long been established that circulating XO activity is increased during hemolytic conditions, it has been assumed that the elevated activity is always pathological due to the increase in ROS production. ROS production at the endothelial surface can damage endothelial cells leading to cell and tissue damage, interference with signaling pathways, and diminished NO bioavailability. These effects can contribute to disease pathologies and lead to worse outcomes in patients. The majority of circulating XO (>50%) originates from the liver; however, the mechanism of release is unclear. Based on our knowledge of hepatic release of XO during hemolytic conditions, we hypothesized that such a significant increase in XO activity during several hemolytic conditions could have beneficial properties. We postulated that XO could still be harmful under basal conditions, but it is present in preparation for a heme crisis event, where it serves to protect the body from excess free heme. Therefore, we designed a project with the goal of identifying the role of XO during heme crisis. We chose to study the role of XO in SCD because sickle patients have higher levels of hemolysis and XO activity compared to healthy individuals, and under stress, they experience crisis events which lead to further hemolysis and increases in XO activity levels. This provided an excellent model to study the role of XO under varying levels of hemolytic stress.

The specific aims of this project are: (1) to investigate the role of XO during basal conditions of SCD by treating wildtype mice with febuxostat (FDA approved XO inhibitor) for 10 weeks and evaluating the effects on hematology, vessel reactivity, and cardiac function (disease markers of SCD), and (2) to explore the role of XO during a heme crisis event in hepatocyte-specific XO knockout SCD mice by injecting mice with hemin and evaluating the effects on

survival, hematology, and XO activity. Additionally, to evaluate the potential protective mechanisms of XO during heme by crisis by investigating its impact on free heme and hemoglobin.

2.0 Xanthine Oxidase Drives Hemolysis and Vascular Malfunction in Sickle Cell Disease

Heidi M. Schmidt¹, Katherine C. Wood², Sara E. Lewis³, Scott A. Hahn², Xena M. Williams³, Brenda McMahon², Jeffrey J. Baust², Shuai Yuan², Timothy N. Bachman², Yekai Wang^{4,5}, Joo-Yeun Oh⁶, Samit Ghosh^{2,7}, Solomon F. Ofori-Acquah^{2,7,8}, Jeffrey D. Lebensburger⁹, Rakesh P. Patel^{6,10}, Jianhai Du^{4,5}, Dario A. Vitturi^{1,2}, Eric E. Kelley³, Adam C. Straub^{1,2}

¹Department of Pharmacology and Chemical Biology, University of Pittsburgh, Pittsburgh, PA;

²Heart, Lung, Blood and Vascular Medicine Institute, University of Pittsburgh, Pittsburgh, PA;

³Department of Physiology and Pharmacology, Health Sciences Center, West Virginia University, Morgantown, WV;

⁴Department of Ophthalmology, West Virginia University, Morgantown, WV;

⁵Department of Biochemistry, West Virginia University, Morgantown, WV;

⁶Center for Free Radical Biology, University of Alabama at Birmingham, Birmingham, AL;

⁷Division of Hematology/Oncology, Department of Medicine, School of Medicine, University of Pittsburgh, Pittsburgh, PA;

⁸School of Biomedical and Allied Health Sciences, University of Ghana, Accra, Ghana;

⁹Department of Pediatrics, University of Alabama at Birmingham, Birmingham, AL;

¹⁰Department of Pathology, University of Alabama at Birmingham, Birmingham, AL

Copyright, Arteriosclerosis, Thrombosis, and Vascular Biology, 2020

2.1 Summary

OBJECTIVE: Chronic hemolysis is a hallmark of sickle cell disease (SCD) and a driver of vasculopathy; however, the mechanisms contributing to hemolysis remain incompletely understood. Although XO (xanthine oxidase) activity has been shown to be elevated in SCD, its role remains unknown. XO binds endothelium and generates oxidants as a byproduct of hypoxanthine and xanthine catabolism. We hypothesized that XO inhibition decreases oxidant production leading to less hemolysis.

APPROACH AND RESULTS: Wild-type mice were bone marrow transplanted with control (AA) or sickle (SS) Townes bone marrow. After 12 weeks, mice were treated with 10 mg/kg per day of febuxostat (Uloric), Food and Drug Administration–approved XO inhibitor, for 10 weeks. Hematologic analysis demonstrated increased hematocrit, cellular hemoglobin, and red blood cells, with no change in reticulocyte percentage. Significant decreases in cell-free hemoglobin and increases in haptoglobin suggest XO inhibition decreased hemolysis. Myographic studies demonstrated improved pulmonary vascular dilation and blunted constriction, indicating improved pulmonary vasoreactivity, whereas pulmonary pressure and cardiac function were unaffected. The role of hepatic XO in SCD was evaluated by bone marrow transplanting hepatocyte-specific XO knockout mice with SS Townes bone marrow. However, hepatocyte-specific XO knockout, which results in >50% diminution in circulating XO, did not affect hemolysis levels or vascular function, suggesting hepatocyte-derived elevation of circulating XO is not the driver of hemolysis in SCD.

CONCLUSIONS: Ten weeks of febuxostat treatment significantly decreased hemolysis and improved pulmonary vasoreactivity in a mouse model of SCD. Although hepatic XO accounts for >50% of circulating XO, it is not the source of XO driving hemolysis in SCD.

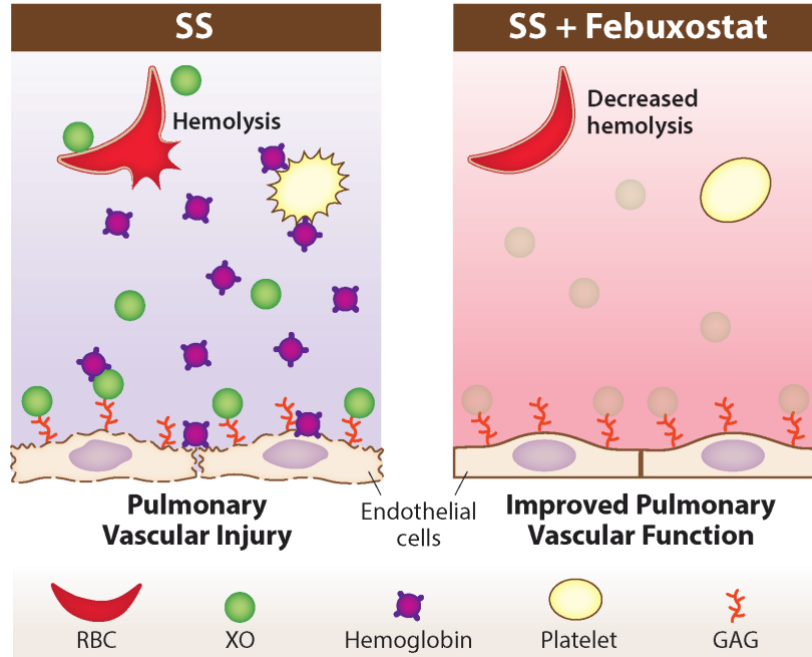


Figure 3. XO is a key driver of hemolysis in SCD

In SS sickle mice XO drives hemolysis of RBCs, releasing hemoglobin into circulation. Free hemoglobin activates platelets and in combination with the ROS produced by XO induces pulmonary vascular injury (left). When SS sickle mice are treated with febuxostat less hemolysis occurs, preventing platelet activation and leading to improved pulmonary vascular function (right). RBC, red blood cell; XO, xanthine oxidase; GAG, glycosaminoglycan; SCD, sickle cell disease; ROS, reactive oxygen species.

2.2 Introduction

Sickle cell disease (SCD) is a major global hemoglobinopathy that affects $\approx 300,000$ newborns worldwide each year¹⁰. It is estimated that there are $\approx 100,000$ affected individuals in the United States¹⁰; however, in other parts of the world, such as Sub-Sahara Africa, SCD is endemic with $\approx 230,000$ new incidences in 2010¹¹⁻¹³, leading the World Health Organization and United Nations to classify SCD as a global public health problem^{10,12}.

SCD presents as multi-organ dysfunction that is the consequence of a single genetic mutation in the β -subunit of Hb (hemoglobin)^{11,14}. Under low pH or deoxygenation conditions, the point mutation in the Hb gene triggers Hb polymerization due to the hydrophobicity change of the amino acid substitution and subsequent sickling of red blood cells (RBCs)^{11,16,17}. Sickled RBCs cause vaso-occlusive crises and RBC hemolysis, releasing cell-free Hb and heme into circulation^{11,18}. Free Hb and heme generate a proinflammatory environment that results in endothelial dysfunction, hyperviscosity, and RBC-leukocyte-platelet interaction on the endothelial surface^{16,18-20}. Despite having a direct impact on Hb structure, function, and RBC shape, the mutation also causes complications such as pulmonary and systemic vasculopathy¹⁷, pulmonary and relative systemic hypertension¹⁶, acute chest syndrome¹⁶, heart failure²⁰, and renal failure¹⁶, which result in accelerated mortality⁸⁶. Treatment options for SCD remain limited, with only four Food and Drug Administration–approved drugs: hydroxyurea^{16,19,23,24}, L-glutamine^{19,26}, crizanlizumab²⁷, and voxelotor^{28,29}. This is due in part to the poor understanding of the molecular drivers of hemolysis in SCD and, therefore, lack of small molecule drugs that can inhibit hemolysis in SCD patients. Chronic blood transfusions are also used to treat SCD; however, benefits for patients with pulmonary hypertension remain inconclusive^{87,88}.

XO (xanthine oxidase) has been shown to be increased in several studies involving human SCD patients and mouse models of SCD^{1,76,89}; however, the role of XO in SCD is yet to be established. XO and XDH (xanthine dehydrogenase) are 2 forms of the enzyme collectively known as XOR (xanthine oxidoreductase)^{42,90}. XOR is transcribed and translated as XDH which catalyzes the oxidation of hypoxanthine to xanthine and xanthine to uric acid at the Molybdenum-cofactor while reducing NAD^+ to NADH at the flavin adenine dinucleotide-cofactor. During inflammation, oxidation of critical cysteine residues, or limited proteolysis converts XDH to XO which catalyzes

the same reactions at the Molybdenum-cofactor, yet reduces oxygen to superoxide ($O_2^{\bullet-}$) and hydrogen peroxide (H_2O_2)¹.

XDH is transcribed and translated primarily in the liver; however, following hepatic stressors, such as ischemia, hypoxia, or inflammation, XDH is released from the liver and enters circulation where it is rapidly converted to XO by plasma proteases^{1,91}. XO binds with considerable affinity ($K_d=6$ nmol/L) to distal endothelial surfaces via electrostatic interactions with glycosaminoglycans, thus increasing XO concentration in organs with low basal levels of the enzyme and amplifying $O_2^{\bullet-}$ or H_2O_2 production at the endothelial surface^{60,61}. Although XO directly produces $O_2^{\bullet-}$ or H_2O_2 , other reactive species such as peroxynitrite and hydroxyl radical can also be generated via reactions with nitric oxide (NO) and iron, respectively¹. This oxidative milieu at the endothelial surface can lead to endothelial and tissue damage, altered signaling, and diminished NO bioavailability⁹⁰. Reactive oxygen species (ROS) produced on the endothelial surface or in circulation can cause RBC membrane fragility, resulting in hemolysis⁹². Therefore, we hypothesized that XO inhibition would decrease hemolysis in a mouse model of SCD.

2.3 Materials and Methods

2.3.1 Animals

C57BL/6J (58 wildtype; stock no. 000664;) mice were ordered from The Jackson Laboratory (Bar Harbor, ME). Colonies of *Xdh*^{floxed/floxed}*Alb-1*^{Cre/Wt} (Albumin-1; 7 hepatocyte-specific *Xdh* knockout)⁹³, *Xdh*^{floxed/floxed}*Alb-1*^{Wt/Wt} (8 littermate floxed [FLX] controls)⁹³, and Townes knock-in sickle (SS) and their control (AA) mice were bred and maintained at the

University of Pittsburgh. All *Xdh*^{flxed/flxed} mice were bred on a C57BL/6J background. All Townes mice were bred on a C57BL/6J and 129S background⁹⁴. Only 6- to 13-week-old male mice were used for experiments because there is currently no indication that male and female mice have major differences in hemolysis in SCD. In the AA control Townes mice, both murine alpha-globin genes are knocked out and replaced by human alpha and beta-globin (Hb) transgenes in the mouse locus. The SS sickle mice contain 2 copies of the human beta sickle globin transgene⁹⁵. All animal experiments were approved by the Institutional Animal Care and Use Committee at the University of Pittsburgh. All mice were supplied standard laboratory diet (no. 5234) and drinking water according to the Guide for the Care and Use of Laboratory Animals of the Department of Laboratory Animal Research at the University of Pittsburgh. All mice were housed in pathogen-free conditions.

2.3.2 Bone Marrow Transplanted Chimeric Mice

The genotype of the *Xdh*^{flxed/flxed} mice was confirmed by polymerase chain reaction analysis of DNA obtained from tail tissue using a Cre-specific probe. Genotypes of the Townes mice were confirmed by peripheral blood Hb electrophoresis. Hb electrophoresis was performed using the reagents provided in the Hb (E) and Hb (E) Acid Kits (Sebia Capillary System; Lisse, France), in accordance with the manufacturer's guidelines. Briefly, 5 μ L of the RBC pellet was lysed in 65 μ L of Sebia hemolysis solution. Samples were run on an agarose gel and stained for identification of Hb fraction by band location. Phoresis software was used to quantify the density of the bands. Four different groups of bone marrow (BM) chimeras were generated: C57BL/6J/AA, C57BL/6J/SS, *Xdh*^{flxed/flxed}*Alb-1*^{Cre/Wt}/SS, and *Xdh*^{flxed/flxed}*Alb-1*^{Wt/Wt}/SS. C57BL/6J/AA mice received BM cells from Townes AA donor mice and C57BL/6J/SS, *Xdh*^{flxed/flxed}*Alb-1*^{Cre/}

Wt/SS , and $Xdh^{floxed/floxed}Alb-I^{Wt/Wt}/SS$ mice received BM cells from Townes SS donor mice. BM transplants were performed as previously described⁹⁶. Briefly, BM cells were isolated from the femurs and tibiae of Townes AA or SS donor mice. C57BL/6J (8 weeks old), $Xdh^{floxed/floxed}Alb-I^{Cre/Wt}$ (6-13 weeks old), or $Xdh^{floxed/floxed}Alb-I^{Wt/Wt}$ (6-13 weeks old) recipient mice were lethally irradiated (two 500–550 rad doses, 3 hours apart) and AA or SS BM ($1.5\text{--}2.5\times 10^6$ cells) was injected retro-orbitally immediately following the second irradiation. Following BM transplant, chimeras were housed in autoclaved cages and provided 0.2% neomycin drinking water for 2 weeks, followed by normal autoclaved drinking water for the remainder of the experiment. At 12 weeks post-BM transplant, 50 to 100 μL of blood was collected via retro-orbital eye bleed to assess BM engraftment of the chimeric mice by Hb electrophoresis using the Sebia Hb Electrophoresis kit described above. Only chimeras with $\geq 80\%$ of the donor Hb phenotype were used for subsequent experiments. At 12 weeks post-BM transplant C57/AA and C57/SS mice were given the clinically relevant dose of febuxostat in drinking water (0.05 mg/mL or ≈ 10 mg/kg per day) for 10 weeks. BM engraftment was confirmed 0-, 3-, and 10-weeks post initiation of febuxostat treatment. Ten weeks post-BM engraftment, mice were weighed and euthanized via heart puncture following right heart catheterization. Blood was collected via heart puncture (200–500 μL) in 5% EDTA. Mice were perfused with 5 mL of PBS and organs were collected and flash-frozen in liquid nitrogen. Mice were then perfused with 5 mL of 4% paraformaldehyde in PBS and organs were weighed and fixed in paraformaldehyde overnight, then transferred to 70% ethanol for paraffin embedding.

2.3.3 Echocardiogram

Echocardiograms were performed by the University of Pittsburgh Rodent Ultrasonography Core. Mice were anesthetized with 3% isoflurane (maintained with 1.5% isoflurane) and body temperature was maintained with a heating pad. Images of the right and left ventricles were acquired using a Vevo 3100 imaging system and the VisualSonic MX400 (20-46 MHz, 50 μ m axial resolution) linear array transducer (FUJIFILM VisualSonics, Toronto, Canada). Heart rate was maintained between 400-500 bpm by adjusting the isoflurane concentration between 1-2%. Image acquisition and analysis was done as previously described⁹⁷.

2.3.4 Closed Chest Right Ventricle (RV) Micro-Catheterization

Micro-catheterization was performed as previously described^{96,98}. Briefly, mice were anesthetized with an intraperitoneal injection of etomidate/urethane (9/1.1 mg/kg, Butler Schein). Body temperature was regulated with a heating pad and heating lamp. While in the supine position, an incision was made between the sternohyoid and sternomastoid muscles of the right neck. Catheterization of an isolated 20 mm section of the external jugular vein was done using two 6-0 silk sutures by tying a surgical knot at the cranial end of the external jugular vein and the other looped lightly on the same vein by the heart. A small incision was made in the vein and a 1.2F micro pressure-volume (PV) catheter was inserted beyond the suture by the heart which was then tightened to prevent bleeding. The catheter was further advanced until it passed through the right atrium and into the right ventricle. Pressure measurements were given five minutes to stabilize before beginning recording. The PV catheter was removed, and the external jugular was ligated to

prevent further bleeding. Pressure waveforms were saved and analyzed using IOX2 Software (EMKA Technologies; Falls Church, VA) and MATLAB (Mathworks, Natick, MA, USA).

2.3.5 Pulmonary, Mesenteric, and Thoracodorsal (TDA) Ex-Vivo Two-Pin Wire

Myography

Myography experiments were performed similarly to those previously described by our lab⁹⁹. Briefly, mice were euthanized by heart puncture, following right heart catheterization (see above). Pulmonary, mesenteric, and TDA arteries were rapidly excised, placed in room temperature physiological salt solution (PSS), cleaned of fat, cut into 2 mm rings fitted with two 25 μm wires, and placed on a wire myograph (DMT 620M) filled with PSS containing (in mM): NaCl 119, KCl 4.7, MgSO_4 1.17, KH_2PO_4 1.18, D-glucose 5.5, NaHCO_3 25, EDTA 0.027, CaCl_2 2.5, pH 7.4 when bubbled with 95% O_2 and 5% CO_2 at 37°C. Vessels were allowed to rest for 30 minutes in PSS buffer. Vessels were then incrementally stretched to a tension equivalent to 80 mmHg. To constrict the arteries and determine viability, 60 mM potassium (K) in PSS (KPSS) was added for 5 minutes. Vessels were washed (3x) and rested in PSS for 30 minutes. For vessels isolated from mice treated with febuxostat, 10 μM febuxostat was added to the PSS following the washes. For pulmonary arteries, vasoconstriction was induced with increasing doses of the constrictor prostaglandin $\text{F}_{2\alpha}$ (PGF) (10^{-7} - 10^{-5} M, Tocris #4214) at 4-minute intervals until the vessels reached maximum constriction. For mesenteric and TDA arteries vasoconstriction was induced with increasing doses of the constrictor U46619 ($10^{-7.5}$ - $10^{-6.5}$ M, Cayman Chemicals) at 4-minute intervals until the vessels reached maximum constriction. Pulmonary, mesenteric, and TDA arteries were then treated with increasing doses of the vasodilator acetylcholine (10^{-8} - 10^{-5} M, Sigma) at 3-minute intervals. Finally, vessels were treated with Ca^{2+} free PSS containing 100 μM

SNP to determine maximal dilation. Data was collected using Lab Chart Software (AD Instruments) and normalized to the change in maximum constriction or maximum dilation to determine the percent relaxation of vessels.

2.3.6 Blood Collection and Hematologic Phenotyping

Blood samples were obtained at 0-, 3-, 6-, and 10-weeks post engraftment via retro-orbital eye bleed. Blood samples were obtained immediately following euthanasia via heart puncture. For retro-orbital eye bleeds, mice were anesthetized with 1% isoflurane and heparin-coated microcapillary tubes were used to collect 50 to 100 μ L of blood. Blood was collected in sterile tubes containing 5% EDTA and maintained at room temperature until analysis of complete blood count (within 2–4 hours). Complete blood counts were measured using a Heska (HemaTrue Inc.; Miami Lakes, FL) according to manufacturer instructions. Reticulocytes were measured from whole blood using flow cytometry. Thiazole Orange (80 pM in 1 \times PBS) was used to stain reticulocytes. Samples were incubated overnight at 4°C and protected from light. The samples were analyzed using flow cytometry, and FACSDIVA software was used for data collection. Whole blood was spun down at 2500 \times g for 10 minutes at 4°C. Plasma was separated from the RBC pellet, aliquoted for additional experiments, and stored at –80°C. Plasma Hp (haptoglobin) levels were measured by ELISA according to the manufacturer’s instructions (Crystal Chem; Elk Grove Village, IL). Plasma Hx (hemopexin) levels were measured by ELISA according to the manufacturer’s instructions (AssayPro; St. Charles, MO). Heme-containing species and their metabolites including methemoglobin, oxyhemoglobin, and hemin were measured in plasma using ultraviolet-visible spectral deconvolution as previously described¹⁰⁰.

2.3.7 XO Activity

Human blood samples from healthy controls (non-SCD pediatric patients undergoing surgery) or SCD patients were obtained from Children's of Alabama Hospital according to University of Alabama at Birmingham Institutional Review Board–approved protocols¹⁰⁰. Blood from AA, AS, and SS chimeric mice was collected via heart puncture. Blood from AA and SS chimeric mice treated with febuxostat was collected via retro-orbital eye bleed at 0 and 3 weeks of treatment and via heart puncture at 10 weeks of treatment. Whole mouse blood was spun down at 2500×g for 10 minutes to collect plasma. Liver, lung, and kidney tissue was collected after perfusion with 5 mL of PBS. Plasma and tissue XO activity was measured, as previously described⁹³. Briefly, XO activity was evaluated by electrochemical detection (ESA Coul-Array System) of uric acid via reverse-phase high-performance liquid chromatography.

2.3.8 Coumarin Boronic Acid (CBA) Assay

Oxidant load (H_2O_2 , $\text{O}=\text{NOO}^-$, and HClO) was measured using coumarin boronic acid (CBA) as previously published with some modifications¹⁰¹. Plasma samples were collected and stored at -80°C . To preserve oxidant production in plasma samples, sodium azide (20 mM) was supplemented to inhibit enzyme activity immediately upon thawing the plasma. CBA probe (Cayman, 14051) was prepared in the assay buffer (0.01% BSA in HBSS) and mixed with plasma samples at 0.5 mM final concentration. Kinetic fluorescence measurement was performed at 350/450 nm, 37°C . The amount of oxidant load was quantified by the production rate of the fluorescent product in the log phase and expressed as fold change.

2.3.9 Trichrome Staining

Trichrome staining was performed as previously described¹⁰². Tissues were stained using the Masson's Trichrome Kit (Thermo Fisher) in accordance with the manufacturer's guidelines. Sections were imaged using the TissueGnostics Microscope with a 20x objective and stitched using NIS Elements Software (Snake Stich, 8% overlap). Quantification of trichrome positive/fibrotic area was done using FIJI software.

2.3.10 Statistics

Outliers were identified using a ROUT analysis with a Q=1% and excluded from the data presented. When 2 groups were included, an unpaired Student t test was used unless otherwise noted. An unpaired Student t test with a Welch correction was used if the standard deviation of the 2 groups was significantly different. Normality was assessed using the Shapiro-Wilk normality test. If the 2 groups were not normally distributed, a Mann-Whitney test was performed. When ≥ 3 groups were included, a 1-way ANOVA with Dunnett multiple comparison test was used when comparing multiple groups to a control group or Sidak multiple comparison test was used when making multiple comparisons. When comparing 2 groups over time or across several doses a 2-way ANOVA with Sidak multiple comparison test was used. Significance was defined as a $P < 0.05$.

2.4 Results

2.4.1 Febuxostat Treatment Significantly Decreases Plasma and Tissue XO Activity

Previous reports have shown a significant increase in XO activity in human patients with SCD compared to healthy controls, as well as in the Townes mouse model of SCD¹. To confirm these findings, we obtained plasma samples from pediatric patients with or without SCD and observed a significant increase (8-fold) in the plasma XO activity of patients with SCD compared with the healthy controls (Figure 4A). We also measured plasma XO activity in wild-type mice transplanted with BM from AA control, AS sickle trait, and SS sickle Townes mice and observed a 1.3-fold increase in the AS sickle trait and a 1.5-fold increase in the SS sickle mice (Figure 4B). To evaluate the role of XO in SCD, 8-week-old wild-type mice were BM transplanted with AA control or SS sickle BM from Townes mice (Figure 4C, Figure 5A). After 12 weeks, mice were fully engrafted with the Townes BM (Figure 5B). The mice were then split into four groups: AA, AA+febuxostat, SS, and SS+febuxostat. They were treated with a clinically relevant dose of febuxostat (10 mg/kg per day) in their drinking water for 10 weeks. Blood was collected at 0-, 3-, 6-, and 10-weeks post initiation of febuxostat treatment, with 10 weeks being the end point of the study (Figure 4C, Figure 5A). Febuxostat treatment resulted in significant decreases in plasma, liver, lung, and kidney XO activity in the AA control (Table I) and in the SS sickle mice (Figure 4D, Table II). XO inhibition was confirmed by measuring hypoxanthine, xanthine, and urate levels. No change in hypoxanthine or xanthine, and a significant decrease in urate was observed in the AA control (Figure 5C) and a significant increase in hypoxanthine, no change in xanthine, and a significant decrease in urate was observed in the SS sickle mice treated with febuxostat (Figure 4E through 4G). Oxidant load was also assessed via a coumarin boronate assay. There was

a significant decrease in oxidant load in the febuxostat-treated SS sickle mice compared with the SS sickle mice (Figure 4H). No difference in body weight between the SS and SS+febuxostat groups was observed (Figure 4I); however, there was a significant 2.4 g weight loss in the AA+febuxostat group compared with the AA control mice (Figure 5D). There was approximately a 7-fold difference in spleen weight between the AA and SS mice; however, febuxostat treatment did not alter the AA or SS spleen weight (Figure 5E).

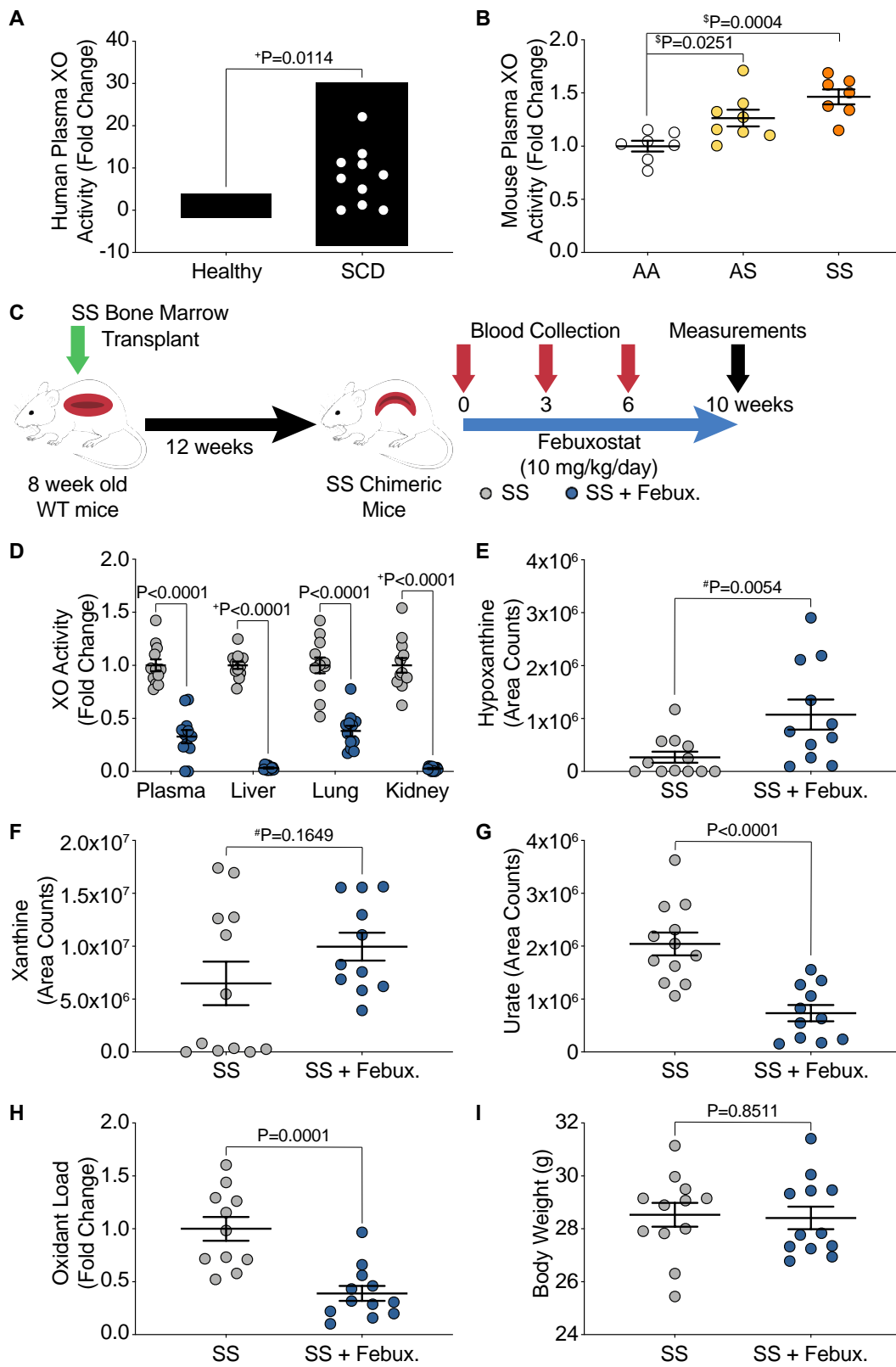


Figure 4. Febuxostat treatment inhibits XO activity in chimeric sickle cell disease mice.

XO activity was assessed in A) human sickle cell disease patients compared with healthy controls and B) chimeric AA control, AS sickle trait, and SS sickle mice. C) Experimental design. D) XO activity of plasma, liver, lung, and kidney after 10 wk of Febux treatment. LC/MS-MS was used for purine metabolite analysis of E) hypoxanthine, F) xanthine, and G) urate. H) A coumarin boronate assay was used to measure plasma oxidant load. I) Febuxostat treatment did not alter body weight. Values are mean \pm SEM using an unpaired Student t test unless otherwise noted. +Values are mean \pm SEM using an unpaired Student t test with Welch correction. \$Values are mean \pm SEM using a 1-way ANOVA with Dunnett multiple comparisons test. #Values are mean \pm SEM using a Mann-Whitney test. WT, wildtype; XO, xanthine oxidase; SCD, sickle cell disease; Febux, febuxostat; LC/MS-MS, liquid chromatography/mass spectrometry-mass spectrometry.

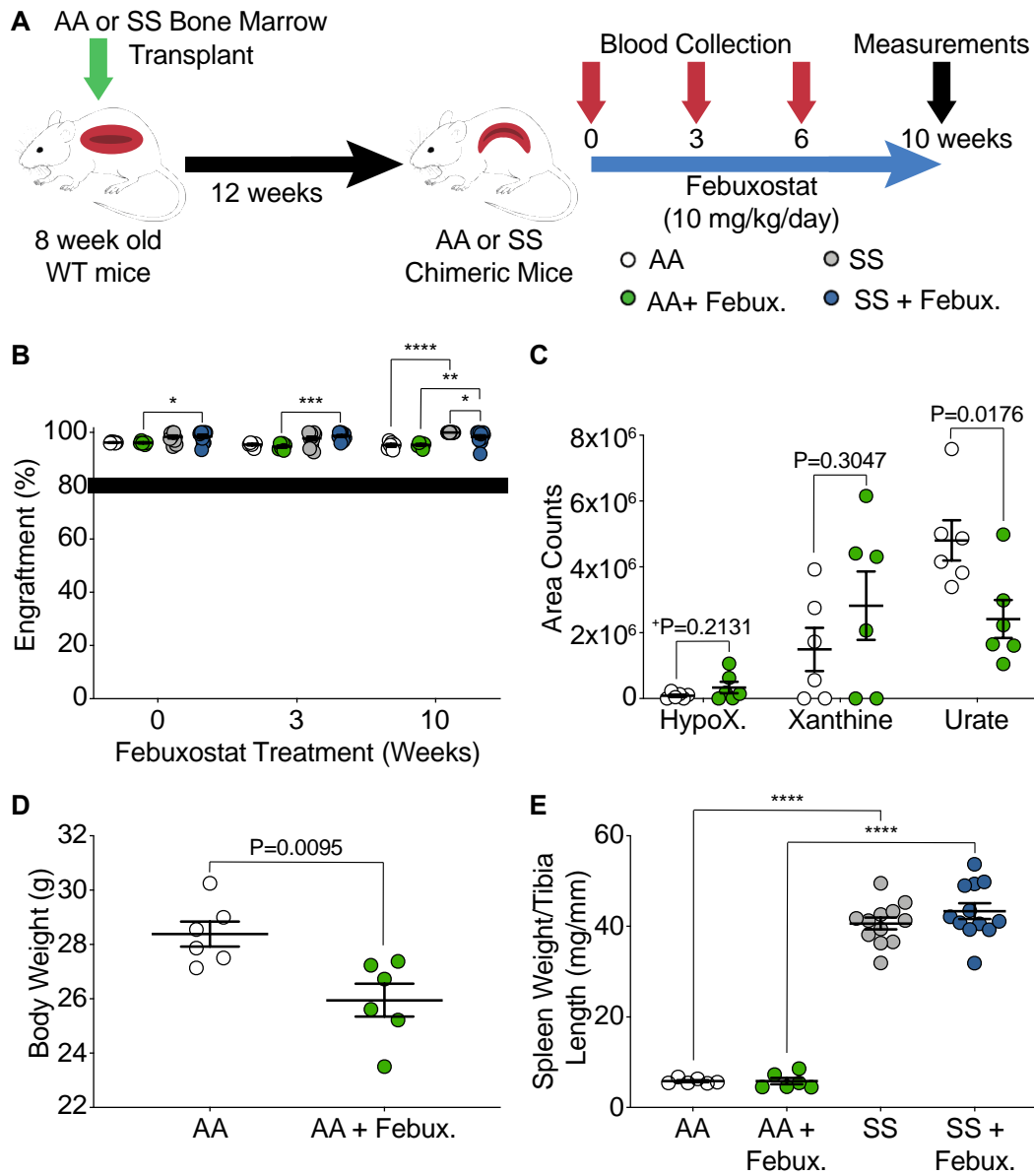


Figure 5. Characterization of chimeric SCD mouse model treated with febuxostat.

A) Experimental design. B) Bone marrow engraftment evaluated by hemoglobin electrophoresis at 0, 3, and 10 weeks post-enugraftment. Eighty percent was used as the threshold for adequate engraftment. Values are mean \pm SEM using a one-way ANOVA with Sidak's multiple comparisons test. * $P < 0.05$, ** $P < 0.01$, *** $P < 0.001$, and **** $P < 0.0001$. C) LC/MS-MS was used for purine metabolite analysis of hypoxanthine, xanthine, and urate. D) Febuxostat treatment decreased body weight of AA mice. Values are mean \pm SEM using an unpaired Student's t test unless otherwise noted. +Values are mean \pm SEM using an unpaired Student's t test with Welch's correction. E)

Spleen weight was normalized to tibia length. Values are mean \pm SEM using a one-way ANOVA with Sidak's multiple comparisons test. ****P<0.0001. WT, wild type; Febux, febuxostat; HypoX, hypoxanthine; SCD, sickle cell disease; LC/MS-MS, liquid chromatography/mass spectrometry-mass spectrometry.

Table I. Febuxostat treatment significantly decreased uric acid concentration and XO activity in plasma and tissues of AA control mice at 10 weeks post-initiation of treatment with effects on plasma detected as early as

3 weeks.

	0 week		3 week		10 week		Significance AA 0 vs AA + Febux. 0 AA 3 vs AA + Febux. 3 <u>AA 10 vs. AA + Febux. 10</u>
	AA (n=6)	AA + Febux. (n=5-6)	AA (n=6)	AA + Febux. (n=6)	AA (n=6)	AA + Febux. (n=6)	
Plasma	Uric Acid, μ M	0.62 \pm 0.09	1.05 \pm 0.07	1.52 \pm 0.15	0.13 \pm 0.05	0.95 \pm 0.10	0.28 \pm 0.06 P=0.011, P<0.001 <u>P=0.001</u>
	XO Activity, μ Units/mL	58.00 \pm 8.81	64.34 \pm 5.05	90.95 \pm 8.92	13.05 \pm 5.96	57.06 \pm 6.13	16.67 \pm 3.46 P=0.894, P<0.001 <u>P=0.001</u>
Liver	Uric Acid, μ M	-	-	-	-	56.43 \pm 3.87	9.97 \pm 2.89 <u>#P=0.002</u>
	XO Activity, mUnits/mg	-	-	-	-	15.86 \pm 0.92	3.04 \pm 0.93 <u>P<0.001</u>
Lung	Uric Acid, μ M	-	-	-	-	13.78 \pm 0.78	8.07 \pm 1.69 <u>P=0.012</u>
	XO Activity, mUnits/mg	-	-	-	-	28.62 \pm 1.24	16.82 \pm 3.46 <u>#P=0004</u>
Kidney	Uric Acid, μ M	-	-	-	-	6.60 \pm 0.32	0.44 \pm 0.17 <u>P<0.001</u>
	XO Activity, mUnits/mg	-	-	-	-	2.13 \pm 0.08	0.14 \pm 0.05 <u>P<0.001</u>

Definition of abbreviations: XO = xanthine oxidase; febux = febuxostat; - = measurement not made. Values are mean \pm SEM using a 2-way ANOVA with Sidak's multiple comparison test for plasma measurements. Values are mean \pm SEM using an unpaired t test for tissue measurements unless otherwise noted. #Values are mean \pm SEM using a Mann-Whitney test. P values are in normal font for AA 0 week vs. AA + febuxostat 0 week, **bolded** for AA 3 week vs. AA + febuxostat 3 week, and underlined for AA 10 week vs. AA + febuxostat 10 week.

Table II. Febuxostat treatment significantly decreased uric acid concentration and XO activity in plasma and tissues of SS sickle mice at 10 weeks post-initiation of treatment with effects on plasma detected as early as 3 weeks.

	0 week		3 week		10 week		Significance	
	SS (n=12)	SS + Febux. (n=12)	SS (n=11-12)	SS + Febux. (n=11)	SS (n=12)	SS + Febux. (n=12)		
Plasma	Uric Acid, μM	1.32 \pm 0.14	1.099 \pm 0.29	0.55 \pm 0.13	0.23 \pm 0.07	2.65 \pm 0.15	0.94 \pm 0.13	P=0.8814, P=0.1189 <u>P<0.0001</u>
	XO Activity, $\mu\text{Units/mL}$	79.08 \pm 8.52	65.95 \pm 17.44	45.62 \pm 9.72	13.56 \pm 4.30	159.1 \pm 8.78	52.20 \pm 9.74	P=0.8814, P=0.0279 <u>P=<0.0001</u>
Liver	Uric Acid, μM	-	-	-	-	85.18 \pm 2.04	2.97 \pm 0.51	<u>P<0.0001</u>
	XO Activity, mUnits/mg	-	-	-	-	29.40 \pm 1.00	0.97 \pm 0.17	<u>P<0.0001</u>
Lung	Uric Acid, μM	-	-	-	-	11.50 \pm 0.60	4.34 \pm 0.54	<u>P<0.0001</u>
	XO Activity, mUnits/mg	-	-	-	-	12.60 \pm 0.94	4.80 \pm 0.62	<u>+P<0.0001</u>
Kidney	Uric Acid, μM	-	-	-	-	10.88 \pm 0.63	0.29 \pm 0.06	<u>#P<0.0001</u>
	XO Activity, mUnits/mg	-	-	-	-	2.78 \pm 0.20	0.08 \pm 0.01	<u>+P<0.0001</u>

Definition of abbreviations: XO = xanthine oxidase; febux = febuxostat; - = measurement not made. Values are mean \pm SEM using a 2-way ANOVA with Sidak's multiple comparison test for plasma measurements. Values are mean \pm SEM using an unpaired t test for tissue measurements unless otherwise noted. #Values are mean \pm SEM using a Mann-Whitney test. +Values are mean \pm SEM using an unpaired t test with Welch's correction. P values are in normal font for SS 0 week vs. febuxostat 0 week, **bolded** for SS 3 week vs. febuxostat 3 week, and underlined for SS 10 week vs. febuxostat 10 week.

2.4.2 XO Inhibition Decreased Hemolysis in Chimeric Sickle Mice

Key hematologic parameters altered in SCD were measured as a delta change from 0 to 10 weeks of febuxostat treatment (Figure 6A). In the SS sickle mice, significant increases in hematocrit, cellular Hb, RBCs, and platelets were observed over the ten weeks of treatment (Figure 6B-E). A complete analysis of blood parameters is included for the AA control and SS sickle mice in Tables III and IV, respectively, at 0, 3, 6, and 10 weeks of febuxostat treatment. Additionally, the febuxostat-treated AA mice demonstrated significant diminution in white blood cells at 3

weeks and a significant increase in RBC distribution width at 6 and 10 weeks of treatment compared to the AA mice (Table III). No additional differences were observed in the hematology between SS and febuxostat-treated SS mice (Table IV). Despite these hematologic improvements, there was no difference in reticulocytes, the RBC precursors (Figure 6F). To further assess hemolysis, cell-free Hb and cell-free hemin were measured along with acute-phase proteins that scavenge these species, Hp and Hx, respectively, after 10 weeks of febuxostat treatment (Figure 7A, Figure 8A). In the SS sickle mice, febuxostat treatment resulted in a significant decrease in cell-free Hb concentration (Figure 7B) which was primarily due to a loss in methemoglobin levels rather than a loss in oxyhemoglobin levels (Figure 8B-C). There was no difference in plasma cell-free hemin concentration or Hx concentration in the SS sickle mice (Figure 7D-E). In the AA control mice, no difference in methemoglobin, oxyhemoglobin, cell-free hemoglobin, cell-free hemin, Hp, or Hx were observed (Figure 8B-G).

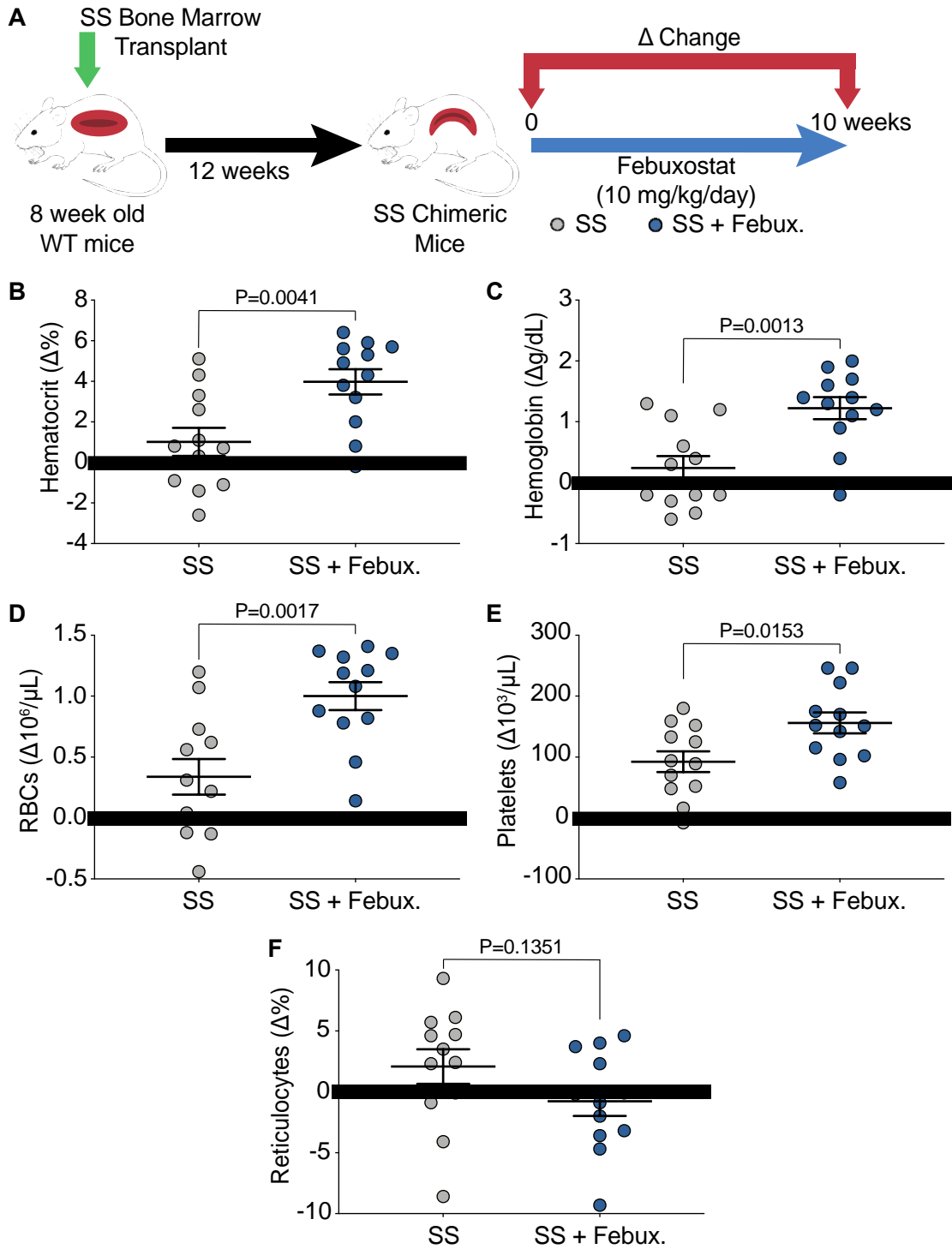


Figure 6. XO inhibition improves hematologic parameters.

A) Experimental design. B–E) Complete blood counts shown as a delta change from 0 to 10 weeks of treatment. F) Flow cytometry was used to measure the delta change of reticulocyte percentage from 0 to 10 weeks of treatment. Values are mean \pm SEM using an unpaired Student t test. Febux, febuxostat; RBCs, red blood cells; WT, wild-type.

Table III. Blood cell indices for Townes AA bone marrow transplanted mice at 0, 3, 6, and 10 weeks of drinking normal water (AA) or febuxostat treated water (AA + Febux).

	0 week		3 week		6 week		10 week		Significance AA 0 vs AA + Febux. 0 AA 3 vs AA + Febux. 3 AA 6 vs AA + Febux. 6 AA 10 vs. AA + Febux. 10
	AA (n=6)	AA + Febux. (n=5-6)	AA (n=5-6)	AA + Febux. (n=4-6)	AA (n=6)	AA + Febux. (n=5)	AA (n=6)	AA + Febux. (n=6)	
WBC, 10 ³ /μL	15.33 \pm 0.69	14.28 \pm 0.16	19.67 \pm 0.72	15.53 \pm 1.06	15.97 \pm 0.65	12.26 \pm 1.30	18.42 \pm 1.40	16.57 \pm 1.17	P=0.918, P=0.017 <i>P=0.052, P=0.551</i>
RBC, 10 ⁶ /μL	10.85 \pm 0.26	10.88 \pm 0.22	10.96 \pm 0.08	11.03 \pm 0.22	10.51 \pm 0.17	11.07 \pm 0.30	10.78 \pm 0.20	11.15 \pm 0.29	P>0.999, P=0.999 <i>P=0.323, P=0.674</i>
HCT, %	35.00 \pm 0.83	35.08 \pm 0.62	34.88 \pm 0.18	35.17 \pm 0.64	33.38 \pm 0.51	35.30 \pm 0.79	34.13 \pm 0.67	35.63 \pm 1.07	P>0.999, P=0.997 <i>P=0.254, P=0.441</i>
MCV, fl	32.35 \pm 0.23	32.20 \pm 0.09	31.83 \pm 0.19	31.87 \pm 0.10	31.78 \pm 0.13	31.88 \pm 0.16	31.65 \pm 0.16	31.92 \pm 0.20	P=0.999, P>0.999 <i>P=0.991, P=0.694</i>
RDW, %	27.35 \pm 0.20	27.30 \pm 0.10	27.20 \pm 0.03	27.28 \pm 0.08	27.27 \pm 0.24	28.34 \pm 0.41	27.27 \pm 0.14	28.52 \pm 0.32	P>0.999, P=0.998 <i>P=0.006, P=0.001</i>
HGB, g/dL	12.15 \pm 0.25	12.37 \pm 0.20	12.38 \pm 0.05	12.30 \pm 0.23	11.93 \pm 0.13	12.62 \pm 0.31	12.18 \pm 0.22	12.67 \pm 0.28	P=0.927, P=0.998 <i>P=0.142, P=0.400</i>
MCH, pg	11.20 \pm 0.10	11.40 \pm 0.07	11.30 \pm 0.05	11.13 \pm 0.09	11.42 \pm 0.10	11.42 \pm 0.05	11.32 \pm 0.05	11.35 \pm 0.06	P=0.221, P=0.388 <i>P>0.999, P=0.996</i>
PLT, 10 ³ /μL	762.50 \pm 19.80	743.83 \pm 16.83	770.33 \pm 17.72	689.67 \pm 33.45	718.17 \pm 39.24	810.00 \pm 24.03	850.67 \pm 16.95	924.33 \pm 46.91	P=0.985, P=0.205 <i>P=0.146, P=0.282</i>
MPV, fl	6.57 \pm 0.03	6.60 \pm 0.05	6.58 \pm 0.08	6.60 \pm 0.00	6.65 \pm 0.07	6.72 \pm 0.06	6.43 \pm 0.06	6.55 \pm 0.02	P=0.986, P=0.999 <i>P=0.847, P=0.414</i>
Retic, %	5.93 \pm 0.40	5.28 \pm 0.12	3.98 \pm 0.18	3.65 \pm 0.22	4.95 \pm 0.21	4.94 \pm 0.30	4.88 \pm 0.22	5.32 \pm 0.27	P=0.259, P=0.821 <i>P>0.999, P=0.640</i>

Definition of abbreviations: febux = febuxostat; WBC = white blood cells; RBC = red blood cells; HCT = hematocrit; MCV = mean corpuscular volume; RDW = red blood cell distribution width; HGB = hemoglobin; MCH = mean corpuscular hemoglobin; PLT = platelets; MPV = mean platelet volume; retic = reticulocytes. Values are mean \pm SEM using a 2 way ANOVA with Sidak's multiple comparison test. P values are in normal font for AA 0 week vs. AA + febuxostat 0 week, **bolded** for AA 3 week vs. AA + febuxostat 3 week, *italicized* for AA 6 week vs. AA + febuxostat 6 week, and underlined for AA 10 week vs. AA + febuxostat 10 week.

Table IV. Blood cell indices for Townes SS bone marrow transplanted mice at 0, 3, 6, and 10 weeks of drinking normal water (SS) or febuxostat treated water (SS + Febux).

	0 week		3 week		6 week		10 week		Significance SS 0 vs SS + Febux. 0 SS 3 vs SS + Febux. 3 SS 6 vs SS + Febux. 6 <u>SS 10 vs. SS + Febux. 10</u>
	SS (n=12)	SS + Febux. (n=12)	SS (n=11-12)	SS + Febux. (n=10-12)	SS (n=12)	SS + Febux. (n=12)	SS (n=11-12)	SS + Febux. (n=12)	
WBC, 10 ³ /μL	16.74 ± 1.20	19.32 ± 1.35	23.72 ± 1.51	21.47 ± 0.94	26.14 ± 0.86	23.73 ± 1.11	26.60 ± 1.43	25.48 ± 1.09	P=0.428, P=0.622 , P=0.494, <u>P=0.942</u>
RBC, 10 ⁶ /μL	6.09 ± 0.16	5.94 ± 0.14	6.52 ± 0.32	6.41 ± 0.08	6.17 ± 0.19	6.61 ± 0.11	6.42 ± 0.17	6.94 ± 0.14	P=0.966, P=0.986 , P=0.290, <u>P=0.151</u>
HCT, %	27.58 ± 0.83	26.67 ± 0.68	27.80 ± 0.79	28.53 ± 0.36	26.44 ± 0.73	28.28 ± 0.56	28.05 ± 0.35	30.64 ± 0.66	P=0.776, P=0.897 , P=0.165, <u>P=0.024</u>
MCV, fl	44.95 ± 0.33	44.73 ± 0.26	44.49 ± 0.35	44.51 ± 0.26	42.92 ± 0.32	42.75 ± 0.37	44.59 ± 0.42	44.13 ± 0.29	P=0.983, P>0.999 , P=0.994, <u>P=0.780</u>
RDW, %	35.00 ± 0.40	35.01 ± 0.23	35.57 ± 0.19	36.41 ± 0.15	36.91 ± 0.26	36.81 ± 0.26	35.93 ± 0.39	36.93 ± 0.29	P>0.999, P=0.147 , P=0.999, <u>P=0.057</u>
HGB, g/dL	9.72 ± 0.25	9.44 ± 0.23	9.82 ± 0.24	10.04 ± 0.17	9.63 ± 0.25	10.18 ± 0.19	9.77 ± 0.10	10.67 ± 0.23	P=0.831, P=0.910 , P=0.234, <u>P=0.017</u>
MCH, pg	15.97 ± 0.09	15.93 ± 0.09	15.76 ± 0.07	15.68 ± 0.11	15.63 ± 0.14	15.43 ± 0.10	15.55 ± 0.20	15.37 ± 0.08	P=0.999, P=0.983 , P=0.648, <u>P=0.717</u>
PLT, 10 ³ /μL	421.00 ± 14.79	417.33 ± 12.69	445.50 ± 31.24	470.10 ± 7.94	535.58 ± 21.88	550.83 ± 18.12	513.50 ± 18.84	573.58 ± 19.45	P=0.999, P=0.866 , P=0.969, <u>P=0.119</u>
MPV, fl	6.37 ± 0.04	6.39 ± 0.04	6.43 ± 0.06	6.58 ± 0.04	6.48 ± 0.03	6.62 ± 0.05	6.47 ± 0.07	6.56 ± 0.05	P=0.993, P=0.130 , P=0.143, <u>P=0.539</u>
Retic, %	44.7 ± 0.99	44.74 ± 0.57	-	-	44.30 ± 0.98	43.08 ± 0.81	46.58 ± 1.16	44.16 ± 1.22	P=0.984, P=0.764, <u>P=0.234</u>

Definition of abbreviations: febux = febuxostat; WBC = white blood cells; RBC = red blood cells; HCT = hematocrit; MCV = mean corpuscular volume; RDW = red blood cell distribution width; HGB = hemoglobin; MCH = mean corpuscular hemoglobin; PLT = platelets; MPV = mean platelet volume; retic = reticulocytes; - = measurement not made. Values are mean ± SEM using a 2 way ANOVA with Sidak's multiple comparison test. P values are in normal font for SS 0 week vs. SS + febuxostat 0 week, **bolded** for SS 3 week vs. SS + febuxostat 3 week, *italicized* for SS 6 week vs. SS + febuxostat 6 week, and underlined for SS 10 week vs. SS + febuxostat 10 week.

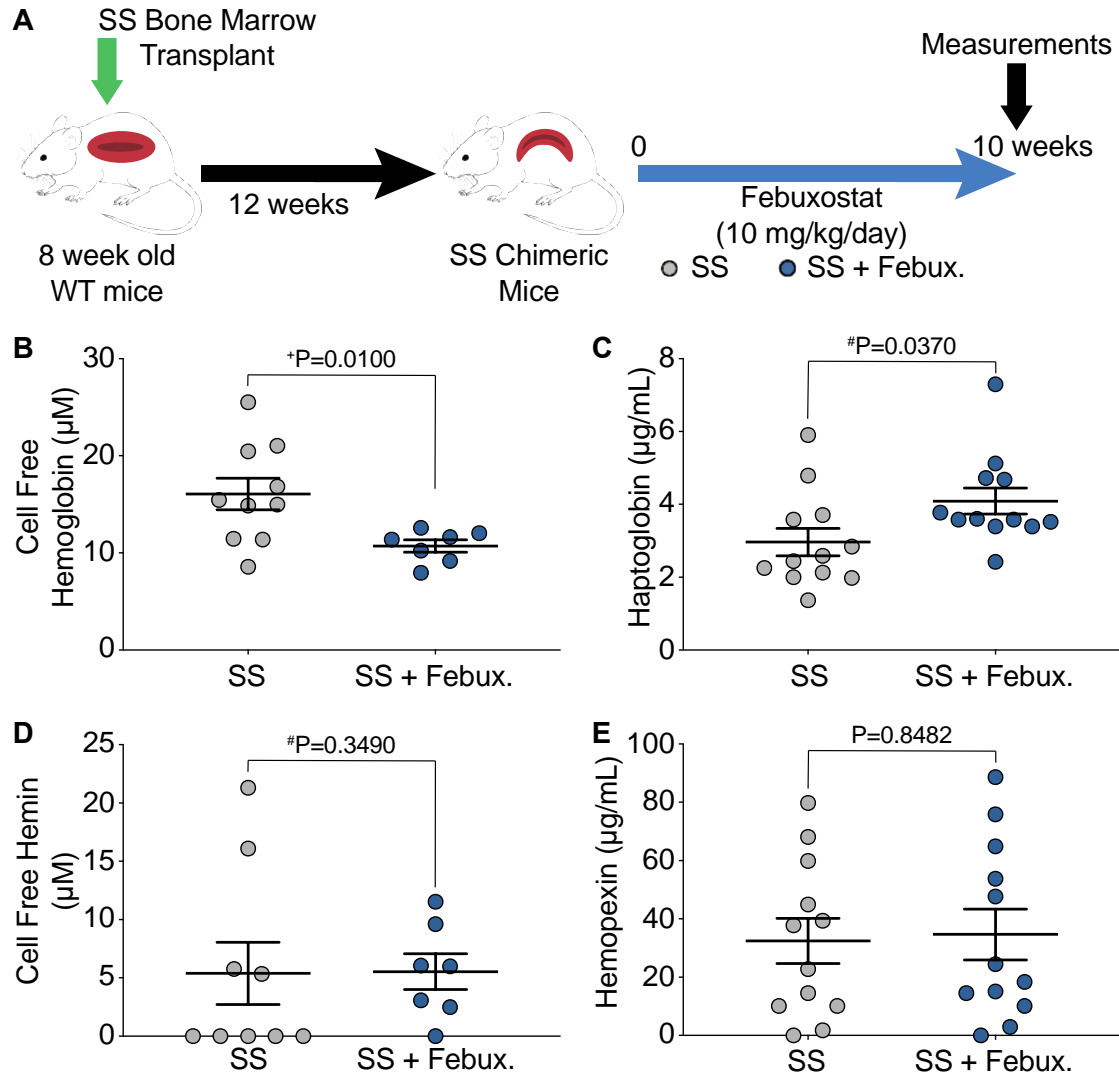


Figure 7. XO inhibition decreases hemolysis.

A) Experimental design. B) Ultraviolet (UV)-visible spectral deconvolution was used to measure plasma cell-free hemoglobin, a combination of oxyhemoglobin and methemoglobin, after 10 weeks of treatment. C) An ELISA was used to measure plasma haptoglobin concentration after 10 weeks of treatment. D) UV-visible spectral deconvolution was used to measure plasma cell-free hemin concentration after 10 weeks of treatment. E) An ELISA was used to measure plasma hemopexin concentration after 10 weeks of treatment. Values are mean \pm SEM using an unpaired Student t test unless otherwise noted. +Values are mean \pm SEM using an unpaired Student t test with Welch correction. #Values are mean \pm SEM using a Mann-Whitney test. Febux, febuxostat; WT, wild-type; XO, xanthine oxidase; ELIA, enzyme linked immunosorbant assay.

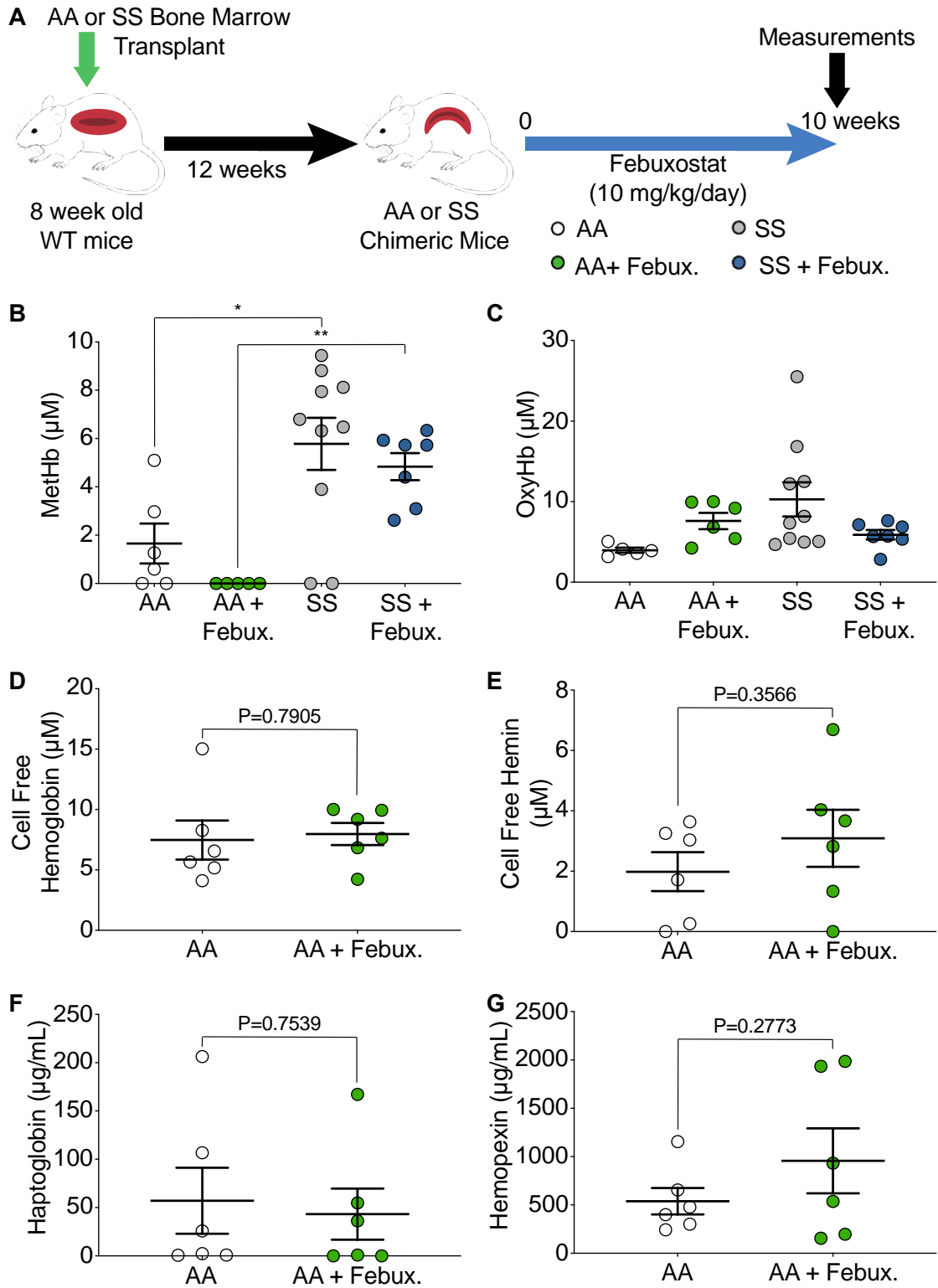


Figure 8. Evaluation of hemolysis in AA and SS mice treated with febuxostat.

A) Experimental design. UV-visible spectral deconvolution was used to measure B) MetHb and C) OxyHb after 10 weeks of treatment. Values are mean \pm SEM using a one-way ANOVA with Sidak's multiple comparisons test. *P<0.05, **P<0.01. UV-visible spectral deconvolution was used to measure D) plasma cell free hemoglobin, a combination of MetHb and OxyHb, and E) cell free hemin after 10 weeks of treatment. An ELISA was used to measure plasma F) haptoglobin and G) hemopexin concentration after 10 weeks of treatment. Values are mean \pm SEM using an unpaired Student's t test. WT, wild type; febux, febuxostat; MetHb, methemoglobin; OxyHb, oxyhemoglobin; ELISA, enzyme linked immunosorbent assay; UV, ultraviolet ELISA, enzyme linked immunosorbant assay.

2.4.3 XO Inhibition Improves Pulmonary Vasoreactivity in Chimeric Sickie Mice

Wire myography was used to assess isolated pulmonary, mesenteric, and thoracodorsal vasoreactivity in SS sickle (Figure 9A) and AA control mice (Figure 10A). Febuxostat treatment significantly decreased constriction in pulmonary, mesenteric, and thoracodorsal arteries of SS sickle mice (Figure 9B-D). In the AA control mice, febuxostat treatment significantly reduced constriction in pulmonary vessels, but no differences in mesenteric or thoracodorsal constriction were observed (Figure 10B-D). A cumulative acetylcholine dose-response was used to assess endothelium-dependent dilation of the 3 vascular beds. In the SS sickle mice, febuxostat treatment significantly improved the dilation of the pulmonary vessels and decreased the EC₅₀ compared with the untreated vessels (Figure 9E); however, this effect was not observed with vessels from the systemic circulation as no difference was observed in the mesenteric or thoracodorsal vessel dilation (Figure 9F-G). No differences in dilation were observed in the AA control mice (Figure 10E-G).

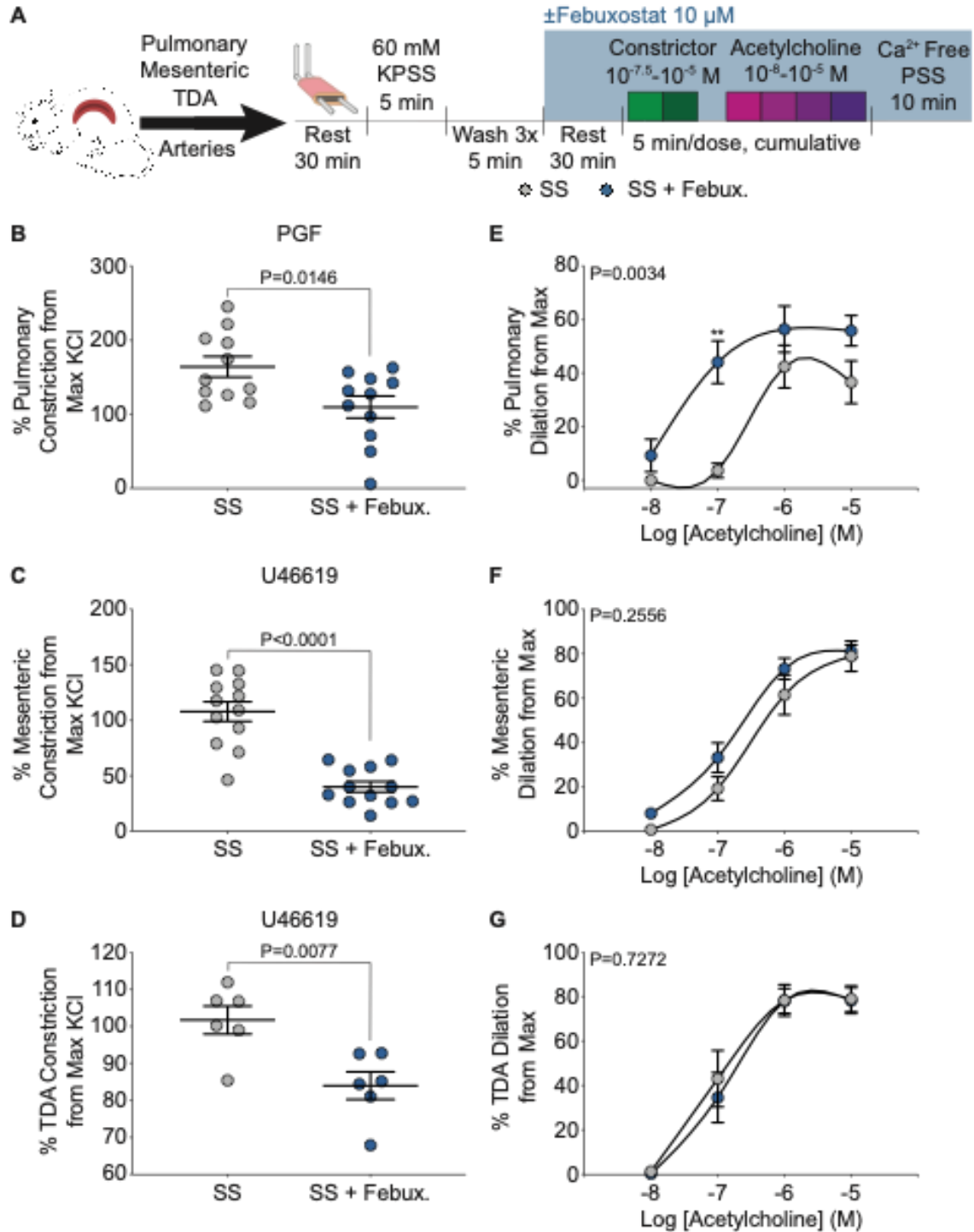


Figure 9. XO inhibition decreases constriction across multiple vascular beds but only improves dilation in pulmonary arteries.

A) Ex vivo wire myography was used to assess vasoreactivity of pulmonary, mesenteric, and TDA arteries. B) Pulmonary (n=8), C) mesenteric (n=12), and D) TDA (n=6) constriction was measured by normalizing to maximum

KCl response. Values are mean \pm SEM using an unpaired Student t test. An acetylcholine dose-response was used to measure dilation of E) pulmonary, F) mesenteric, and G) TDA arteries. Values are mean \pm SEM using a 2-way ANOVA with Sidak multiple comparisons test. ** $P < 0.01$. TDA, thoracodorsal; Febux, febuxostat; KPSS; potassium physiological salt solution; PGF, prostaglandin F $_{2\alpha}$; and PSS, physiological salt solution; max, maximum; XO, xanthine oxidase.

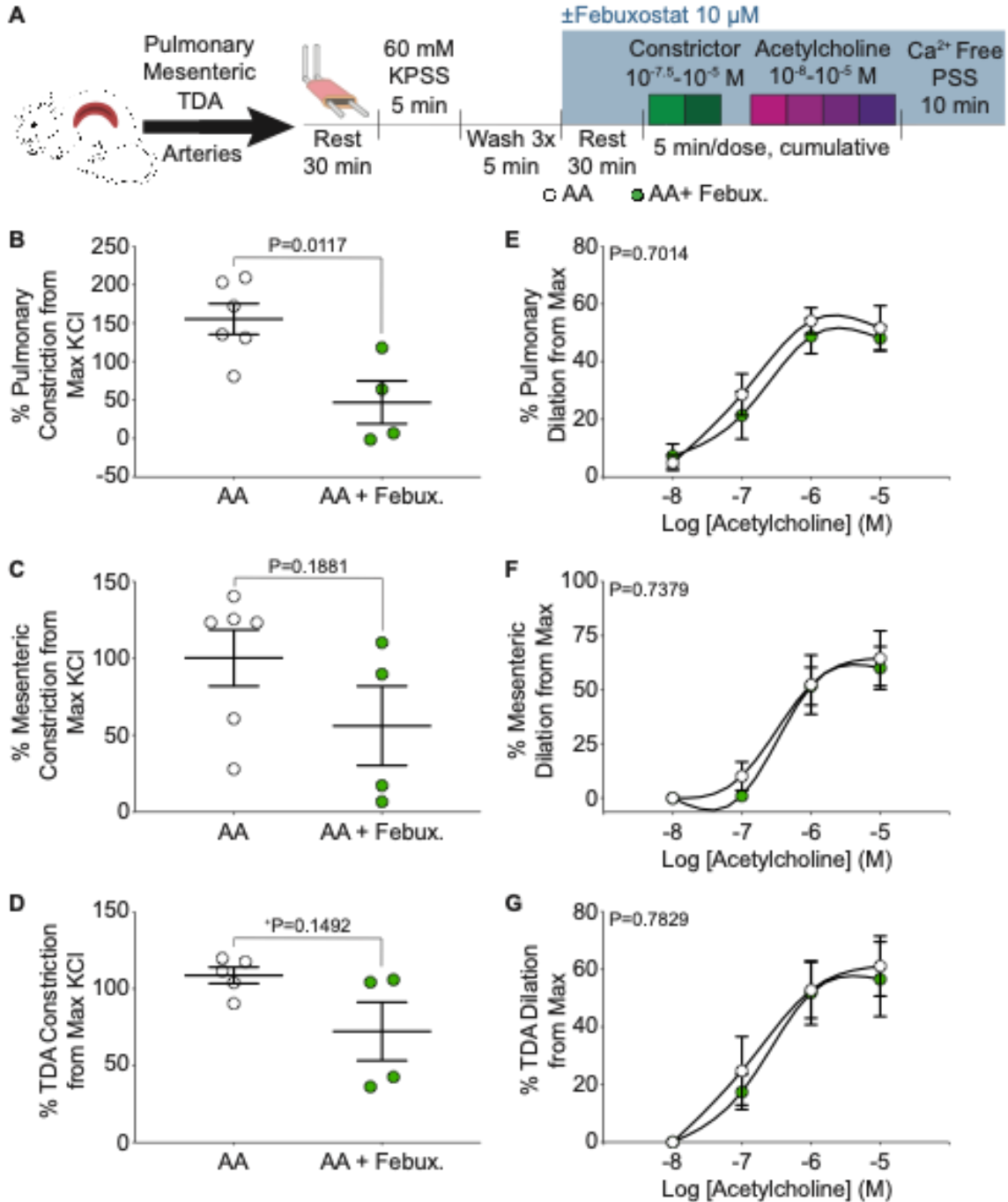


Figure 10. Ex-vivo wire myography of AA mice treated with febuxostat.

A) Ex vivo wire myography was used to assess vasoreactivity of pulmonary, mesenteric, and TDA arteries. B) Pulmonary, C) mesenteric, and D) TDA constriction was measured by normalizing to maximum KCl response. Values are mean \pm SEM using an unpaired Student's t test unless otherwise noted. +Values are mean \pm SEM using an unpaired Student's t test with Welch's correction. An acetylcholine dose response was used to measure dilation

of E) pulmonary (AA n=12, AA + Febux. n=4), F) mesenteric (AA n=6, AA + Febux. n=4), and G) TDA (AA n=6, AA + Febux. n=4) arteries. Values are mean \pm SEM using a two-way ANOVA with Sidak's multiple comparisons test. TDA, thoracodorsal; KPSS, potassium physiological salt solution; PSS, physiological salt solution; febux, febuxostat; max, maximum.

2.4.4 Improvements in Pulmonary Vasoreactivity Did Not Manifest into Cardiac Changes

We hypothesized that improved pulmonary vasoreactivity would also result in decreased pulmonary artery pressure and improved cardiac function. To assess cardiac function, closed-chest right heart catheterization, right ventricle (RV) weight, and left ventricle + septum (LV+S) weight were measured after ten weeks of treatment. Additionally, echocardiograms were performed at 0 and 10 weeks of treatment, and changes in parameters are shown as a delta change from baseline to ten weeks of treatment (Figure 11A). Febuxostat treatment did not alter the RV maximum pressure or heart rate of the SS sickle mice (Figure 11B-C). A complete list of parameters from the RV catheterization is included in Table V. No differences were observed in the AA control or SS sickle mice when treated with febuxostat; however, significant increases in RV maximum dP/dt and RV contractile index were observed in the SS mice in comparison to the AA mice (Table V). The RV was separated from the LV+S and weighed and normalized to tibia length to assess hypertrophy of the ventricles. No significant differences in RV or LV+S weight were observed in the SS sickle (Figure 11D-E) or the AA control (Figure 12A-B) mice. Trichrome staining was also performed to measure fibrosis of the right and left ventricles. Fibrosis was observed in the SS sickle and SS sickle mice treated with febuxostat; however, when quantified, no difference in fibrosis was observed in the RV or LV+S (Figure 12C-E). Echocardiograms were performed before and after 10 weeks of febuxostat treatment to assess the effects of febuxostat treatment on

cardiac function. No differences were observed in end-systolic volume, end-diastolic volume, stroke volume, or cardiac output in the SS sickle mice (Figure 11F-I). A complete list of right ventricle echocardiogram parameters is included in Table VI. Febuxostat treatment significantly increased the tricuspid valve peak velocity of early diastolic transmitral flow to peak velocity of early diastolic mitral annular motion ratio (TV E/e') in the SS sickle mice but did not affect any other measurement (Table VI). In comparing the SS sickle to the AA control mice, the SS sickle mice had significantly increased tricuspid valve peak velocity of early diastolic transmitral flow (TV E) and the ratio of tricuspid valve peak velocity of early diastolic transmitral flow to peak velocity of late transmitral flow (TV E/A) (Table VI). A complete list of left ventricle echocardiogram parameters is included in Table VII. Febuxostat treatment did not significantly alter any left ventricle parameters assessed in the AA control or SS sickle mice (Table VII). SS febuxostat-treated mice had significantly decreased isovolumic contraction time and significantly increased cardiac output, LV mass, LV mass corrected, and left ventricle anterior wall thickness during systole and diastole compared with AA febuxostat-treated mice (Table VII).

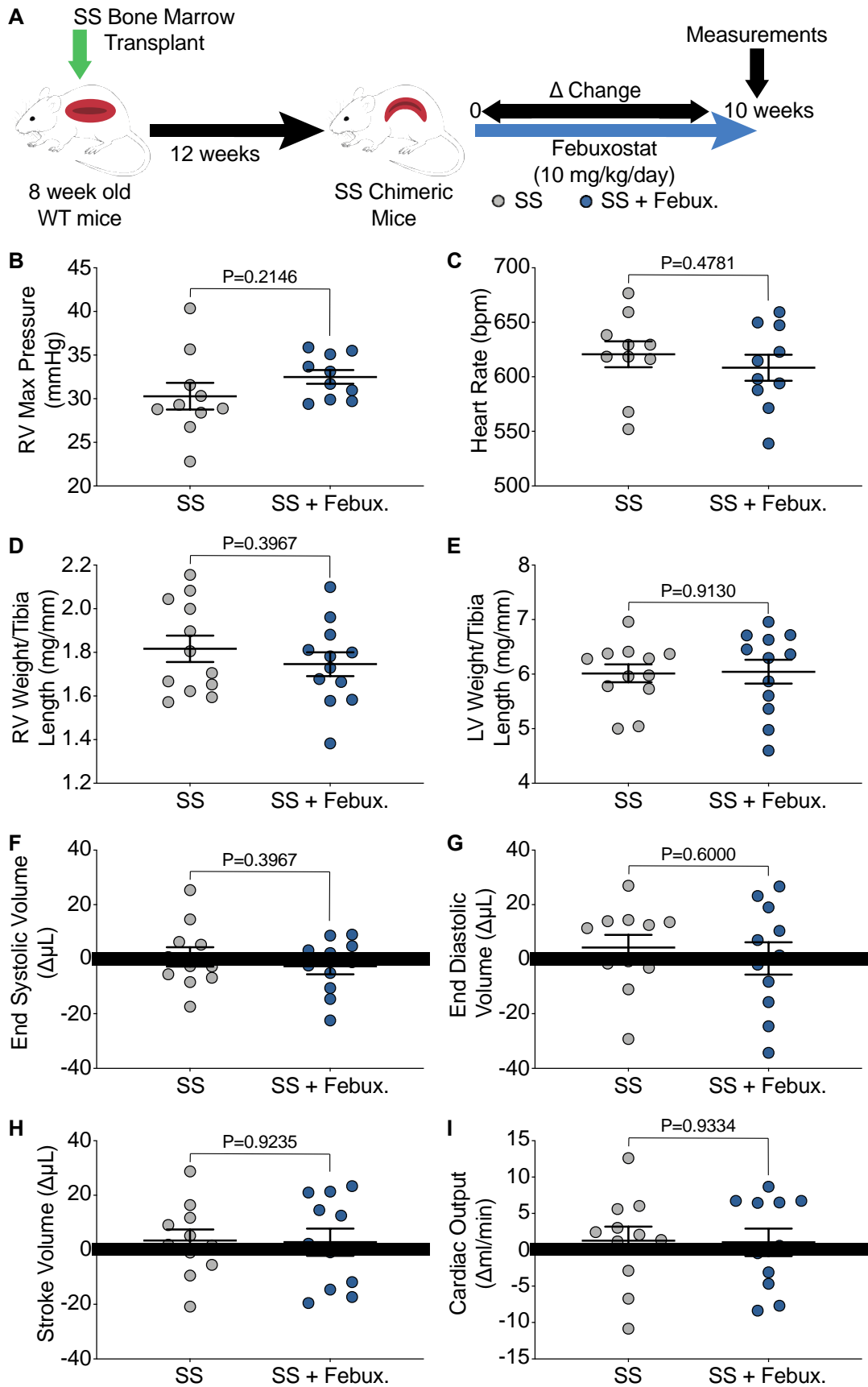


Figure 11. XO inhibition did not affect pulmonary pressure or cardiac function.

A) Experimental design. Closed-chest right heart catheterization was used to measure B) RV maximum pressure and C) heart rate after 10 weeks of treatment. D) RV weight and E) LV + septum weight was normalized to tibia length. Echocardiogram was used to assess cardiac function as a delta change from 0 to 10 weeks of febuxostat treatment: F) systolic volume, G) diastolic volume, H) stroke volume, and I) cardiac output. Values are mean \pm SEM using an unpaired Student t test. WT, wild-type; Febux, febuxostat; RV, right ventricle; Max, maximum; LV, left ventricle; XO, xanthine oxidase.

Table V. Closed chest right heart catheterization indices for Townes AA, AA+febuxostat, SS, SS+febuxostat, Xdh^{fl/fl}, and HXdh^{-/-} chimeras ten weeks post-engraftment.

	AA (n=6)	AA + Febux. (n=6)	SS (n=9-10)	SS + Febux. (n=10)	XDH ^{fl/fl} (n=8)	XDH ^{-/-} (n=7)	AA vs AA + Febux SS vs SS + Febux. AA vs SS AA + Febux. vs. SS + Febux.	XDH ^{fl/fl} vs. XDH ^{-/-}
RV Max Pressure mmHg	28.21 \pm 1.15	29.19 \pm 1.40	30.29 \pm 1.52	32.50 \pm 0.79	32.53 \pm 0.58	33.65 \pm 0.87	P=0.983, P=0.550 , P=0.720, <u>P=0.302</u>	P=0.294
Heart Rate bpm	581.38 \pm 32.11	592.70 \pm 21.25	620.69 \pm 11.84	608.46 \pm 12.03	610.11 \pm 18.97	639.46 \pm 11.39	P=0.992, P=0.972 , P=0.451, <u>P=0.958</u>	P=0.224
RV End Diastolic Pressure mmHg	3.07 \pm 0.37	3.13 \pm 0.20	2.28 \pm 0.25	2.63 \pm 0.17	2.39 \pm 0.23	2.95 \pm 0.21	P>0.999, P=0.720 , P=0.139, <u>P=0.532</u>	P=0.096
RV Max dP/dt	1716.33 \pm 163.67	1910.50 \pm 181.50	2309.80 \pm 138.69	2546.20 \pm 102.23	2395.38 \pm 100.78	2564 \pm 117.02	P=0.876, P=0.583 , P=0.030, <u>P=0.018</u>	P=0.291
RV Min dP/dt	-1670.50 \pm 141.90	-1777.83 \pm 156.67	-1703.00 \pm 138.30	-1890.80 \pm 79.29	-1940.63 \pm 86.39	-2035.71 \pm 112.33	P=0.977, P=0.689 , P>0.999, <u>P=0.958</u>	P=0.508
RV Contractile Index 1/s	60.33 \pm 3.67	64.80 \pm 3.01	75.99 \pm 1.73	78.13 \pm 1.40	73.53 \pm 2.38	75.98 \pm 1.73	P=0.651, P=0.912 , P<0.001, <u>P=0.001</u>	P=0.431
PA Mean Pressure mmHg	18.89 \pm 0.74	19.52 \pm 0.91	20.24 \pm 0.99	21.67 \pm 0.51	21.70 \pm 0.38	22.42 \pm 0.56	P=0.983, P=0.550 , P=0.720, <u>P=0.302</u>	P=0.294
Tau (W) ms	5.45 \pm 0.17	6.20 \pm 0.40	5.79 \pm 0.38	6.27 \pm 0.86	6.13 \pm 0.55	5.82 \pm 0.32	P=0.917, P=0.960 , P=0.994, <u>P>0.999</u>	P=0.650

Definition of abbreviations: febux = febuxostat; RV = right ventricle; PA = pulmonary artery. Values are mean \pm SEM using a 1 way ANOVA with Sidak's multiple comparison test for WT AA and SS mice. P values are in normal font for AA vs. AA + febuxostat, **bolded** for SS vs. SS + febuxostat, *italicized* for AA vs. SS, and underlined for AA + febuxostat vs. SS + febuxostat 10. Values are mean \pm SEM using an unpaired t test for Xdh mice.

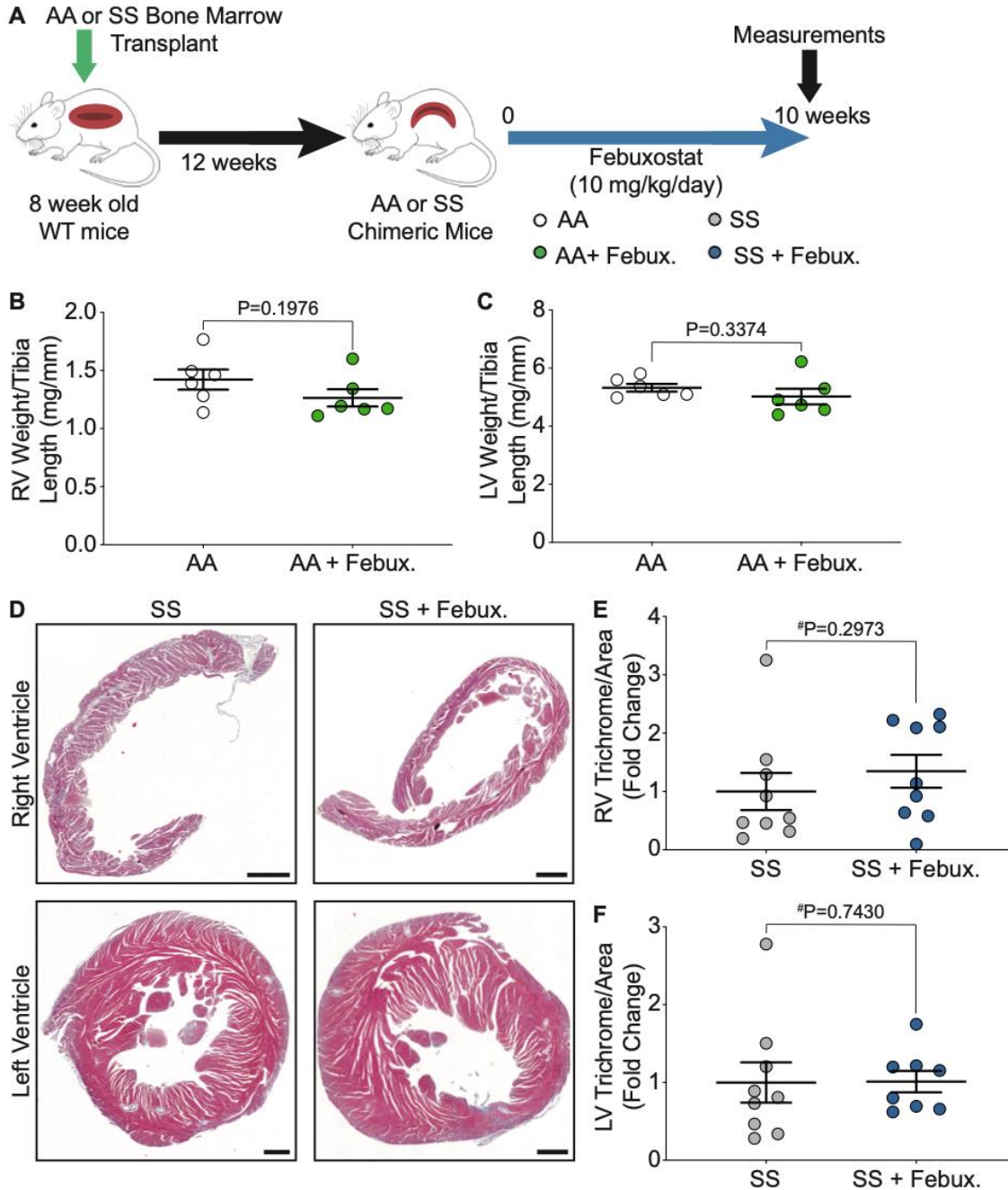


Figure 12. XO inhibition did not affect the cardiac fibrosis observed in SS sickle mice.

A) Experimental design. B) RV weight and C) LV + septum weight were normalized to tibia length. D) Trichrome staining of RV (top) and LV (bottom) heart sections. Scale bar = 100 μ m. Quantification of E) RV and F) LV trichrome staining using FIJI software. Values are mean \pm SEM using an unpaired Student's t test unless otherwise noted. #Values are mean \pm SEM using a Mann-Whitney test. WT, wild type; febux, febuxostat; RV, right ventricle; LV, left ventricle; XO, xanthine oxidase.

Table VI. Right ventricle echocardiogram indices for Townes AA, AA+febuxostat, SS, SS+febuxostat, Xdh^{fl/fl}, and HXdh^{-/-} chimeras ten weeks post-engraftment.

	AA (n=5-6)	AA + Febux. (n=5-6)	Right Ventricle		XDH ^{fl/fl} (n=5-8)	XDH ^{-/-} (n=3-7)	Significance	Significance
			SS (n=8-11)	SS + Febux. (n=7-11)			AA vs AA + Febux SS vs SS + Febux. AA vs SS	XDH ^{fl/fl} vs. XDH ^{-/-}
TV A mm/s	334.05 ± 24.30	339.16 ± 14.01	327.43 ± 19.15	320.51 ± 28.81	325.22 ± 76.76	362.41 ± 22.69	P>0.999, P=0.999 , P>0.999, <u>P=0.981</u>	#P=0.656
TV E ms	192.97 ± 3.82	198.63 ± 25.32	439.54 ± 25.44	360.25 ± 32.00	330.07 ± 39.41	375.28 ± 72.33	P>0.999, P=0.126 , P<0.001, <u>P=0.004</u>	P=0.567
TV LW A' mm/s	-36.36 ± 4.03	-32.82 ± 3.71	-33.01 ± 3.19	-40.73 ± 3.10	-30.73 ± 5.66	-33.06 ± 2.77	P=0.949, P=0.343 , P=0.940, <u>P=0.435</u>	P=0.744
TV LW E' ms	-28.17 ± 3.36	-29.27 ± 2.57	-28.84 ± 2.78	-38.58 ± 3.23	-25.15 ± 5.33	-27.65 ± 6.25	P=0.999, P=0.088 , P>0.999, <u>P=0.186</u>	P=0.768
TV E/A ms	0.55 ± 0.03	0.58 ± 0.06	1.40 ± 0.12	1.22 ± 0.16	1.24 ± 0.22	1.02 ± 0.17	P>0.999, P=0.711 , P=0.001, <u>P=0.020</u>	P=0.469
TV E/e' mm/s	-8.53 ± 0.96	-7.02 ± 1.06	-16.58 ± 2.98	-7.85 ± 1.61	-15.11 ± 2.79	-10.32 ± 1.85	P=0.988, P=0.025 , P=0.073, <u>P=0.998</u>	P=0.272
PAT mm/s	22.59 ± 0.78	20.51 ± 0.99	20.96 ± 0.80	20.73 ± 0.57	20.60 ± 1.59	22.62 ± 1.33	P=0.405, P=0.999 , P=0.516, <u>P>0.999</u>	P=0.349
PET	58.98 ± 1.64	57.04 ± 1.04	63.23 ± 1.44	60.48 ± 2.23	66.88 ± 3.23	70.67 ± 2.70	P=0.956, P=0.675 , P=0.438, <u>P=0.634</u>	P=0.385
PA Peak Velocity	-529.39 ± 26.32	-571.45 ± 29.89	-599.00 ± 18.97	-573.34 ± 24.52	-458.73 ± 35.32	-470.89 ± 23.80	P=0.782, P=0.876 , P=0.234, <u>P>0.999</u>	P=0.780
PAT/PET	0.39 ± 0.02	0.36 ± 0.01	0.33 ± 0.02	0.34 ± 0.01	0.31 ± 0.02	0.32 ± 0.01	P=0.845, P=0.962 , P=0.202, <u>P=0.984</u>	P=0.601
FAC %	50.76 ± 2.80	43.99 ± 3.87	39.41 ± 1.31	46.85 ± 3.45	34.82 ± 0.67	46.30 ± 4.25	P=0.546, P=0.184 , P=0.053, <u>P=0.944</u>	*P=0.036
RVID mm	1.38 ± 0.04	1.38 ± 0.15	1.68 ± 0.06	1.60 ± 0.10	1.80 ± 0.08	1.88 ± 0.06	P>0.999, P=0.931 , P=0.139, <u>P=0.385</u>	P=0.4618
RVFW mm	0.40 ± 0.02	0.38 ± 0.01	0.40 ± 0.02	0.34 ± 0.01	0.39 ± 0.02	0.43 ± 0.03	P=0.987, P=0.115 , P=0.999, <u>P=0.622</u>	P=0.305
TAPSE mm	1.15 ± 0.07	1.14 ± 0.09	1.24 ± 0.07	1.36 ± 0.09	1.07 ± 0.10	1.22 ± 0.07	P>0.999, P=0.737 , P=0.925, <u>P=0.320</u>	P=0.266

Definition of abbreviations: febux = febuxostat; TV = tricuspid valve; A = peak velocity of late transmitral flow; E = peak velocity of early diastolic transmitral flow; LW = left wall; A' = peak velocity of diastolic mitral annular motion; E' = peak velocity of early diastolic mitral annular motion; PAT = pulmonary acceleration time; PET = pulmonary ejection time; PA = pulmonary artery; FAC = fractional area change; RVID = right ventricular internal diameter; RVFW = right ventricular free wall; TAPSE = tricuspid annular plane systolic excursion. Values are mean ± SEM using a 1 way ANOVA for WT AA and SS mice. P values are in normal font for AA vs. AA + febuxostat, **bolded** for SS vs. SS + febuxostat, *italicized* for AA vs. SS, and underlined for AA + febuxostat vs. SS + febuxostat 10. Values are mean ± SEM using an unpaired t test for XDH mice unless otherwise noted. #Values are mean ± SEM using a Mann-Whitney test.

Table VII. Left ventricle echocardiogram indices for Townes AA, AA+febuxostat, SS, SS+febuxostat, Xdh^{fl/fl}, and HXdh^{-/-} chimeras ten weeks post-graftment.

	AA (n=5-6)	AA + Febux. (n=6)	Left Ventricle		XDH ^{fl/fl} (n=6-8)	XDH ^{-/-} (n=7)	Significance	Significance
			SS (n=10-11)	SS + Febux. (n=9-11)			AA vs AA + Febux SS vs SS + Febux. AA vs SS <u>AA + Febux. vs. SS + Febux.</u>	XDH ^{fl/fl} vs. XDH ^{-/-}
A' mm/s	-22.02 ± 2.16	-21.48 ± 2.07	-27.77 ± 2.34	-23.76 ± 1.31	-23.03 ± 2.08	-22.40 ± 2.32	P>0.999, P=0.437 , P=0.241, <u>P=0.916</u>	P=0.843
AET ms	56.53 ± 0.92	55.28 ± 1.37	57.83 ± 1.61	55.40 ± 1.55	56.01 ± 2.21	56.56 ± 3.59	P=0.983, P=0.637 , P=0.969, <u>P>0.999</u>	P=0.894
E' mm/s	-29.30 ± 2.43	-32.22 ± 2.41	-32.06 ± 1.64	-33.60 ± 2.25	-30.41 ± 2.07	-28.84 ± 3.56	P=0.887, P=0.967 , P=0.857, <u>P=0.988</u>	P=0.710
IVCT ms	14.77 ± 0.88	15.97 ± 0.88	13.16 ± 0.88	12.31 ± 0.70	13.78 ± 2.10	12.91 ± 1.52	P=0.876, P=0.894 , P=0.610, <u>P=0.027</u>	P=0.748
IVRT ms	15.51 ± 1.11	15.51 ± 1.74	15.13 ± 0.62	15.68 ± 1.86	17.55 ± 0.13	15.03 ± 1.53	P>0.999, P=0.997 , P>0.999, <u>P>0.999</u>	+P=0.151
MV A mm/s	463.06 ± 58.69	378.48 ± 28.71	451.34 ± 17.25	437.95 ± 31.43	398.37 ± 40.40	457.05 ± 58.75	P=0.414, P=0.996 , P=0.997, <u>P=0.638</u>	P=0.416
MV E mm/s	721.20 ± 38.57	723.46 ± 58.07	760.50 ± 24.40	777.47 ± 39.33	598.22 ± 46.68	694.53 ± 39.95	P>0.999, P=0.994 , P=0.936, <u>P=0.825</u>	P=0.147
LV MPI IV	0.54 ± 0.03	0.57 ± 0.04	0.49 ± 0.02	0.47 ± 0.03	0.58 ± 0.06	0.49 ± 0.04	P=0.926, P=0.971 , P=0.762, <u>P=0.110</u>	P=0.222
MV E/A	1.66 ± 0.17	1.94 ± 0.16	1.71 ± 0.07	1.67 ± 0.09	1.61 ± 0.21	1.65 ± 0.20	P=0.458, P=0.999 , P=0.998, <u>P=0.393</u>	P=0.899
MV E/E'	-25.03 ± 1.41	-23.00 ± 2.41	-24.27 ± 1.25	-23.65 ± 1.68	-21.69 ± 1.96	-25.35 ± 1.88	P=0.920, P=0.997 , P=0.996, <u>P=0.998</u>	P=0.203
Heart Rate bpm	490.02 ± 15.76	472.49 ± 22.76	459.62 ± 10.51	465.10 ± 10.83	441.43 ± 16.43	447.17 ± 11.10	P=0.911, P=0.996 , P=0.465, <u>P=0.994</u>	P=0.7831
Diameter;s mm	2.78 ± 0.09	2.64 ± 0.14	2.75 ± 0.12	2.61 ± 0.09	2.75 ± 0.18	2.92 ± 0.17	P=0.911, P=0.782 , P>0.999, <u>P>0.999</u>	P=0.519
Diameter;d mm	3.90 ± 0.11	3.77 ± 0.14	4.14 ± 0.11	4.06 ± 0.10	4.05 ± 0.17	4.11 ± 0.14	P=0.937, P=0.963 , P=0.507, <u>P=0.332</u>	P=0.765
Volume;s μL	29.35 ± 2.51	26.17 ± 3.27	29.24 ± 2.93	25.34 ± 2.03	29.69 ± 4.79	33.82 ± 5.13	P=0.934, P=0.700 , P>0.999, <u>P=0.999</u>	P=0.566
Volume;d μL	66.34 ± 4.60	61.48 ± 5.58	76.66 ± 4.56	73.03 ± 4.00	73.28 ± 7.28	75.75 ± 6.34	P=0.956, P=0.955 , P=0.473, <u>P=0.363</u>	P=0.804
Stroke Volume μL	36.99 ± 2.38	35.32 ± 2.79	47.41 ± 3.15	47.69 ± 3.29	43.59 ± 3.30	41.93 ± 3.42	P=0.997, P>0.999 , P=0.144, <u>P=0.059</u>	P=0.733
Ejection Fraction %	55.87 ± 1.29	58.06 ± 2.30	62.28 ± 2.64	65.17 ± 2.43	60.90 ± 3.03	56.09 ± 3.83	P=0.977, P=0.837 , P=0.334, <u>P=0.241</u>	P=0.337
Fractional Shortening %	28.70 ± 0.85	30.20 ± 1.50	33.64 ± 1.97	35.62 ± 1.75	32.49 ± 2.13	29.30 ± 2.64	P=0.981, P=0.861 , P=0.276, <u>P=0.200</u>	P=0.359
Cardiac Output mL/min	18.08 ± 1.13	16.44 ± 0.75	20.50 ± 0.83	22.06 ± 1.43	19.09 ± 1.32	18.81 ± 1.73	P=0.881, P=0.772 , P=0.553, <u>P=0.012</u>	P=0.900
LV Mass mg	116.73 ± 1.33	115.37 ± 7.12	143.48 ± 5.52	159.86 ± 9.27	130.30 ± 10.74	136.08 ± 12.10	P>0.999, P=0.350 , P=0.136, <u>P=0.002</u>	P=0.726
LV Mass Cor mg	93.38 ± 1.06	92.30 ± 5.69	114.78 ± 4.42	127.89 ± 7.42	104.24 ± 8.59	108.86 ± 9.68	P>0.999, P=0.350 , P=0.136, <u>P=0.002</u>	P=0.726
LVAW;s mm	1.15 ± 0.05	1.14 ± 0.05	1.28 ± 0.03	1.39 ± 0.03	1.15 ± 0.04	1.10 ± 0.05	P=0.999, P=0.104 , P=0.093, <u>P<0.001</u>	P=0.459
LVAW;d mm	0.89 ± 0.02	0.85 ± 0.04	0.97 ± 0.04	1.07 ± 0.04	0.89 ± 0.03	0.89 ± 0.04	P=0.947, P=0.281 , P=0.568, <u>P=0.004</u>	P=0.933
LVPW;s mm	1.10 ± 0.02	1.12 ± 0.04	1.29 ± 0.07	1.30 ± 0.05	1.18 ± 0.09	1.16 ± 0.06	P=0.997, P>0.999 , P=0.089, <u>P=0.143</u>	P=0.887
LVPW;d mm	0.80 ± 0.03	0.84 ± 0.02	0.86 ± 0.05	0.89 ± 0.04	0.80 ± 0.05	0.81 ± 0.03	P=0.963, P=0.985 , P=0.779, <u>P=0.917</u>	#P=0.463
Left Atrial Area mm ²	4.04 ± 0.27	4.08 ± 0.31	4.07 ± 0.21	4.09 ± 0.17	4.07 ± 0.36	3.84 ± 0.27	P>0.999, P>0.999 , P>0.999, <u>P>0.999</u>	P=0.620

Definition of abbreviations: A' = peak velocity of diastolic mitral annular motion; AET = aortic ejection time; E' = peak velocity of early diastolic mitral annular motion; IVCT = isovolumic contraction time; IVRT = isovolumic relaxation time; MV = mitral valve; A = peak velocity of late transmitral flow; E = peak velocity of early diastolic transmitral flow; LV = left ventricle; MPI = myocardial performance index; s = systolic; d = diastolic; LVAW = left ventricle anterior wall; LVPW = left ventricle posterior wall. Values are mean ± SEM using a one way ANOVA for WT AA and SS mice. P values are in normal font for AA vs. AA + febuxostat, **bolded** for SS vs. SS + febuxostat, *italicized* for AA vs. SS, and underlined for AA + febuxostat vs. SS + febuxostat. Values are mean ± SEM using a students t test for Xdh mice unless otherwise noted. +Values are mean ± SEM using an unpaired t test with Welch's correction. #Values are mean ± SEM using a Mann-Whitney test.

2.4.5 Hepatic XO is Not the Driver of Hemolysis in Chimeric Sickle Mice

To evaluate the role of hepatic-derived XO during hemolysis in SCD mice, 6- to 13-week-old, $Xdh^{floxed/floxed}Alb-1^{Cre/Wt}$ ($HXdh^{-/-}$, hepatocyte-specific XO knockout [KO]) and $Xdh^{floxed/floxed}Alb-1^{Wt/Wt}$ ($Xdh^{fl/fl}$, littermate control) mice were BM transplanted with SS sickle BM from Townes mice (Figure 13A, Figure 14A). After 12 weeks, the mice were fully engrafted with the SS sickle Townes BM (Figure 14B). The mice were aged an additional 10 weeks to match the experimental timeline of the febuxostat-treated groups. Blood was collected at 0-, 3-, 6-, and 10-weeks post engraftment with 10 weeks being the end point of the study (Figure 13A). Hepatocyte-specific XO KO ($HXdh^{-/-}$) significantly decreased plasma and liver XO activity but did not impact lung or kidney XO activity levels (Figure 13B, Table VIII). Decreased XO activity was further evaluated in plasma via measurement of hypoxanthine, xanthine, and urate concentrations. Consistent with pharmacological XO inhibition, the $HXdh^{-/-}$ mice had no change in hypoxanthine and a significant decrease in xanthine and urate concentration compared with the $Xdh^{fl/fl}$ mice (Figure 14C). Hepatocyte-specific XO KO did not alter the body weight of the mice compared with the $Xdh^{fl/fl}$ mice (Figure 14D). In contrast to the febuxostat-treated SS sickle mice, there was no significant difference in hematocrit, Hb, RBCs, platelets, or any hematologic parameter measured between the $HXdh^{-/-}$ and $Xdh^{fl/fl}$ mice (Figure 13C-F, Table IX). Additional measurements of hemolysis confirmed hepatocyte-specific XO KO has no effect on hemolysis. No differences were observed in Hp, cell-free Hb (methemoglobin and oxyhemoglobin), cell-free hemin, or Hx (Figure 13G-H, Figure 14E-G). Wire myography was again used to assess pulmonary, mesenteric, and thoracodorsal vasoreactivity in the $Xdh^{fl/fl}$ and $HXdh^{-/-}$ mice. Despite the improvement in pulmonary artery dilation observed in the febuxostat-treated mice, the $Xdh^{fl/fl}$ and $HXdh^{-/-}$ pulmonary arteries had comparable dilation (Figure 13I). There was no difference in

pulmonary, mesenteric, or thoracodorsal constriction or mesenteric or thoracodorsal dilation (Figure 15A-F). Finally, we evaluated changes in cardiac function and pulmonary pressure between the *Xdh^{fl/fl}* and *HXdh^{-/-}* mice. No difference was observed in RV or LV+S weight normalized to tibia length (Figure 15G-H) and closed-chest RV catheterization parameters (Table V). Echocardiograms of *Xdh^{fl/fl}* and *HXdh^{-/-}* mice showed a significant increase in fractional area change in the *HXdh^{-/-}* mice (Table VI), but no other differences in RV or LV parameters (Tables VI and VII). FAC is a measure of the percent RV area change between systole and diastole, and an increase in the *HXdh^{-/-}* mice could suggest improved RV function.

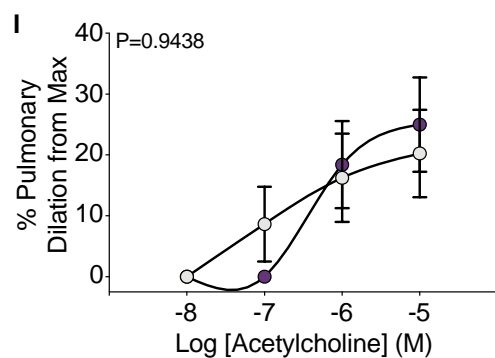
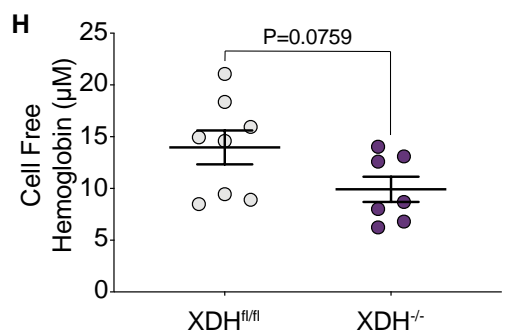
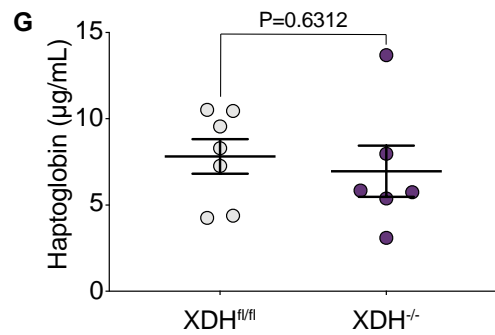
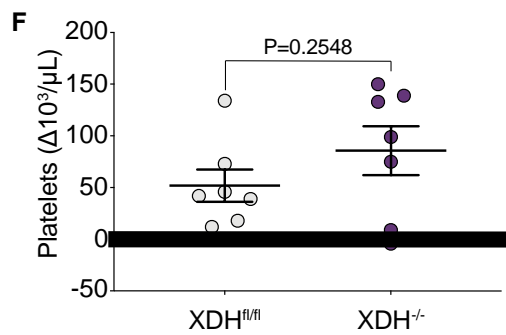
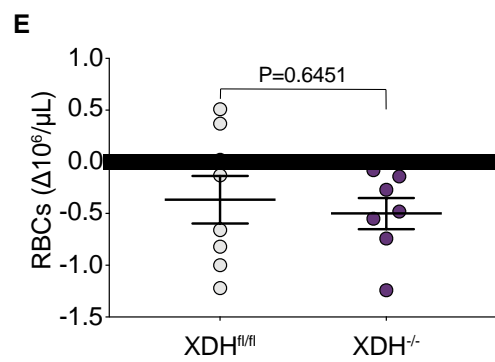
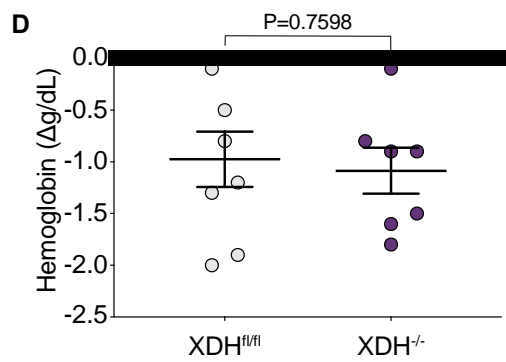
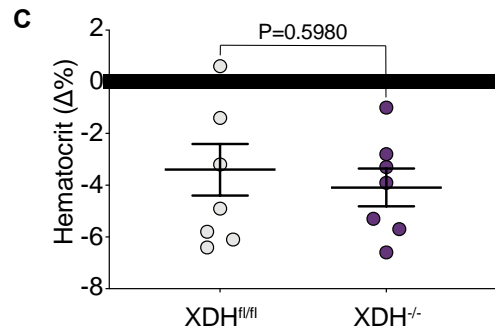
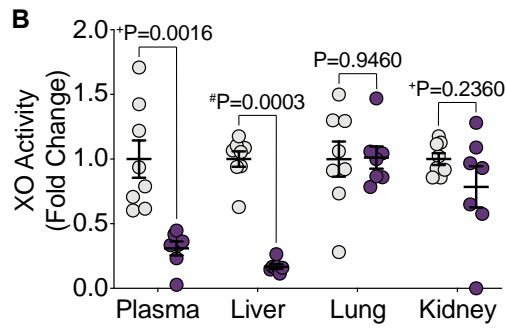
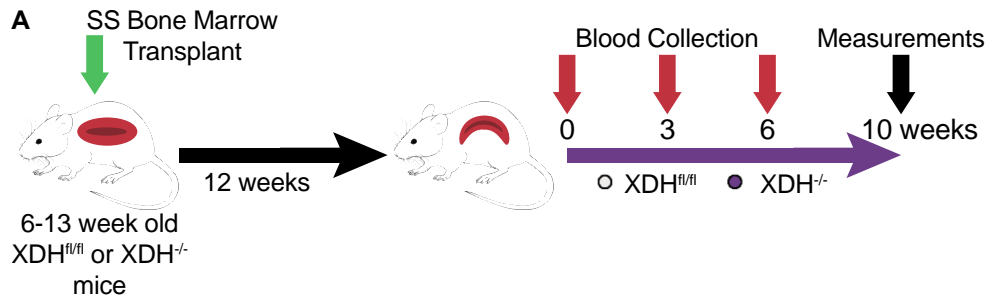


Figure 13. Hepatocyte-specific XO knockout did not decrease hemolysis or alter pulmonary vasoreactivity.

A) Experimental design. B) High-performance liquid chromatography was used to measure plasma, liver, lung, and kidney XO activity. Complete blood counts show the hematologic parameters C) hematocrit, D) hemoglobin, E) red blood cells, and (F) platelets, as a delta change from 0 to 10 weeks postengraftment. G) An ELISA was used to measure plasma haptoglobin concentration 10 weeks post-engraftment. H) Ultraviolet-visible spectral deconvolution was used to measure plasma cell-free hemoglobin, a combination of oxyhemoglobin and methemoglobin, 10 weeks post-engraftment. Values are mean \pm SEM using an unpaired Student t test unless otherwise noted. +Values are mean \pm SEM using an unpaired Student t test with Welch correction. #Values are mean \pm SEM using a Mann-Whitney test. I) An acetylcholine dose-response was used to measure dilation of pulmonary arteries 10 weeks post-engraftment (Xdhfl/fl n=8, Xdh^{-/-} n=7). Values are mean \pm SEM using a 2-way ANOVA with Sidak multiple comparisons test. Max, maximum; XDH, xanthine dehydrogenase; XO, xanthine oxidase; RBCs, red blood cells; ELISA, enzyme linked immunosorbant assay.

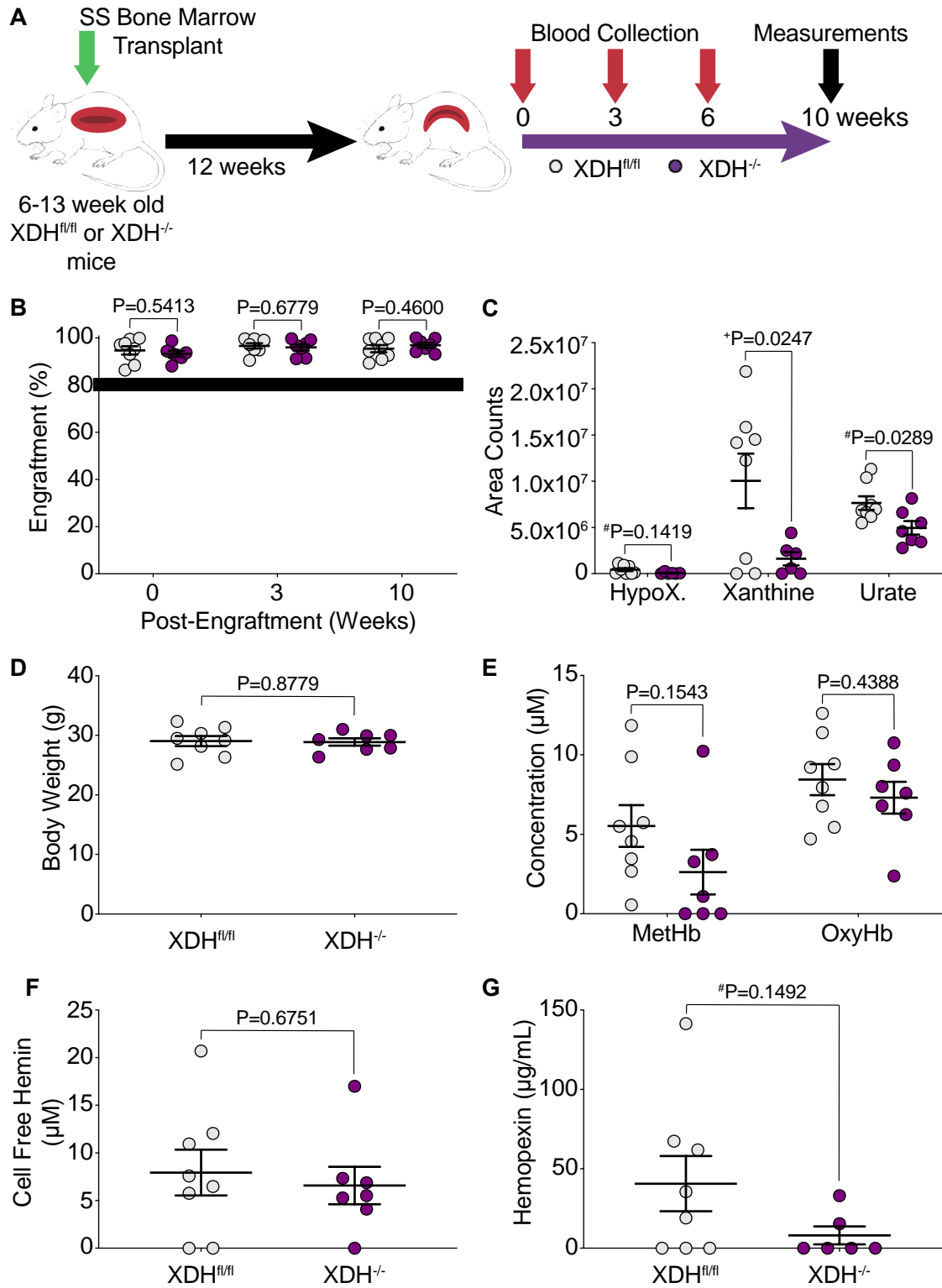


Figure 14. Characterization and evaluation of hemolysis in hepatocyte-specific XO KO mice.

A) Experimental design. B) Bone marrow engraftment evaluated by hemoglobin electrophoresis at 0, 3, and 10 weeks post-engraftment. Eighty percent was used as the threshold for adequate engraftment. C) LC/MS-MS was used for purine metabolite analysis of hypoxanthine, xanthine, and urate. D) Hepatocyte-specific XO KO did not alter body weight of HXdh^{-/-} mice. UV-visible spectral deconvolution was used to measure E) plasma MetHb and OxyHb and F) cell free hemin 10 weeks post-engraftment. G) An ELISA was used to measure plasma hemopexin concentration after 10 weeks of treatment. Values are mean ± SEM using an unpaired Student's t test unless otherwise noted. #Values are mean ± SEM using a Mann-Whitney test. +Values are mean ± SEM using an unpaired Student's t test with Welch's correction. XDH, xanthine dehydrogenase; HypoX, hypoxanthine; MetHb, methemoglobin; OxyHb, oxyhemoglobin; XO, xanthine oxidase; KO, knockout; LC/MS-MS, liquid chromatography/mass spectrometry-mass spectrometry; UV, ultraviolet; ELISA, enzyme linked immunosorbent assay.

Table VIII. Hepatocyte-specific XO knockout significantly decreased uric acid concentration and XO activity in plasma and liver tissue of *HXdh*^{-/-} mice at 10 weeks post-engraftment with effects on plasma detected as early as 3 weeks.

	0 week		3 week		10 week		Significance	
	<i>XDH</i> ^{fl/fl} (n=8)	<i>XDH</i> ^{-/-} (n=6-7)	<i>XDH</i> ^{fl/fl} (n=8)	<i>XDH</i> ^{-/-} (n=6-7)	<i>XDH</i> ^{fl/fl} (n=7-8)	<i>XDH</i> ^{-/-} (n=6-7)		
Plasma	Uric Acid, μ M	1.52 \pm 0.16	1.16 \pm 0.10	1.88 \pm 0.16	1.05 \pm 0.09	1.00 \pm 0.14	0.31 \pm 0.05	P=0.231, P=0.003 <i>XDH</i>^{fl/fl} 3 vs. <i>XDH</i>^{-/-} 3 <i>XDH</i>^{fl/fl} 10 vs. <i>XDH</i>^{-/-} 10
	XO Activity, μ Units/mL	91.21 \pm 9.70	72.82 \pm 6.07	112.83 \pm 9.49	68.26 \pm 2.01	229.40 \pm 33.13	70.74 \pm 12.27	P=0.355, P=0.006 P=0.005
Liver	Uric Acid, μ M	-	-	-	-	93.44 \pm 1.44	14.84 \pm 1.11	<u>P<0.001</u>
	XO Activity, mUnits/mg	-	-	-	-	24.56 \pm 1.47	4.13 \pm 0.43	#P<0.001
Lung	Uric Acid, μ M	-	-	-	-	20.46 \pm 2.78	20.70 \pm 1.76	P=0.946
	XO Activity, mUnits/mg	-	-	-	-	12.67 \pm 1.88	13.92 \pm 0.87	P=0.575
Kidney	Uric Acid, μ M	-	-	-	-	15.31 \pm 0.79	12.29 \pm 2.54	<u>+P=0.294</u>
	XO Activity, mUnits/mg	-	-	-	-	4.87 \pm 0.22	3.82 \pm 0.78	<u>+P=0.236</u>

Definition of abbreviations: XO = xanthine oxidase; - = measurement not made. Values are mean \pm SEM using a two-way ANOVA with Sidak's multiple comparison test for plasma measurements. Values are mean \pm SEM using an unpaired t-test unless otherwise noted. #Values are mean \pm SEM using a Mann-Whitney test. +Values are mean \pm SEM using an unpaired t test with Welch's correction. P values are in normal font for *Xdh* fl/fl 0 week vs. *HXdh*^{-/-} 0 week, **bolded** for *Xdh* fl/fl 3 week vs. *HXdh*^{-/-} 3 week, and underlined for *Xdh* fl/fl 10 week vs. *HXdh*^{-/-} 10 week.

Table IX. Blood cell indices for Townes SS bone marrow transplanted $Xdh^{fl/fl}$ and $HXdh^{-/-}$ chimeras at weeks 0, 3, 6, and 10 weeks post-engraftment.

	0 week		3 week		6 week		10 week		Significance SS + XDH fl/fl 0 vs SS + XDH -/- 0 SS + XDH fl/fl 3 vs SS + XDH -/- 3 SS + XDH fl/fl 6 vs SS + XDH -/- 6 SS + XDH fl/fl 10 vs. SS + XDH -/- 10
	SS + XDH fl/fl (n=8)	SS + XDH -/- (n=7)	SS + XDH fl/fl (n=7-8)	SS + XDH -/- (n=7)	SS + XDH fl/fl (n=8)	SS + XDH -/- (n=7)	SS + XDH fl/fl (n=8)	SS + XDH -/- (n=7)	
WBC, $10^3/\mu\text{L}$	16.03 ± 1.19	20.44 ± 0.98	20.13 ± 1.05	22.04 ± 1.34	22.74 ± 1.57	25.17 ± 1.23	27.16 ± 0.54	30.76 ± 2.30	P=0.095, P=0.805 <i>P=0.605, P=0.263</i>
RBC, $10^6/\mu\text{L}$	6.27 ± 0.15	6.23 ± 0.11	5.79 ± 0.08	6.04 ± 0.15	5.55 ± 0.16	6.03 ± 0.17	5.90 ± 0.22	5.73 ± 0.12	P>0.999, P=0.681 <i>P=0.105, P=0.898</i>
HCT, %	30.54 ± 0.58	30.34 ± 0.61	27.25 ± 0.31	28.47 ± 0.92	26.19 ± 0.79	28.21 ± 0.81	27.14 ± 0.98	26.26 ± 0.69	P>0.999, P=0.680 <i>P=0.212, P=0.873</i>
MCV, fl	48.75 ± 0.44	48.73 ± 0.41	47.09 ± 0.46	47.09 ± 0.57	47.23 ± 0.47	46.73 ± 0.39	45.99 ± 0.47	45.80 ± 0.45	P>0.999, P>0.999 <i>P=0.909, P=0.997</i>
RDW, %	34.23 ± 0.42	34.01 ± 0.36	36.39 ± 0.58	37.01 ± 1.08	36.35 ± 0.42	36.56 ± 0.46	36.81 ± 0.62	36.89 ± 0.46	P=0.998, P=0.908 <i>P=0.999, P>0.999</i>
HGB, g/dL	10.54 ± 0.19	10.56 ± 0.16	9.74 ± 0.11	10.13 ± 0.24	9.275 ± 0.24	9.96 ± 0.26	9.56 ± 0.27	9.47 ± 0.20	P>0.999, P=0.602 <i>P=0.114, P=0.997</i>
MCH, pg	16.86 ± 0.19	16.94 ± 0.16	16.84 ± 0.19	16.79 ± 0.17	16.75 ± 0.15	16.54 ± 0.17	16.26 ± 0.20	16.56 ± 0.13	P=0.996, P=0.999 <i>P=0.872, P=0.657</i>
PLT, $10^3/\mu\text{L}$	464.00 ± 18.74	425.71 ± 8.25	476.63 ± 19.25	511.14 ± 34.93	444.75 ± 24.52	515.00 ± 16.41	489.00 ± 30.01	511.57 ± 25.23	P=0.695, P=0.769 <i>P=0.152, P=0.939</i>
MPV, fl	6.25 ± 0.04	6.24 ± 0.04	6.33 ± 0.06	6.34 ± 0.05	6.38 ± 0.07	6.33 ± 0.03	6.41 ± 0.07	6.34 ± 0.05	P>0.999, P=0.999 <i>P=0.957, P=0.837</i>
Retic, %	47.75 ± 1.15	47.83 ± 0.69	49.50 ± 1.10	47.90 ± 1.43	43.89 ± 0.82	42.33 ± 1.21	47.50 ± 1.19	47.60 ± 0.49	P>0.999, P=0.747 <i>P=0.764, P>0.999</i>

Definition of abbreviations: WBC = white blood cells; RBC = red blood cells; HCT = hematocrit; MCV = mean corpuscular volume; RDW = red blood cell distribution width; HGB = hemoglobin; MCH = mean corpuscular hemoglobin; PLT = platelets; MPV = mean platelet volume; Retic = reticulocyte. Values are mean ± SEM using a two-way ANOVA with Sidak's multiple comparison test. P values are in normal font for SS $Xdh^{fl/fl}$ 0 week vs. SS + $HXdh^{-/-}$ 0 week, **bolded** for SS + $Xdh^{fl/fl}$ 3 week vs. SS + $HXdh^{-/-}$ 3 week, *italicized* for SS + $Xdh^{fl/fl}$ 6 week vs. SS + $HXdh^{-/-}$ 6 week, and underlined for SS + $Xdh^{fl/fl}$ 10 week vs. SS + $HXdh^{-/-}$ 10 week.

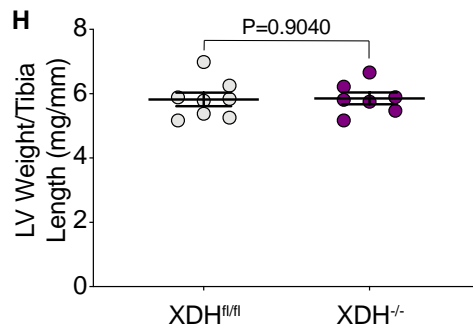
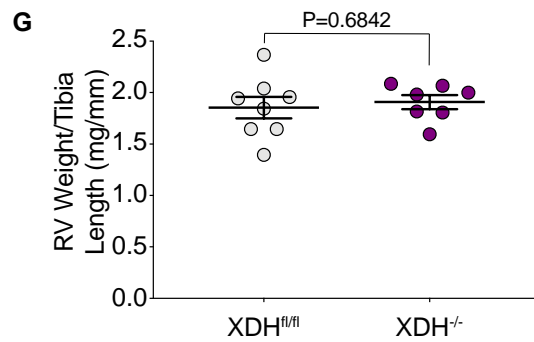
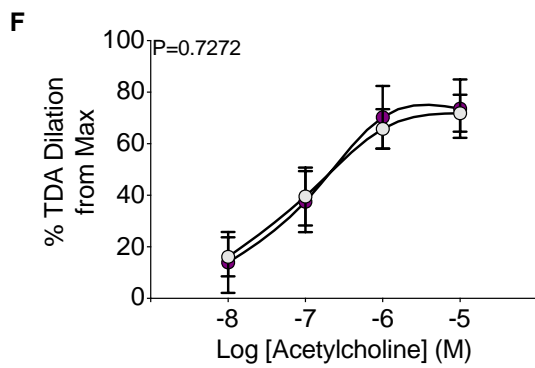
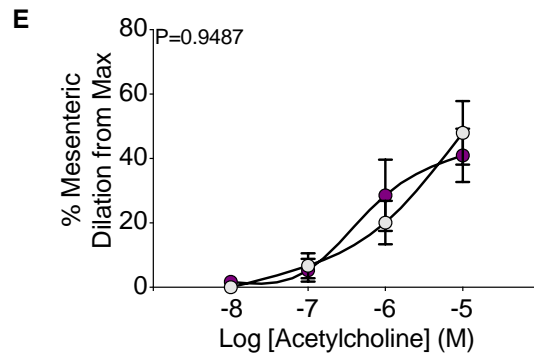
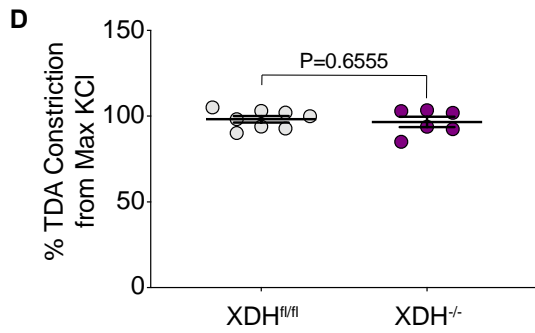
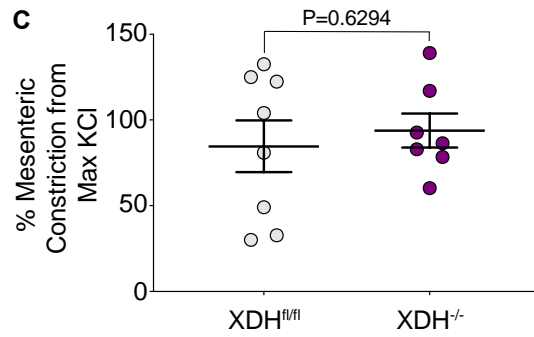
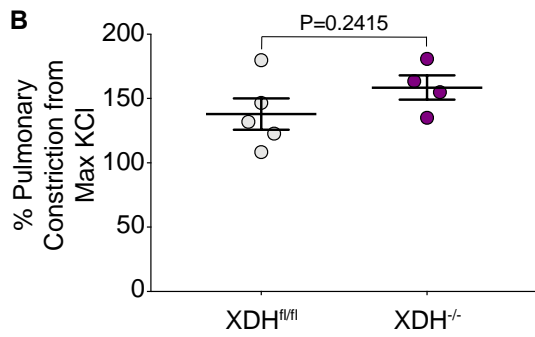
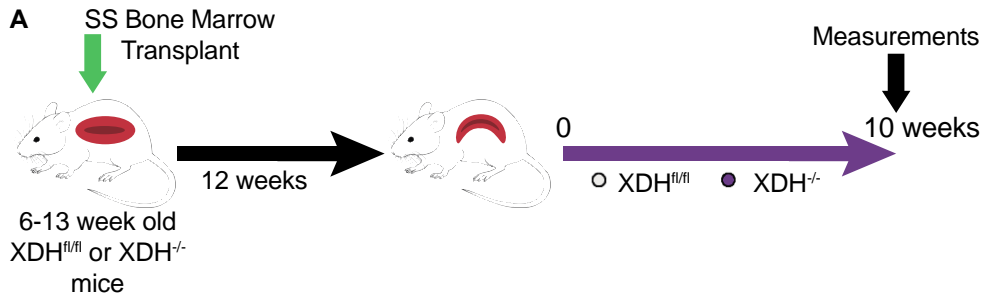


Figure 15. Evaluation of vasoreactivity and cardiac function of HXdh^{-/-} mice.

A) Experimental design. B) Pulmonary, C) mesenteric, and D) TDA constriction was measured by normalizing to maximum KCl response. Values are mean \pm SEM using an unpaired Student's t test. An acetylcholine dose response was used to measure dilation of E) mesenteric (Xdhfl/fl n=8, Xdh^{-/-} n=7), and F) TDA (Xdhfl/fl n=8, Xdh^{-/-} n=6) arteries. Values are mean \pm SEM using a two-way ANOVA with Sidak's multiple comparisons test. G) RV weight and H) LV + septum weight was normalized to tibia length. Values are mean \pm SEM using an unpaired Student's t test. XDH, xanthine dehydrogenase; max, maximum; TDA, thoracodorsal; RV, right ventricle; LV, left ventricle.

2.5 Discussion

SCD affects \approx 300,000 new patients worldwide each year¹⁰; however, treatment options are limited, with no Food and Drug Administration–approved drugs specifically inhibiting hemolysis. The molecular drivers of hemolysis are not well understood, leaving a gap in the overall understanding of the disease and a target for therapeutics that could improve sickle pathologies. We have identified XO as a key driver of hemolysis in a chimeric mouse model of SCD. Bone marrow transplanted SS sickle mice treated with febuxostat, a Food and Drug Administration–approved XO inhibitor, have increased hematocrit, cellular Hb, and RBC number (Figure 6B-D), with no impact on reticulocyte percentage (Figure 6F). Since there is no difference in reticulocyte percentage, the improvements in hematocrit, cellular Hb, and RBCs is likely due to less hemolysis, rather than increased RBC production; however, it is also possible that RBC storage sites such as the liver, are releasing red cells in response to the hepatocellular damage mediated by SCD. Decreased hemolysis is further supported by an increase in Hp concentration and a decrease in cell-free Hb (Figure 7B-C). Less cell-free Hb and an increase in Hp, a Hb scavenging protein, suggest less Hb is being released from RBCs, thus less Hp is required for clearance. No difference

was observed in Hx or cell-free hemin concentration (Figure 7D-E). We hypothesize that only changes in Hp/cell-free Hb occurred as inhibition of circulating XO decreases ROS production, thus limiting the oxidation of heme molecules, and preventing their release from Hb. This is crucial as H_2O_2 and $\text{O}_2^{\cdot-}$, both products of XO, are noted to be intimately involved in degrading Hb and oxidizing histidine and cysteine heme-binding residues, resulting in heme dissociation^{103,104}. It has been shown that ferric heme interacts with H_2O_2 to produce biliverdin IX α and carbon monoxide, similar to the canonical heme degrading enzyme, heme oxygenase-1³⁴. ROS play a critical role in Hb modulation as $\text{O}_2^{\cdot-}$ can react with Hb to form methemoglobin or oxyhemoglobin and under certain conditions may lead to release of heme molecules; however, it has not yet been determined if XO-derived ROS directly act on Hb³⁴. Thus, we have identified XO as a specific target capable of mediating hemolysis in chimeric SCD mice. The exact mechanism in which XO inhibition decreases hemolysis was not identified in this study; however, we hypothesize a reduction in oxidant production from XO activity protects RBCs from ROS-induced damage and hemolysis. Further studies will explore this hypothesis.

Vascular injury and pulmonary hypertension are major complications experienced by SCD patients^{16,20}. By inhibiting XO activity, we were able to significantly reduce constriction in 3 vascular beds (pulmonary, mesenteric, and thoracodorsal) of chimeric SCD mice (Figure 9B-D). Less constriction of the vessels will allow for larger vessel diameter and therefore, improved blood flow in the febuxostat-treated mice. Additionally, XO inhibition was able to significantly improve endothelium-dependent pulmonary artery dilation while having no effect on mesenteric or thoracodorsal arteries (Figure 9E-G). This suggests that XO inhibition was able to specifically protect the endothelium in the pulmonary vasculature. It is also important to note the 2 key physiological differences in the pulmonary vasculature compared to other vascular beds that may

impact our results: (1) pulmonary circulation has a lower pressure than systemic circulation and (2) pulmonary artery dilation is primarily NO-dependent, whereas systemic circulation has multiple mechanisms of dilation¹⁰⁵.

XO is released into circulation and binds to the surface of endothelial cells via electrostatic interactions with glycosaminoglycans, specifically heparin sulfate and chondroitin sulfate^{60,62,67}. Therefore, endothelial bound XO concentration is dependent on the composition of the glycocalyx of each vascular bed. Glycosaminoglycan composition varies depending on the vascular bed and can also be altered under disease conditions. For example, heparin sulfate and chondroitin sulfate composition percentage is affected in human patients with lung cancer¹⁰⁶; however, to our knowledge glycosaminoglycan composition in SCD remains unexplored. We posit that differences in glycosaminoglycan composition between vascular beds is responsible for the pulmonary-specific improvement in endothelial-dependent vasodilation. Alternatively, XOR produced in lung endothelial cells could be released and adhere to the endothelium resulting in endothelial damage. Despite improved pulmonary vasoreactivity, there was no indication of improved pulmonary pressure or cardiac function (Figure 11). Based on our results, 10 weeks of XO inhibition has no effect on pulmonary pressure or cardiac function in sickle mice. It is possible that a longer treatment time may be required to impact pulmonary pressure and cardiac output or that the vessels become tolerant to the febuxostat treatment requiring more acute studies. Hematologic improvements did not occur before 10 weeks of treatment (Table IV), also affirming the potential value of a long-term model.

A hepatocyte-specific XO knockout mouse model demonstrated that $\approx 50\%$ of circulating XO is released from the liver⁹³. Therefore, we BM transplanted $Xdh^{floxed/floxed}Alb-1^{Wt/Wt}$ ($Xdh^{fl/fl}$, littermate control) and $Xdh^{floxed/floxed}Alb-1^{Cre/Wt}$ ($HXdh^{-/-}$, hepatocyte-specific XO KO) mice with

SS sickle Townes BM to evaluate the effects of hepatic-derived XO in SCD. Global pharmacological inhibition of XO resulted in marked improvements in hematology and ex vivo pulmonary vasoreactivity; however, *HXdh*^{-/-} mice showed no indications of reduced hemolysis or alteration in pulmonary vasoreactivity compared to *Xdh*^{fl/fl} mice (Figure 13). This suggests hepatic-derived XO is not the driver of hemolysis in SCD or there are compensatory effects due to the loss of hepatic XO from birth. An alternative source of XO, such as endothelial-derived XO, may be responsible for causing hemolysis in SCD. The presence and activity of XOR in endothelial cells has been confirmed by numerous studies¹⁰⁷⁻¹⁰⁹. Endothelial-derived XOR could be an important driver of hemolysis and vascular dysfunction in SCD because endothelial XO could produce oxidants that damage endothelial cells and when released into circulation generate oxidants that induce hemolysis. Exploring this hypothesis is warranted. One limitation to our febuxostat studies is the possibility that febuxostat could have off-target effects. Although febuxostat has a high affinity for XO ($K_i=0.12$ nmol/L), it has also been shown to bind and inhibit ABCG2 (ATP-binding cassette transporter), which has significant expression in the small intestine and kidney^{110,111}. ABCG2 inhibition could be important in our model as it can control PPIX (protoporphyrin IX) efflux from cells¹¹⁰. PPIX is an important intermediate in the heme biosynthesis pathway¹¹²; therefore, interference with PPIX efflux via off-target effects of febuxostat could potentially play a role in our model.

In conclusion, we identified XO as a key driver of hemolysis in SCD. Febuxostat, a Food and Drug Administration–approved drug, can improve hematologic parameters and pulmonary vascular function by decreasing hemolysis in chimeric SCD mice. We propose that modulation of XO activity could be used alone or in combination with current SCD therapies to improve the

hemolysis-driven pathologies of SCD patients. Although we determined hepatic XO is not the driver of hemolysis in SCD, future studies will define the role of endothelial-derived XO.

2.6 Acknowledgements

The Center for Biologic Imaging at the University of Pittsburgh was utilized for imaging and image analysis of the trichrome staining.

2.7 Sources of Funding

This work was supported, in whole or in part, by National Institutes of Health Grants: F31 HL149241 (H.M. Schmidt); R25 HL128640-03 (K.C. Wood); 1S10OD023684-01A1 (B. McMahon); K01 HL133331 (D.A. Vitturi); R01 HL106192 and U01HL117721 (S.F. Ofori-Acquah); National Institutes of Health (NIH) R01 DK124510-01 and American Heart Association 19TPA34850089 (E.E. Kelley); NIH R01 EY026030 and Retina Research Foundation (J. Du); and R01 HL133864, R01 HL128304 and American Heart Association Established Investigator Award (A.C. Straub).

3.0 Xanthine Oxidase Binds and Degrades Heme During Hemolytic Crisis in Sickle Cell Disease

Heidi M. Schmidt¹, Evan R. DeVallance^{2,3}, Sara E. Lewis³, Katherine C. Wood⁴,
Gowtham K. Annarapu⁴, Mara Carreño¹, Scott A. Hahn⁴, Madison Seman³, Brooke A. Maxwell³,
Emily A. Hileman³, Werner J. Geldenhuys^{5,6}, Dario A. Vitturi^{1,4}, Sruti Shiva^{1,4}, Eric E. Kelley³,
Adam C. Straub^{1,4}

¹Department of Pharmacology and Chemical Biology, University of Pittsburgh, Pittsburgh, PA;

²Center for Inhalation Toxicology, West Virginia University School of Medicine, Morgantown,
WV;

³Department of Physiology and Pharmacology, Health Sciences Center, West Virginia
University, Morgantown, WV;

⁴Heart, Lung, Blood and Vascular Medicine Institute, University of Pittsburgh, Pittsburgh, PA;

⁵Department of Pharmaceutical Sciences, School of Pharmacy, West Virginia University,
Morgantown, WV;

⁶Department of Neuroscience, School of Medicine, West Virginia University, Morgantown, WV.

3.1 Summary

Xanthine oxidase (XO) catalyzes the catabolism of hypoxanthine to xanthine and xanthine to uric acid, generating reactive oxygen species (ROS) as a byproduct of these reactions. Hepatic

stress releases xanthine dehydrogenase (XDH) from hepatocytes into circulation where it is rapidly converted to XO and binds to the endothelium via interactions with glycosaminoglycans. The current dogma in the field suggests increased XO activity contributes to pathology via increased ROS production. XO activity is elevated in numerous hemolytic conditions including sickle cell disease (SCD); however, the role of XO in this context has not been fully elucidated. Identifying XO's role during heme crisis could improve understanding of pathologies involving hemolysis and identify new targets for treatment. We hypothesized that XO is protective during heme crisis by acting as a secondary mechanism of heme scavenging when canonical pathways become saturated. Heme challenge (40 $\mu\text{mol/kg}$) resulted in significantly more hemolysis and elevation in plasma XO activity in SS sickle mice compared to AA control mice. Mechanistic studies in AML12 cells demonstrated that hepatic XO release is dependent on heme-toll like receptor 4 (TLR4) signaling. Additionally, the importance of hepatic-derived XO was highlighted by repeating the heme challenge model in hepatocyte-specific XO knockout mice transplanted with SS sickle Townes bone marrow. The hepatocyte-specific knockout mice had increased death compared to the littermate controls. Molecular modeling identified a potential heme-XO binding site in the FAD domain of XO ($K_d=128$ nM). We confirmed binding by incubating purified XO and hypoxanthine with heme and running the samples on a dot blot. When heme-induced human platelet activation and aggregation was assessed, pre-incubation of platelets with XO and hypoxanthine prevented heme-induced activation and aggregation which was reversed by febuxostat. Lastly, spectrophotometry and EPR demonstrated that XO can degrade hemoglobin and release iron and an NO consumption assay showed that XO activity prevented oxyhemoglobin from scavenging NO. Our experiments have identified a novel and protective role for XO during hemolytic crisis in SCD. We find that XO is released from hepatocytes through heme-TLR4

signaling, resulting in an increase in plasma and endothelial bound XO which creates a microenvironment on the endothelial surface capable of binding free heme, degrading hemoglobin, and chelating free iron with uric acid.

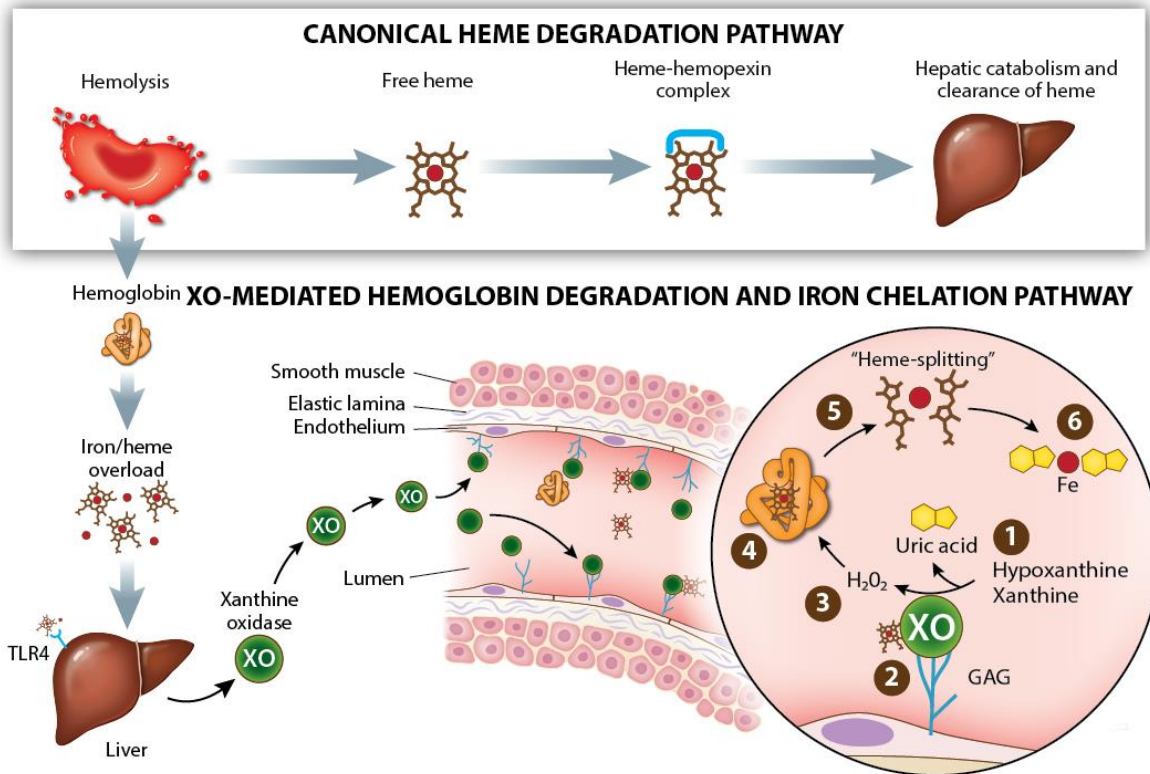


Figure 16. XO mediated hemoglobin degradation and iron chelation pathway.

Hemolytic conditions, such as SCD, can saturate canonical heme degradation pathways resulting in free iron and heme overload. Heme signals through TLR4 to release XO from hepatocytes into circulation. XO binds to the surface of distal endothelium to create a microenvironment designed to protect endothelial cells from heme induced injury. Hypoxanthine and xanthine catabolism generates H₂O₂ which can break down hemoglobin, release heme, and cause a heme-splitting reaction. In doing so, iron is released and can be chelated by the uric acid generated by XO. XO, xanthine oxidase; TLR4, toll like receptor 4; GAG, glycosaminoglycan; Fe, iron; SCD, sickle cell disease.

3.2 Introduction

Hemolytic conditions encompass many diseases, affecting millions of people worldwide each year. These include but are not limited to sickle cell disease (SCD) (~300,000 new patients per year)¹⁰, malaria (~214 million cases and 429,000 deaths per year)¹¹³, sepsis (30 million cases resulting in 8 million deaths per year)^{114,115}, and complications related to cardiac bypass (one of the most common surgical procedures performed on 44 per 100,000 people annually)¹¹⁶, and transplantation (~140,000 solid organ transplants in 2019)¹¹⁷. Hemolysis releases heme and hemoglobin into circulation at rates that can saturate canonical scavenging mechanisms (hemopexin and haptoglobin, respectively) leading to an excess of circulating free heme and hemoglobin³³. Free heme can directly generate reactive oxygen species (ROS) that damage the endothelium and indirectly by stimulating enzymatic sources of ROS such as xanthine oxidase (XO) ultimately leading to endothelial and organ damage^{33,90}. Heme is also a known agonist of toll-like receptor 4 (TLR4), a receptor that can activate endothelial cells and macrophages to induce an inflammatory response¹¹⁸.

SCD is caused by a single point mutation in the beta chain of the hemoglobin gene that causes polymerization of hemoglobin resulting in the characteristic sickling of red blood cells (RBCs)¹¹⁹⁻¹²¹. Sickled RBCs become lodged in small vasculature, resulting in vaso-occlusive crises and are also prone to frequent hemolysis due to auto-oxidation of sickle oxyhemoglobin and elevated RBC free heme concentration (1 μM)¹²²⁻¹²⁴. Free heme and hemoglobin are two of the key drivers of pathology in SCD. The combination of cell free hemoglobin and increased oxidant production decreases nitric oxide (NO) bioavailability, a critical molecule for vasorelaxation²². In excess, free heme can generate ROS and signal through toll-like receptor 4 (TLR4) to activate endothelial cells and macrophages inducing an inflammatory response⁹⁰. In the Cooperative Study

of Sickle Cell Disease, sickle patients actively experiencing a hemolytic crisis event demonstrated cell free hemoglobin concentrations of 3.6 g/dL or ~2.23 mM hemin and these two factors were strong predictors of death¹²⁵. Increases in free heme deplete the scavenging molecule hemopexin and accordingly, SCD patients have been reported to have hemopexin concentrations as low as 0.24 mg/mL or 0.33 μ M¹²⁶⁻¹²⁸. The chronic hemolysis in SCD leaves patients unable to manage the high amounts of heme released during a crisis event. While there have been recent drug developments, there are currently no Food and Drug Administration approved drugs to target hemolysis in SCD.

One enzyme that has been reported to have elevated activity in the circulation of SCD patients and mouse models, as well as several other hemolytic conditions is XO^{1,76,89,90}. XO is one form of the enzyme collectively known as xanthine oxidoreductase (XOR) with the other form being xanthine dehydrogenase (XDH)^{42,90}. XOR is a key enzyme in the purine degradation pathway, oxidizing hypoxanthine to xanthine and xanthine to uric acid¹. This pathway is critical in sickle cell disease and other hemolytic conditions as hemolysis releases millimolar concentrations of ATP, and possibly one of the reasons XO levels are elevated in SCD⁵⁶. XOR consists of three domains: a molybdenum cofactor domain, two non-identical iron-sulfur clusters, and an FAD domain¹. XDH is converted to XO via stress-mediated post translational modifications that alter the structure of the FAD domain, the main structural difference between XDH and XO¹. XDH utilizes NAD⁺ as its electron acceptor; however, the conformational changes in XO alter its binding affinity for NAD⁺ causing it to use O₂ as its electron acceptor¹. As a result, XO produces hydrogen peroxide (H₂O₂) and superoxide (O₂^{•-}) as a byproduct of hypoxanthine/xanthine oxidation¹. XDH demonstrates its greatest specific activity in the liver; however, following hepatic stressors such as inflammation, ischemia, and hypoxia, XDH is released into circulation and

rapidly converted into XO via plasma proteases⁶¹. The mechanism of hepatic XO release has yet to be identified. Once in circulation, XO can bind to distal endothelium via electrostatic interactions with glycosaminoglycans thus producing ROS directly at the endothelial surface⁶¹. For this reason, excess XO has always been described as a harmful enzyme in pathological conditions; however, we hypothesized that XO activity is increased in hemolytic conditions for a reason and that it may have a protective role during heme crisis.

3.3 Materials and Methods

3.3.1 Animals

Eight-week-old C57BL/6J (23 wildtype; stock no. 000664) mice were ordered from the Jackson Laboratory (Bar Harbor, ME). *Xdh*^{flxed/flxed}*Alb-1*^{Cre/Wt} (Albumin-1; 6 hepatocyte-specific Xdh knockout)⁹³, *Xdh*^{flxed/flxed}*Alb-1*^{Wt/Wt} (5 littermate floxed [FLX] controls)⁹³, and sickle (SS) and control (AA) Townes knock-in mice were bred and maintained at the University of Pittsburgh. The *Xdh*^{flxed/flxed} mice were bred on a C57BL6J background and the SS and AA Townes mice were bred on a combination of a C57BL/6J and 129S background⁹⁴. Seven- to fourteen-week-old male mice were used for experiments. Female mice were not included in this study because there is currently no evidence of sex differences in hemolysis in SCD. In the Townes mice, the murine alpha and beta genes are knocked out and replaced with human hemoglobin genes⁹⁵. The AA control mice contain two human alpha and beta hemoglobin transgenes, while the SS sickle mice contain two alpha and two mutant sickle beta hemoglobin transgenes⁹⁵. All animal experiments were reviewed and approved by the Institutional Animal Care and Use Committee at the University

of Pittsburgh. The mice were all supplied a normal chow diet (no. 5234), had free access to drinking water, and were housed in pathogen free conditions in accordance with the Guide for the Care and Use of Laboratory Animals from the Department of Laboratory Animal Research at the University of Pittsburgh.

3.3.2 Bone Marrow Transplanted Chimeric Mice

Genotyping of the *Xdh*^{flxed/flxed} mice was performed using polymerase chain reaction analysis of DNA isolated from tail tissue using a probe specific for Cre. Peripheral hemoglobin electrophoresis was used to genotype the AA and SS Townes mice using Hb (E) and Hb (E) Acid kits (Sebia Capillary System; Lisse, France), according to the guidelines provided by the manufacturer. The blood was spun down at 2,500xg for 10 minutes and the plasma was removed. Five μ L of the RBC pellet was combined with 65 μ L of Sebia hemolysis solution, vortexed, and incubated at room temperature for 10 minutes. Samples were then incubated in a humidity chamber for 5 minutes before running on an agarose gel and staining of hemoglobin bands. The C57BL/6J-AA mice received bone marrow from AA Townes mice and the C57BL/6J-SS, *Xdh*^{flxed/flxed}*Alb-I*^{Cre/Wt/SS}, and *Xdh*^{flxed/flxed}*Alb-I*^{Wt/Wt/SS} groups received bone marrow from SS Townes mice. The bone marrow transplants were performed as previously described⁹⁶. Briefly, bone marrow cells were collected from the femurs and tibias of AA and SS Townes donor mice. C57BL/6J (8 weeks old), *Xdh*^{flxed/flxed}*Alb-I*^{Cre/Wt} (7-14 weeks old), and *Xdh*^{flxed/flxed}*Alb-I*^{Wt/Wt} (7-14 weeks old) recipient mice were lethally irradiated (two 500–550 rad doses, 3 hours apart) before retro-orbital injection of isolated AA or SS Townes bone marrow cells ($1.5\text{--}2.5 \times 10^6$ cells). After irradiation the mice were placed in fresh autoclaved cages and provided autoclaved chow and 0.2% neomycin drinking water for two weeks before returning to normal autoclaved drinking water. The mice were

allowed 12 weeks to fully engraft, at which point 50-100 μL of blood was collected retro-orbitally to assess engraftment efficiency. Mice were anesthetized with 1% isoflurane and blood was collected using heparin coated microcapillary tubes. The whole blood was spun down at 2,500xg for 10 minutes to separate the RBC pellet and the plasma. Engraftment of the AA and SS Townes bone marrow was evaluated using the Sebia hemoglobin electrophoresis kit described above using the RBC pellet. The percentage of mouse wildtype versus AA or SS bone marrow was quantified using Phoresis software. Any mouse with <85-90% of the donor hemoglobin was excluded from the experiment. The mice were rested for two weeks before heme challenge.

3.3.3 Hemin Challenge and Hematologic Phenotyping

Heme challenge was performed by injecting 40 $\mu\text{mol/kg}$ of hemin (Frontier Scientific, H651-9) via tail vein into each mouse (200 μL). Hemin was made fresh for each experiment in 0.25 N NaOH (Fisher Chemical, S318-500) and brought to a pH of 7.4 using HCl. The mice were observed over a 24-hour period at which point the surviving mice were euthanized for blood and tissue collection. Blood (300-600 μL) was collected via the vena cava in 5% 0.5 M, pH 8.0 EDTA (Promega, V4231). Blood was spun down at 2,500xg for 10 minutes to separate the plasma and RBC pellet. Complete blood counts were measured using a Heska (HemaTrue Inc.; Miami Lakes, FL) in accordance with the manufacturer's instructions. Reticulocytes were measured from whole blood using flow cytometry as described previously¹²⁹. Briefly, Thiazole orange (80 pM in 1 \times PBS; Santa Cruz, sc-215967) was used to stain reticulocytes overnight at 4°C and protected from light. Reticulocyte percentage was analyzed using flow cytometry (LSR-Fortessa; Becton Dickinson), and FACSDIVA software was used for data collection. Plasma was aliquoted and stored at -80°C

until further experiments. Mice were then perfused with 5 mL of 1xPBS, and organs were collected and snap-frozen in liquid nitrogen.

3.3.4 Primary Murine Hepatocyte Isolation and Culture

Primary hepatocytes were isolated from mice (12 week old, C57BL/6J mice) as described in detail elsewhere¹³⁰, and then plated at 80% confluency on collagen-coated 6-well plates. Collagen-coated plates were prepared at 6.25 $\mu\text{g}/\text{cm}^2$ using collagen 1 (Cat#: C3867, Sigma), according to the manufacturer's protocol. Seeded plates were left in the incubator at 37 °C and 5% CO₂ for 5 hours to allow the cells to attach, then each well was washed with 3 mL of Waymouth medium (Cat#: W1625, Sigma) to remove unattached cells. The medium was replaced with 1.5 mL of M199 (Cat#: M5015, Sigma), and returned to the incubator.

3.3.5 AML12 Cell Culture Conditions and Treatment

AML12 hepatocytes were grown in DMEM/F12 (ThermoFisher Scientific, Waltham, MA) media supplemented with dexamethasone, (ThermoFisher Scientific, Waltham, MA) growth supplement (ThermoFisher Scientific, Waltham, MA), and 10% FBS (ThermoFisher Scientific, Waltham, MA). For experiments cells were seeded in 6-well plates. For genetic knockdown, cells at 70% confluency were transfected with 10nM scrambled or TLR4 targeted siRNA (silencer select, ThermoFisher Scientific, Waltham, MA) using Lipofectamine 3000 (ThermoFisher Scientific, Waltham, MA). After cells reached 90% confluency cells were washed with sterile PBS, then 1 ml of MEM alpha supplemented with 16 μM hypoxanthine was added along with indicated treatments (10 μM hemin, 2.5 μM oxyhemoglobin, 10 μM TAK-242). Cells were cultured in MEM

alpha for the indicated periods of time and the media was collected and snap frozen to analyze XO activity while the cells were collected in PBS with HALT phosphatase and protease inhibitors (ThermoFisher Scientific, Waltham, MA) or Qiagen RLT buffer for RNA extraction.

3.3.6 XO Activity

Plasma and tissue (liver, lung, and kidney) XO activity were assessed as previously described^{93,129}. Briefly, blood was collected at baseline via the retro-orbital vein and at the end point via the vena cava and plasma was isolated as described above. Tissue was snap frozen in liquid nitrogen. For cell culture experiments, media was collected from cells. XO activity was measured from all sources with electrochemical detection (Dionex UltiMate 3000 RS Electrochemical Detector) of uric acid post reverse-phase high-performance liquid chromatography separation.

3.3.7 XOR Protein Quantification

Samples were prepared with Laemmli sample buffer and β -mercaptoethanol and run on a 4-20% gradient gel (Biorad, Hercules, California) at 70 V. Samples were then transferred to 0.45 μ m nitrocellulose membranes, dried, reconstituted with ddiH₂O. Membranes were blocked with Li-Cor (Lincoln, Nebraska) TBS blocking buffer, and incubated in primary antibody overnight at 4 °C. Primary antibodies include β -actin (Santa Cruz Biotechnology, Dallas, Texas) and xanthine oxidoreductase (Santa Cruz Biotechnology, Dallas, Texas). Membranes were then washed with TBS containing 1% tween (TBST), incubated in Li-Cor near-infrared secondary antibodies for 1 hour at room temperature, washed again with TBST, and finally imaged with the Li-Cor Odyssey

Clx. Densitometry analysis was conducted in Image-J (National Institutes of Health, Bethesda, Maryland) and reported as target normalized to β -actin and fold change calculated from control.

3.3.8 XOR RNA Quantification

RNA was extracted from AML12 cells by Qiagen RNeasy Kit per manufacturer's instructions. Following RNA extraction RNA concentration was analyzed by nano-drop spectrophotometer and 1 μ g of RNA used in High-Capacity RNA-to-cDNA kit (Applied Biosystems ThermoFisher Scientific, Waltham, MA). Real-time PCR was then performed using iTaq SYBRgreen Supermix (Biorad, Hercules, California) on an Applied Biosystem Real-time PCR instrument. Primers: mouse *XDH* (IDT) and mouse GAPDH (IDT). Data shown as fold change from control.

3.3.9 Molecular Modeling of XO and Heme

Molecular modeling was done using the Molecular Operating Environment (MOE 2020.09) from the Chemical Computing Group. The crystallographic structure of XO was obtained from the Protein Data Bank and downloaded as a PDB file: 1V97. In MOE, the structure was prepared for analysis by adding missing hydrogens and optimizing the structure to remove any steric clashes. The pH was set at 7.4.

3.3.10 Heme Binding Dot Blot

Heme binding was assessed by incubating mixtures of hemin (25 μM , Frontier Scientific, H651-9), xanthine oxidase (50 μM ; obtained from Kelley lab) and hypoxanthine (100 μM ; Sigma, H9377-5G) in the presence or absence of febuxostat (50 μM ; Axon, TEI 6720) in PBS at room temperature for 20 min. An additional control in which albumin (50 μM) was incubated with hemin was included. Aliquots obtained at different timepoints were diluted in Laemmli buffer to stop the reaction and hemin binding was assessed by dot-blotting in nitrocellulose followed by chemiluminescent detection with Clarity Western ECL reagent (Bio-Rad). Images were acquired using a ChemiDoc XRS + imaging station and dot density was quantified with the included ImageLab Software 5.2.1 (Bio-Rad).

3.3.11 Platelet Activation

Whole blood was collected from healthy human volunteers, according to University of Pittsburgh Institutional Review Board–approved protocols, in acid-citrate dextrose (ACD) solution-A anticoagulant and platelet rich plasma (PRP) was separated by centrifugation at 500xg, for 20 minutes at 25°C in swinging buckets. Prostaglandin I₂ (PGI₂; 1 $\mu\text{g}/\text{mL}$) was added to the PRP, and platelets were pelleted down by centrifugation at 1500xg, 25°C for 10 minutes. The platelets were washed with erythrocyte lysis buffer containing PGI₂ to remove residual red cells (centrifuged at 1500xg, 25°C for 5 minutes) and resuspended in modified Tyrode’s buffer (20 mM HEPES, 128 mM NaCl, 12 mM sodium bicarbonate, 0.4 mM sodium phosphate monobasic, 5 mM dextrose, 1 mM MgCl₂, 2.8 mM KCl, pH 7.4). The platelet count was determined by Hemavet[®] 950. The platelet count was adjusted to 2.0-2.5x10⁶/mL with modified Tyrode’s buffer for all

treatments. The platelets were pretreated with purified XO (10 mU/mL; obtained from Kelley lab), and hypoxanthine (200 μ M; Sigma, H9377-5G) or purified XO (10 mU/mL; obtained from Kelley lab), hypoxanthine (200 μ M; Sigma, H9377-5G) and febuxostat (20 μ M; Axon, TEI 6720) for 30 minutes at room temperature and followed by hemin (2.5 μ M; Frontier Scientific, H651-9) treatment for 20 minutes. Treated platelets were stained with anti-CD41a-PE (BD Pharmingen, 555467) and anti-CD62P (P-selectin)-APC (BD Pharmingen, 550888) and the platelet activation was measured using flow cytometry (LSR-Fortessa; Becton Dickinson) by estimating the surface level of P-selectin on CD41a positive population. Data was analyzed using FlowJo™ v10.8.1 software.

3.3.12 Platelet Aggregation

PRP was separated from whole blood collected from healthy human volunteers, according to University of Pittsburgh Institutional Review Board–approved protocols, in sodium citrate (3.2%) anticoagulant by centrifuging at 500xg, 25°C in swinging buckets. The collected PRP was treated with the combinations of febuxostat (20 μ M; Axon, TEI 6720), purified XO (10 mU/mL; obtained from Kelley lab), and hypoxanthine (200 μ M; Sigma, H9377-5G) for 30 min and followed by hemin (2.5 μ M; Frontier Scientific, H651-) treatment for 20 min at room temperature. The treated PRP was subjected to ristocetin-induced platelet aggregation (RIPA) with 0.5 mg/mL of ristocetin (Bio/Data™ 100970) using CHRONO-LOG® Model 700 Optical Aggregometer. The data was analyzed using AGGRO/LINK®8.

3.3.13 Generation of Oxyhemoglobin

The pd10 desalting column was prepared by rinsing with 50 mL of water, followed by 50 mL of PBS. Human hemoglobin (Sigma Aldrich, H7379) was dissolved in PBS (20 mg/mL) and mixed gently. The hemoglobin was spun down at 7,000xg for 5 minutes and the supernatant was isolated. Dithionite (50 mM; Sigma) was added to the hemoglobin and passed through the column in 500 μ L aliquots. The oxyhemoglobin was flash frozen in liquid nitrogen and stored at -80°C until future experiments.

3.3.14 XO/OxyHb UV-VIS

Oxyhemoglobin (17 μ M; Sigma Aldrich, H7379) was incubated with combinations of purified XO (50 mU/mL; obtained from Kelley lab), xanthine (400 μ M; Sigma), and catalase (10 U/mL; Calbiochem) in PBS for 20 minutes. Color change was observed by eye. Absorbance was measured with a spectrophotometer (UV-VIS recording spectrophotometer UV-2401 PC, Shimadzu Scientific Instruments) every couple of minutes for 20 minutes following initiation of the reaction.

3.3.15 Electron Paramagnetic Resonance (EPR) Spectroscopy

Combinations of Sodium ascorbate (1 mM; Sigma-Aldrich, #255564), oxyhemoglobin (17 μ M; Sigma Aldrich, H7379), purified XO (50 mU/mL; obtained from Kelley lab), xanthine (400 μ M; Sigma), catalase (1 kU/mL; Calbiochem), diethylenetriaminepentaacetic acid (DTPA; 50 μ M; Sigma), and H₂O₂ (80.85 μ M; Fischer) were incubated for 20 minutes at room temperature. After

incubation, the samples were snap frozen in liquid nitrogen and stored at -80°C until EPR experiments/analysis were carried out. Ascorbate (EPR silent) is oxidized by reactive/Fe(III) species to form the ascorbyl radical (EPR active). EPR spectroscopy was used to measure the formation of ascorbyl radical¹³¹. At the time of EPR measurements, frozen samples were rapidly thawed and loaded (50 µL) into a glass capillary tube (Ref: 9600150; Hirschmann Laborgerate GmbH & Co. KG, D-74246 Eberstadt, Germany). The sample loaded capillary tubes were sealed on one end using Critoseal clay and placed inside the 4 mm (O.D) EPR quartz tube (Catalog: 707-SQ-250 M; Wilmad LabGlass, Vineland, NJ, USA). The quartz tube was positioned inside the cavity/resonator and EPR spectra were recorded at room temperature. EPR spectra were recorded using a Bruker EMXnano spectrometer (Bruker BioSciences, Billerica, MA, USA) operating at X-band with a 100 kHz modulation frequency as described previously^{132,133}. The following EPR instrument parameters were used: microwave frequency, 9.617 GHz; center field, 3425 G; sweep width, 20 G; microwave power, 20 mW; modulation amplitude, 0.5 G; modulation frequency, 100 kHz; receiver gain, 60 dB; time constant, 5.12 ms; conversion time, 37.5 ms; sweep time, 30 s; number of scans, 10. Data acquisition was performed using Bruker Xenon_nano software. The signal intensity was measured using first peak (low field) height of the EPR spectrum. Data processing was performed using GraphPad Prism 9 (GraphPad software, San Diego, CA).

3.3.16 Nitric Oxide (NO) Consumption Assay

Oxyhemoglobin (17 µM; Sigma Aldrich, H7379) was incubated with combinations of purified XO (5 µM; obtained from Kelley lab), and xanthine (400 µM; Sigma), and NO consumption was measured as previously described¹³⁴. Briefly, 40 µM of the NO donor (Z)-1-[2-(2-Aminoethyl)-N-(2-ammonioethyl)amino]diazene-1-ium-1,2-diolate (DETA NONOate;

Cayman) in PBS (pH 7.4) was added to a glass container with a continuous flow of helium. Once the NO signal stabilized at ~20 mV, the reaction mixtures were added to the glass container. Measurements of the decrease in NO with each reaction were recorded using a Sievers Nitric Oxide Analyzer (General Electric) and quantified using ImageJ by calculating the area under the curve as a measure of NO consumption.

3.3.17 Statistics

ROUT analysis with a Q=1% was used to identify outliers and if identified they were excluded from the dataset. When comparing two groups, a Shapiro-Wilk test was used to assess the normality of the data. If the data was normally distributed an unpaired Student t test was used to compare the groups. If the standard deviation of the groups was significantly different a Welch's correction was added. If the data was not normally distributed the two groups were compared using a Mann-Whitney test. When three or more groups were compared a 1-way ANOVA with Dunnett multiple comparison test was used when comparing multiple groups to a control group or Sidak multiple comparison test if multiple comparisons were made. Significance for all statistical tests were defined as $P < 0.05$.

3.4 Results

3.4.1 XO is released into circulation in response to heme crisis

To investigate the effects of hemolysis on circulating XO activity we transplanted AA control or SS sickle Townes bone marrow into 8 week old C57BL6/J mice (Figure 17A). The mice were allowed 12-weeks to fully engraft at which point the WT SS mice developed SCD and mice less than 90% AA or SS engraftment were excluded (Figure 18A). Blood was collected at baseline and 14 days later the mice were challenged with 40 $\mu\text{mol/kg}$ hemin via tail vein injection. The mice were euthanized 24 hours later for blood and tissue collection. The WT AA mice had 100% survival over the 24-hour period; however, only 75% (9/12) of the WT SS mice survived (Figure 18B). Complete blood counts were used to assess the degree of hemolysis as a delta change from baseline to 24 hours post-heme challenge. The WT AA and WT SS mice both had some degree of hemolysis as demonstrated by a decrease in RBCs, hematocrit, and hemoglobin; however, the WT SS mice had a significantly greater loss in hematocrit ($P < 0.0001$) and hemoglobin ($P = 0.0018$) compared to the WT AA mice (Figure 17B-D). A complete list of hematological parameters is included in Table X. There was a significantly greater decrease in mean corpuscular volume (MCV) and reticulocytes, and a significantly greater increase in red cell distribution width (RDW) and mean platelet volume (MPV) in the WT SS mice compared to the WT AA mice (Table X). This could suggest that hemin challenge in WT SS mice has greater effects on RBC and platelet size which could be the result of formation of more RBC-platelet aggregates compared to the WT AA mice. Next, we assessed the extent of XO release into circulation by measuring plasma XO activity as a delta change from baseline to 24 hours post-hemin injection. While the WT AA mice had a modest 58.67 $\mu\text{U/mL}$ increase in plasma XO activity, the WT SS demonstrated a 20-fold

(1,216 $\mu\text{U/mL}$) greater increase in plasma XO activity, with similar trends in the plasma uric acid concentration (Figure 17E and Table XI). The WT SS mice were more susceptible to the heme challenge, resulting in a greater increase in plasma XO activity.

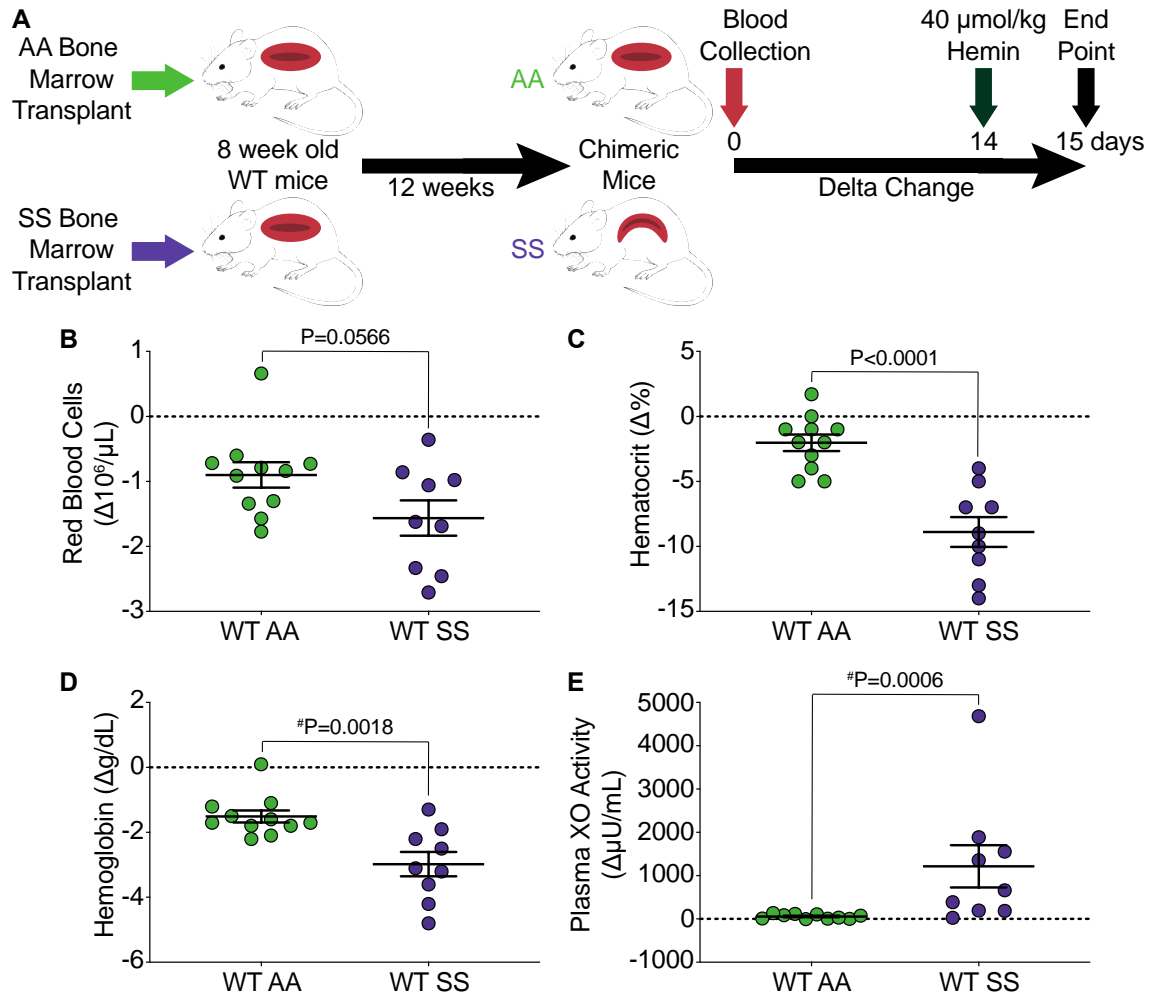


Figure 17. WT SS mice have a significant increase in plasma XO activity in response to heme crisis.

A) Experimental design. Complete blood counts shown as a delta change from baseline to 24 hours post-hemin challenge including B) red blood cells, C) hematocrit, and D) hemoglobin. E) Plasma XO activity was measured using HPLC as a delta change from baseline to 24 hours post-hemin challenge. Values are mean \pm SEM using an unpaired Student t test unless otherwise noted. #Values are mean \pm SEM using a Mann Whitney test. WT, wildtype;

XO, xanthine oxidase; HPLC, high performance liquid chromatography.

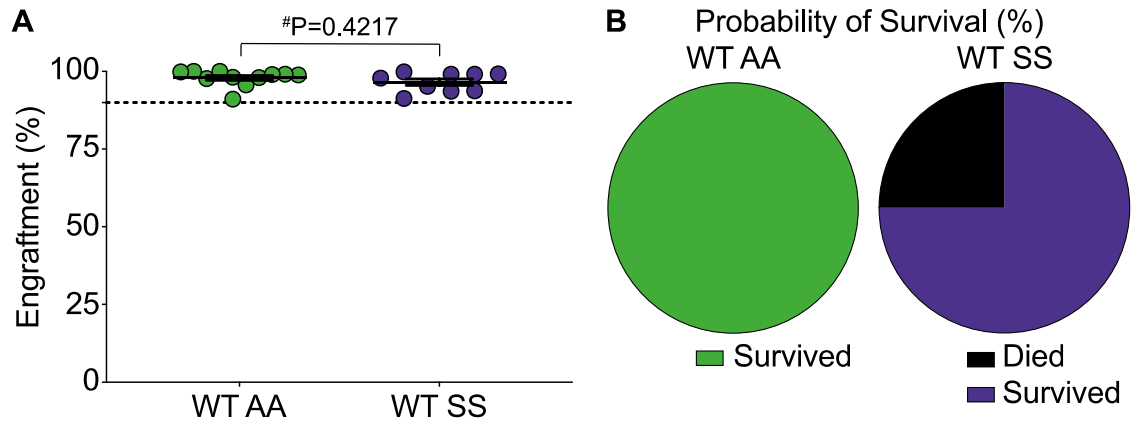


Figure 18. WT SS mice had a 75% survival rate following heme crisis.

A) AA control and SS sickle bone marrow engraftment was measured using hemoglobin electrophoresis. Ninety percent engraftment was used as a cutoff for inclusion in the experiments. Values are mean \pm SEM using a Mann Whitney test. B) Survival was measured over the 24 hours following heme challenge in WT AA (n=11) and WT SS mice (n=12). The WT SS mice had a 75% survival rate. WT, wildtype.

Table X. Blood cell indices for Townes AA bone marrow transplanted mice at baseline and 24 hours post-heme challenge.

	Baseline		Post-Heme Challenge		Delta Change		Significance WT AA vs WT SS Delta Change
	WT AA (n=11)	WT SS (n=9)	WT AA (n=11)	WT SS (n=9)	WT AA (n=11)	WT SS (n=9)	
WBC, 10 ³ /μL	16.36 ± 0.96	17.44 ± 1.43	15.72 ± 1.62	17.11 ± 2.84	-0.65 ± 1.08	-0.29 ± 2.49	+P=0.8978
RBC, 10 ⁶ /μL	10.78 ± 0.19	5.65 ± 0.16	9.88 ± 0.15	4.08 ± 0.21	-0.90 ± 0.19	-1.56 ± 0.27	P=0.0566
HCT, %	35.45 ± 0.76	28.11 ± 0.70	33.64 ± 0.65	19.22 ± 0.85	-2.03 ± 0.63	-8.89 ± 1.15	P<0.0001
MCV, fl	32.79 ± 0.22	49.58 ± 0.39	33.84 ± 0.34	47.20 ± 0.54	1.05 ± 0.20	-2.38 ± 0.50	+P<0.0001
RDW, %	26.82 ± 0.50	34.89 ± 0.79	26.93 ± 0.34	37.83 ± 0.58	0.11 ± 0.29	2.94 ± 0.87	+P=0.0117
HGB, g/dL	11.91 ± 0.16	9.39 ± 0.30	10.40 ± 0.15	6.41 ± 0.31	-1.51 ± 0.19	-2.98 ± 0.37	#P=0.0018
MCH, pg	11.04 ± 0.13	16.66 ± 0.19	10.52 ± 0.08	15.79 ± 0.22	-0.52 ± 0.07	-0.87 ± 0.20	+P=0.1235
PLT, 10 ³ /μL	674.73 ± 18.16	376.56 ± 21.43	597.00 ± 31.65	351.22 ± 31.18	-77.73 ± 35.65	-25.33 ± 36.03	P=0.3194
MPV, fl	6.78 ± 0.06	6.41 ± 0.07	6.62 ± 0.10	6.70 ± 0.11	-0.16 ± 0.10	0.29 ± 0.09	P=0.0033
Retic, %	5.09 ± 0.23	50.09 ± 0.76	5.18 ± 0.25	45.99 ± 1.50	0.09 ± 0.18	-4.10 ± 1.32	+P=0.0128

Definition of abbreviations: WBC = white blood cells; RBC = red blood cells; HCT = hematocrit; MCV = mean corpuscular volume; RDW = red blood cell distribution width; HGB = hemoglobin; MCH = mean corpuscular hemoglobin; PLT = platelets; MPV = mean platelet volume; retic = reticulocytes. Values are mean ± SEM using an unpaired Students t test unless noted otherwise (# Mann Whitney test, + unpaired Students t test with Welch's correction)

Table XI. Hemin injection significantly increased uric acid concentration and XO activity in plasma of SS sickle mice compared to AA control mice 24 hours post-hemin challenge of treatment.

	Baseline		Post-Heme Challenge		Delta Change		Significance WT AA vs WT SS Delta Change
	WT AA (n=10)	WT SS (n=9)	WT AA (n=10)	WT SS (n=9)	WT AA (n=10)	WT SS (n=9)	
Uric Acid, μM	0.53 ± 0.15	1.91 ± 0.41	1.51 ± 0.40	22.18 ± 8.38	0.98 ± 0.28	20.27 ± 8.13	#P=0.0006
XO Activity, μUnits/mL	31.62 ± 9.03	114.65 ± 24.76	90.29 ± 24.14	1330.62 ± 502.84	58.67 ± 16.85	1215.97 ± 487.55	#P=0.0006

Definition of abbreviations: XO = xanthine oxidase. #Values are mean ± SEM using a Mann Whitney test.

3.4.2 Hepatic XO release occurs through heme-TLR4 signaling

Next, we were interested in understanding how heme challenge resulted in such a large increase in circulating XO activity. We began by isolating primary murine hepatocytes from a C57BL6/J mouse and culturing the cells with vehicle or 10 μ M hemin. After 24 hours the media was collected from the cells and HPLC was used to assess XO activity in the media as a measure of hepatocyte XO release. The hemin treated primary murine hepatocytes had a 78-fold increase in media XO activity compared to the vehicle treated cells (Figure 19A), confirming the hepatic XO release we observed in the mouse model. Next, alpha mouse liver 12 (AML12) cells were used to determine the mechanism of XO release from hepatocytes. AML12 cells were treated with 10 μ M hemin and media was collected for XO activity measurement 0 minutes, 5 minutes, and 8 hours after hemin treatment. Media XO activity began to increase within the first five minutes after hemin treatment, with a significant increase in XO release by 8 hours (Figure 19B).

Heme is a known agonist for TLR4¹¹⁸, and we hypothesized that heme-TLR4 signaling was involved in the mechanism for hepatic XO release. To test this hypothesis, TLR4 was knocked down using siRNA from AML12 cells for 48 hours followed by treatment with 10 μ M hemin. Knockdown of TLR4 resulted in complete inhibition of hemin-mediated XO release in AML12 cells 24 hours after treatment (Figure 19C). Additionally, pharmacologic inhibition of TLR4 with the inhibitor TAK242 for 30 minutes prior to treatment with 10 μ M hemin also resulted in complete inhibition of hemin-mediated hepatic XO release 24 hours after treatment (Figure 19D). The specificity of heme-TLR4 mediated hepatic XO release was evaluated by treating AML12 cells with 2.5 μ M oxyhemoglobin and measuring XO activity from the media of the cells. Oxyhemoglobin did not result in an increase in XO release from AML12 cells and pre-incubation with TAK242 for 30 minutes prior to oxyhemoglobin treatment had no effect on media XO activity

(Figure 19E). To test if XO was merely released from hepatocytes or expression was upregulated, XO RNA and protein levels were measured from AML12 cells treated with TAK242 for 30 minutes prior to treatment with 10 μ M hemin. Hemin treatment resulted in a 2.8-fold increase in XOR mRNA; however, pre-treatment with TAK242 prevented the increase in mRNA expression (Figure 19F). Similarly, hemin treatment resulted in a 2.2-fold increase in XOR protein expression that was reduced to a 1.4-fold increase in XOR when pre-treated with TAK242 (Figure 19G and Figure 20), suggesting that heme-TLR4 signaling releases XO from hepatocytes and upregulates XOR expression.

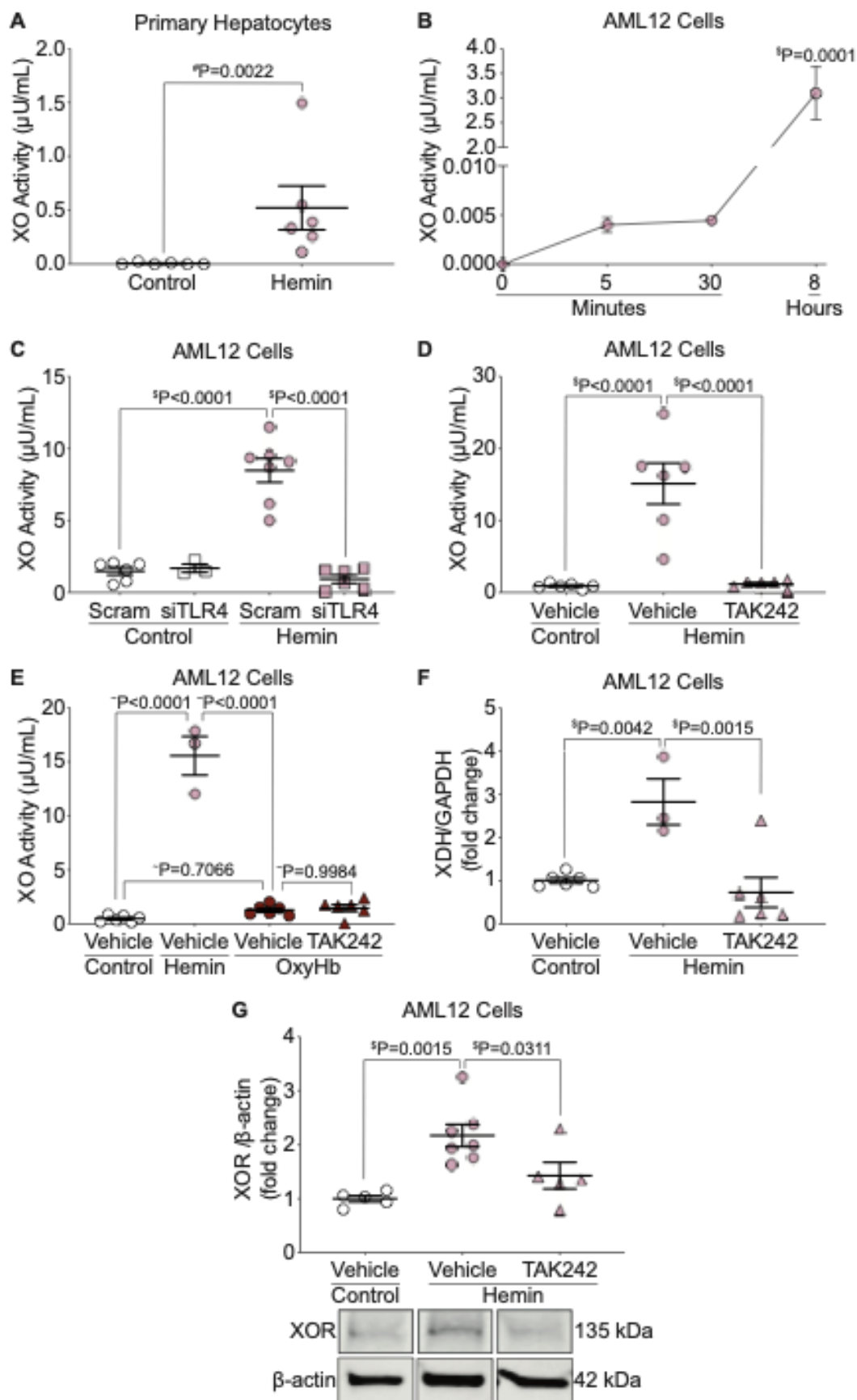


Figure 19. Heme-TLR4 signaling releases XO from primary murine hepatocytes and AML12 cells.

A) Primary murine hepatocytes were isolated from C57BL/6J mice and cultured before treatment with 10 μ M hemin. XO activity was measured in the media from the cells using HPLC. B) AML12 cells were treated with 10 μ M hemin and media was collected between 0 minutes and 8 hours after treatment for XO activity measurement. C) AML12 cells were treated with scrambled or siTLR4 for 48 hours prior to treatment with 10 μ M hemin. Media was collected and XO activity was measured. D) AML12 cells were treated with the TLR4 inhibitor TAK242 for 30 minutes prior to treatment with 10 μ M hemin. Media was collected and XO activity was measured. E) AML12 cells were treated with TAK242 for 30 minutes prior to treatment with 10 μ M hemin or 2.5 μ M oxyhemoglobin. Media was collected and measured for XO activity. AML12 cells were treated with TAK242 for 30 minutes prior to treatment with 10 μ M hemin. Cellular XOR F) mRNA and G) protein were measured from the cells. #Values are mean \pm SEM using a Mann Whitney test. \$Values are mean \pm SEM using a 1-way ANOVA with Dunnett multiple comparisons test. ~Values are mean \pm SEM using a 1-way ANOVA with Sidak's multiple comparisons test. XO, xanthine oxidase; AML, alpha murine liver; Scram, scrambled; TLR4, toll like receptor 4; OxyHb, oxyhemoglobin; XOR, xanthine oxidoreductase; HPLC, high performance liquid chromatography.

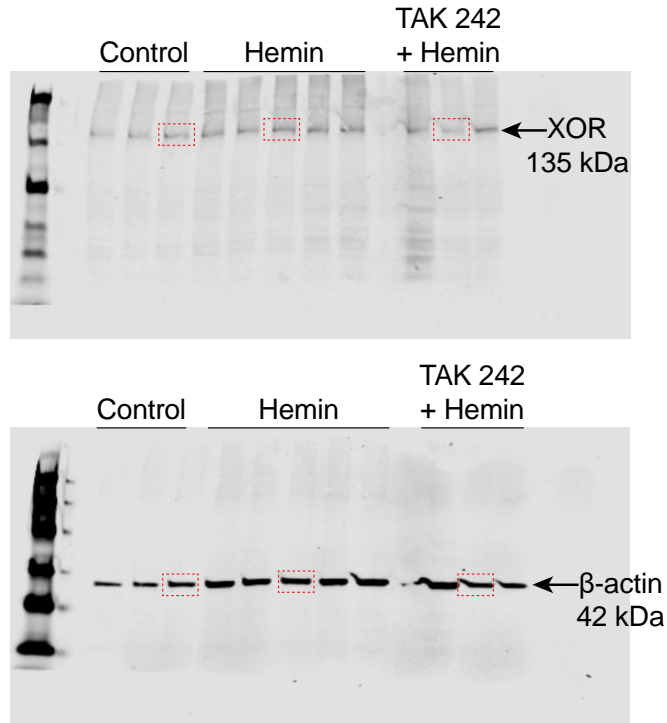


Figure 20. Knockdown and pharmacological inhibition of TLR4 in AML12 cells.

Full Western blot image from AML12 cells pre-treated with TAK242 for 30 minutes prior to treatment with 10 μ M hemin. Red boxes indicate bands included in Figure 19. TLR4, toll like receptor 4; AML, alpha murine liver.

3.4.3 Hepatocyte-specific XDH knockout accelerates death in response to heme challenge

Next, we assessed the role of XO during heme challenge using a hepatocyte-specific XDH knockout mouse. SS sickle Townes bone marrow was transplanted into 7-14 week old *Xdh^{flox/flox}Alb-1^{Cre/Wt}* (HXdh^{-/-}) or *Xdh^{flox/flox}Alb-1^{Wt/Wt}* (HXdh^{fl/fl}) mice and allowed 12 weeks to fully engraft (Figure 21A). Bone marrow engraftment was assessed after 12 weeks using hemoglobin gel electrophoresis and 85% was used as a cutoff for inclusion in the experiment (Figure 22). Blood was collected for baseline measurements and 14 days later the mice were challenged with 40 μ mol/kg hemin. The mice were observed for 24 hours following hemin injection and tissue was collected (Figure 21A). All the HXdh^{-/-} mice (n=6) died between 4-20

hours post-hemin injection; however, the $HXdh^{fl/fl}$ mice (n=5) had a 40% survival rate over 24 hours post-hemin injection (Figure 21B). The hepatocyte-specific XO knockout mice had increased death in response to heme challenge. To evaluate the efficacy of the mouse model we measured liver, lung, and kidney XO activity following heme challenge. As expected, the $HXdh^{-/-}$ mice demonstrated a significant reduction in liver XO activity with no impact on lung or kidney XO activity (Figure 21C, Table XII).

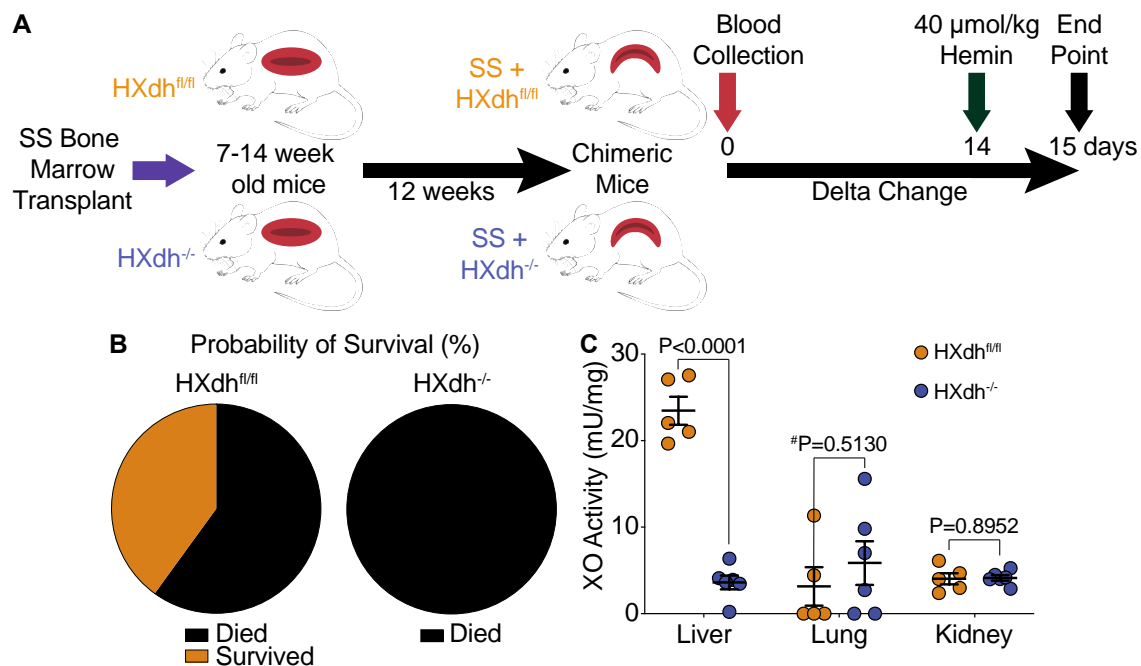


Figure 21. Hepatocyte Specific XO Knockout Increases Death Following Heme Challenge

A) Experimental design. B) Survival was measured over the 24 hours following heme challenge in $HXdh^{fl/fl}$ (n=5) and $HXdh^{-/-}$ mice (n=6). The $HXdh^{fl/fl}$ mice had a 40% survival rate, while all the $HXdh^{-/-}$ mice died within 20 hours. C) Liver, lung, and kidney tissue was collected at time of death or 24 hours post-hemin injection and XO activity was measured using HPLC. Values are mean \pm SEM using an unpaired Student t test unless otherwise noted. #Values are mean \pm SEM using a Mann Whitney test. Xdh, xanthine dehydrogenase; XO, xanthine oxidase;

HPLC, high performance liquid chromatography.

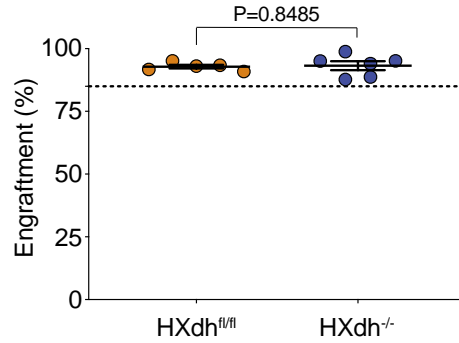


Figure 22. Bone Marrow Engraftment of Hepatocyte Specific XO Knockout Mice

SS sickle bone marrow engraftment was measured by gel electrophoresis in HXdh^{fl/fl} and HXdh^{-/-} mice. Eighty-five percent engraftment was used as a cutoff for inclusion in the experiments. Values are mean ± SEM using an unpaired Student t test. Xdh, xanthine dehydrogenase; XO, xanthine oxidase.

Table XII. Hepatocyte specific XO knockout decreased liver XO activity without impacting lung or kidney

XO activity.

	Post-Heme Challenge		Significance	
	HXdh ^{fl/fl} (n=5)	HXdh ^{-/-} (n=6)		
Liver	Uric Acid, μM	99.76 ± 7.37	14.24 ± 3.20	P<0.0001
	XO Activity, mU/mg	23.46 ± 1.61	3.62 ± 0.81	P<0.0001
Lung	Uric Acid, μM	4.01 ± 2.82	6.69 ± 3.06	#P=0.3939
	XO Activity, mU/mg	3.16 ± 2.22	5.86 ± 2.52	#P=0.5130
Kidney	Uric Acid, μM	13.70 ± 2.15	13.35 ± 1.30	P=0.8898
	XO Activity, mU/mg	4.04 ± 0.65	4.14 ± 0.32	P=0.8952

Definition of abbreviations: XO = xanthine oxidase. Values are mean ± SEM using an unpaired t test unless otherwise noted. #Values are mean ± SEM using a Mann-Whitney test.

3.4.4 XO binds free heme and protects against platelet activation and aggregation

After establishing a protective role for XO during heme crisis, we hypothesized that reduction in plasma XO during heme crisis resulted in an increase in death because XO has a previously uncharacterized function as a heme scavenging enzyme. Computational modeling of XO and heme identified a predicted heme binding site ($K_d=128$ nM) within the FAD domain of XO (Figure 23A). To assess the possibility of heme-XO interaction, a heme binding dot blot was performed by incubating hemin with XO for 20 minutes and the reactions were stopped using Laemmli buffer. Hemin binding was assessed by dot-blotting in nitrocellulose followed by chemiluminescent detection. Hemin alone was used to normalize the other conditions. Incubation of hemin and XO resulted in a 2-fold increase in signal, indicating a hemin-XO interaction (Figure 23B). When hemin was incubated with XO and hypoxanthine, there was a four-fold increase in signal, suggesting XO activity could play a role in the ability of XO to bind heme (Figure 23B). Addition of febuxostat to the reaction mixture completely blunted the increase in dot density, confirming an activity dependent interaction of heme and XO (Figure 23B). Albumin accounts for 55-60% of all plasma proteins and can bind a wide range of ligands in the blood¹³⁵. To confirm the specificity of XO-heme interaction, we incubated heme and albumin for 20 minutes and observed a 3-fold increase in signal, which was less than the 4-fold increase in signal with heme, XO, and hypoxanthine (Figure 24A).

Scavenging of heme by XO could provide some mechanism of protection during heme challenge so we investigated the ability of XO to mediate heme-induced platelet activation and aggregation. Platelets were isolated from healthy human blood and incubated with combinations of XO, hypoxanthine, and febuxostat for 30 minutes prior to activation with hemin. Flow cytometry was used as a measurement of platelet aggregation, while aggregation was measured

using an aggregometer (Figure 23C). Platelet activation was evaluated by staining for the platelet marker CD41a and the platelet activation marker CD62p. The non-treated platelets had a minimal amount of platelet activation (10%), while 94% of the platelets were activated by the positive control thrombin and 72% of platelets were activated by hemin alone (Figure 23D-E). When the platelets were pre-incubated with XO and hypoxanthine for 30 minutes prior to hemin addition, platelet activation was reduced almost to baseline levels of activation (16%) (Figure 23D-E). Febuxostat partially restored hemin-induced platelet activation with 45% of platelets being activated (Figure 23D-E). Mean fluorescent intensity of the platelets showed similar trends (Figure 24B). Platelet aggregation was measured in a similar manner and calculated based on the area under the curve (AUC). Platelets were treated with ristocetin as a positive control, which showed comparable levels of platelet aggregation as hemin (Figure 23F). Pre-incubation of platelets with XO and hypoxanthine for 30 minutes prior to hemin addition completely prevented platelet aggregation (Figure 23F). Addition of febuxostat to the reaction mixture restored hemin's ability to induce platelet aggregation (Figure 23F).

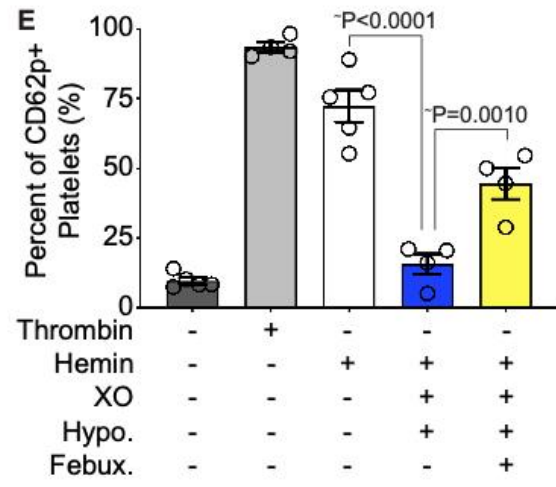
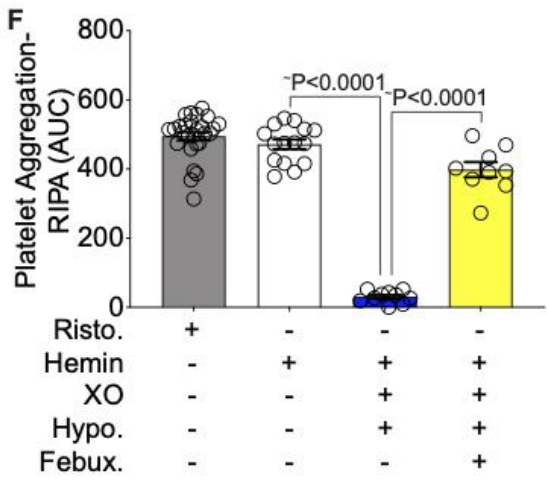
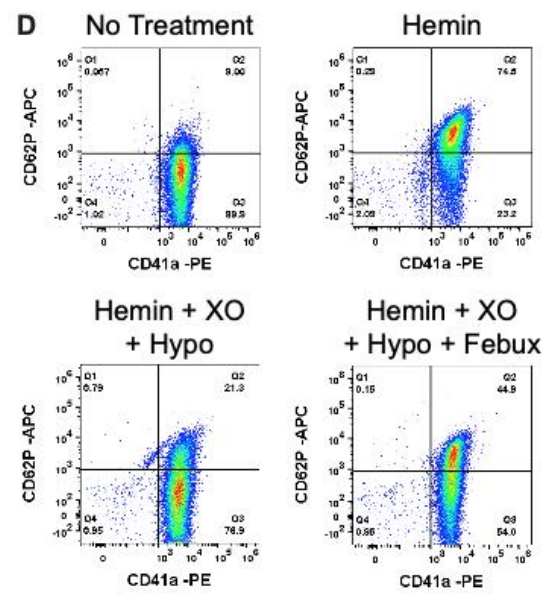
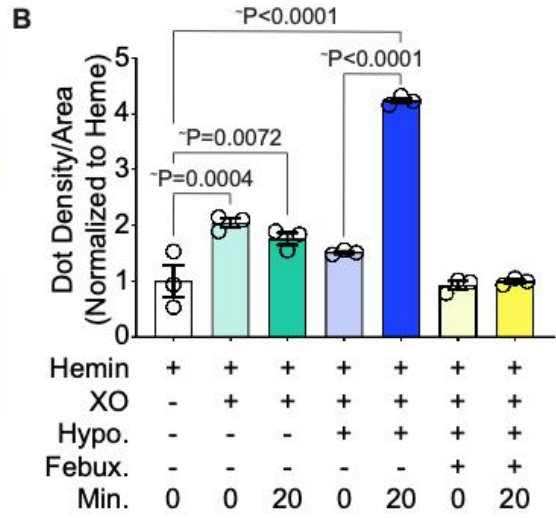
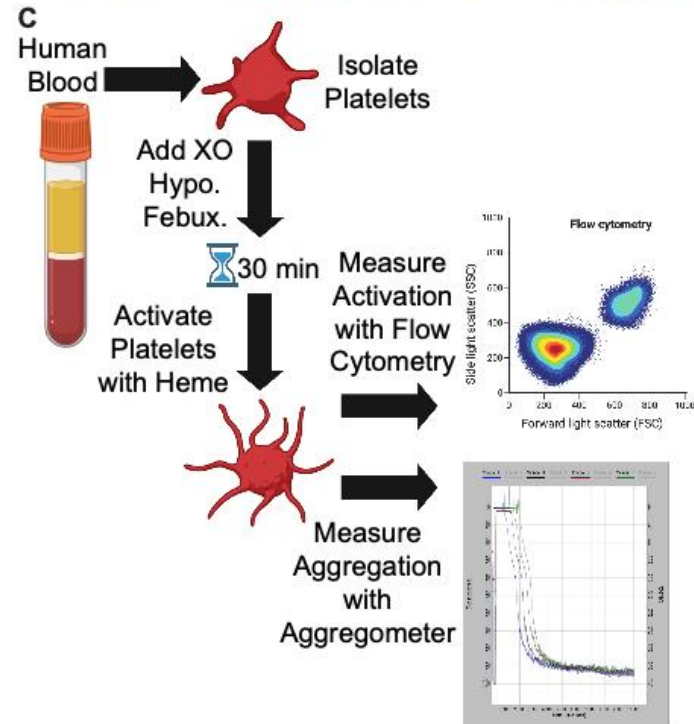
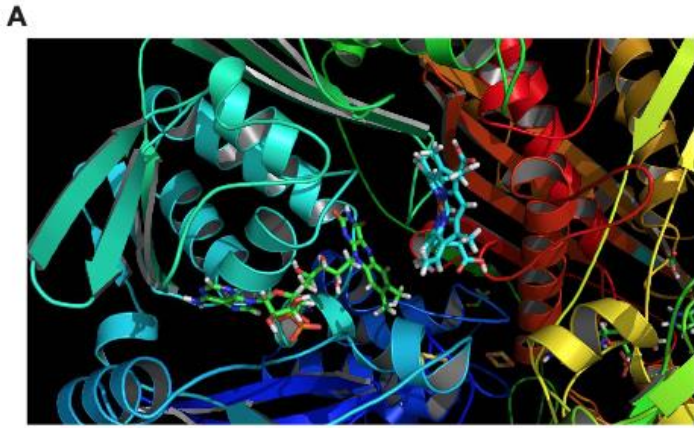


Figure 23. XO binds hemin and prevents platelet activation and aggregation.

A) Molecular modeling of heme and XO identified a predicted heme binding site within the FAD domain of XO. B) Hemin-XO interaction was evaluated via a heme binding dot blot. Reactions were incubated for 20 minutes and stopped with Laemmli buffer. Samples were added to a nitrocellulose dot blot and chemiluminescent detection was used to identify heme binding. C) Schematic of platelet activation and aggregation experiments. Platelets were isolated from healthy human blood and incubated with XO, hypoxanthine and febuxostat for 30 minutes prior to stimulation with hemin. Platelet activation was measured using flow cytometry and platelet aggregation was measured using an aggregometer. This schematic was created using biorender.com. D-E) Platelets were stained with the platelet marker CD41a and the platelet activation marker CD62p to determine the percentage of activated platelets in the sample. Untreated platelets were used as a negative control and thrombin was used as a positive control. Quantification of the flow scatter plots in D are shown in E. F) Platelet aggregation was measured using an aggregometer and calculated as the AUC. Ristocetin was used as a positive control. [~]Values are mean \pm SEM using a 1-way ANOVA with Sidak's multiple comparisons test. XO, xanthine oxidase; Hypo, hypoxanthine; Febux, febuxostat; Min, minute; RIPA, ristocetin-induced platelet activation; AUC, area under the curve; Risto, ristocetin.

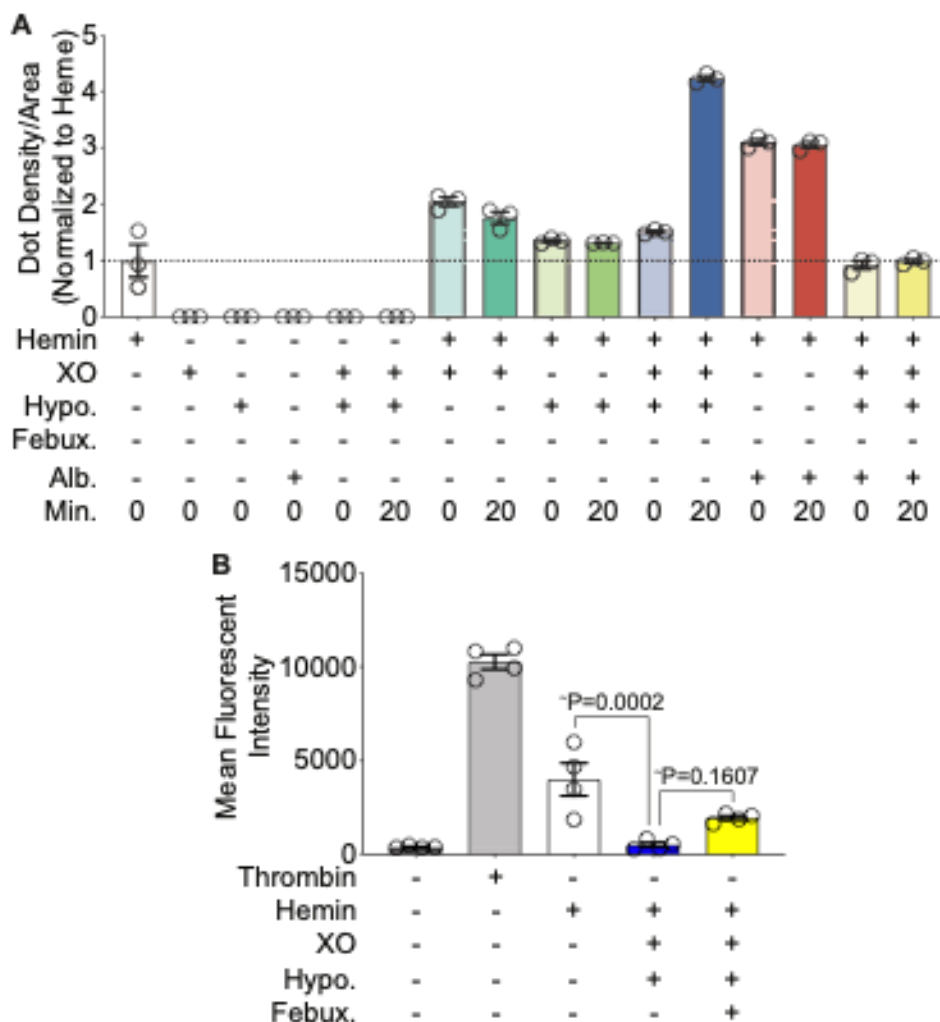


Figure 24. Hemin-XO binding is stronger than hemin-albumin interaction.

A) Heme-XO interaction was evaluated via a heme binding dot blot. Reactions were incubated for 20 minutes and stopped with Laemelli buffer. Samples were added to a nitrocellulose dot blot and chemiluminescent detection was used to identify heme binding. Controls included XO alone, hypoxanthine alone, albumin alone, XO + hypoxanthine and albumin + hemin. B) Platelet activation was measured by flow cytometry with the platelet marker CD41a and the platelet activation marker CD62p. Platelets were incubated for 30 minutes with different combinations of XO, hypoxanthine or febuxostat before activation with thrombin (positive control) or hemin. ~Values are mean \pm SEM using a 1-way ANOVA with Sidak's multiple comparisons test. XO, xanthine oxidase; Hypo, hypoxanthine; Febux, febuxostat; Alb, albumin; Min, minute.

3.4.5 XO activity facilitates hemoglobin degradation

In addition to heme, hemolysis also releases hemoglobin which can exert pathological effects if it is not scavenged and degraded. To investigate the effects of XO activity on hemoglobin, we incubated 17 μM oxyhemoglobin with 50 mU/mL XO and 400 μM xanthine for 20 minutes and observed a visible color change in the reaction mixture compared to the oxyhemoglobin alone (Figure 25A, left and middle). When 1 kU/mL of catalase, converts H_2O_2 to water and oxygen, was added to the reaction mixture there was no visible color change in the oxyhemoglobin, suggesting oxyhemoglobin degradation is H_2O_2 dependent (Figure 25A, right). The visible color change was then measured with a spectrophotometer over 20 minutes. Oxyhemoglobin (17 μM) was incubated with XO (50 mU/mL) and xanthine (400 μM) for 21 minutes and the absorbance was measured every couple of minutes. There was a time-dependent decrease in absorbance at the 415 nm peak (Soret band) as well as at the doublet peaks between 500-600 nm, consistent with the color change observed by eye and suggestive of hemoglobin degradation (Figure 25B). When zooming in on the doublet peaks between 500-600 nm, there is also formation of two isosbestic points at ~ 525 and ~ 580 nm (Figure 25C). This suggests there is oxyhemoglobin degradation and formation of additional hemoglobin species.

Assessment of ascorbyl radical production from oxidation of ascorbate using electron paramagnetic resonance (EPR) was used as a measure of oxidative stress and iron release ($\text{Fe}^{3+} + \text{AscH}^- \rightarrow \text{Fe}^{2+} + \text{Asc}$). Reactions were incubated for 20 minutes prior to EPR measurement. Ascorbate alone produced a small amount of ascorbyl radical as observed by the two peaks and oxyhemoglobin alone did not cause any additional ascorbate radical formation (Figure 25D). However, incubation of ascorbate and hemoglobin with H_2O_2 or xanthine + XO greatly increased ascorbyl radical formation which can be attributed to ferric iron being released from

oxyhemoglobin and reacting with ascorbate (Figure 25D). Next, we added catalase or DTPA to the reaction mixture and observed a significant reduction in the production of ascorbate radical (Figure 25D). This suggests that the breakdown of oxyhemoglobin and formation of ascorbyl radicals is dependent on H₂O₂ production and iron release.

NO binds specifically to the ferrous form (Fe²⁺) of hemoglobin, known as oxyhemoglobin (K_d=10⁻¹⁰-10⁻¹¹ M) to form methemoglobin and nitrate¹³⁶. This deoxygenation reaction scavenges NO and inhibits NO mediated signaling¹³⁶. Therefore, we hypothesized that XO activity could have a role in preventing oxyhemoglobin from scavenging NO. To test this hypothesis, we performed an NO consumption assay. The addition of oxyhemoglobin to the continuous flow of NO results in a drop in mV, indicating oxyhemoglobin scavenges the NO as expected (Figure 25E). When oxyhemoglobin is incubated with XO for 20 minutes prior to addition, there is a small, but insignificant decrease in the area under the curve; however, when xanthine was added to the reaction mixture to provide substrate for XO activity, the area under the curve was significantly reduced (Figure 25E-F). This suggests that XO activity prevents oxyhemoglobin from scavenging NO and provides further evidence of a protective mechanism for XO during heme crisis.

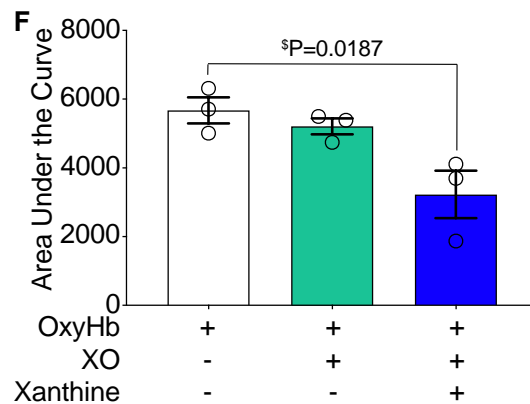
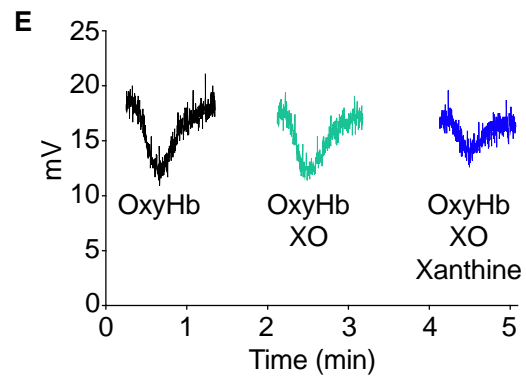
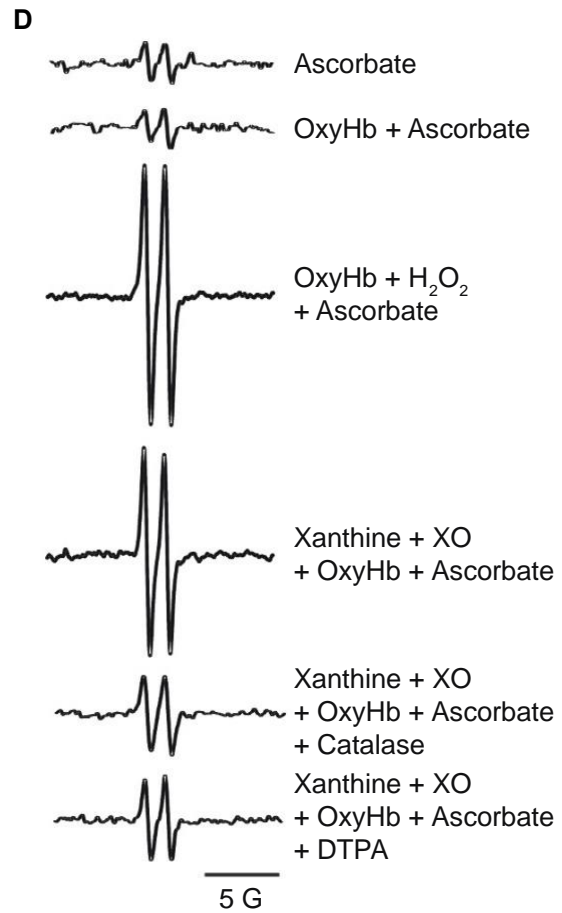
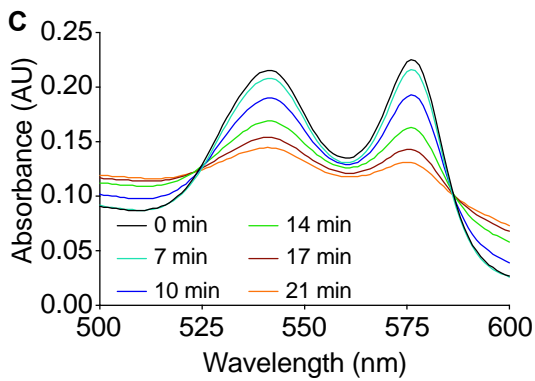
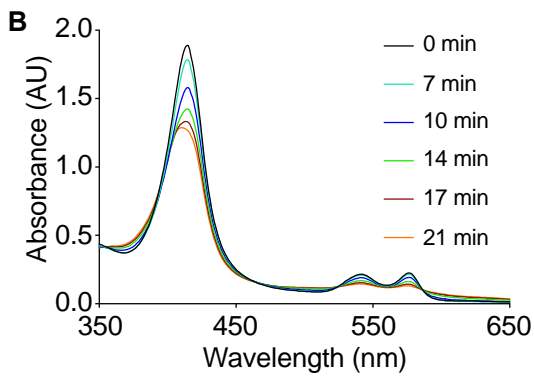
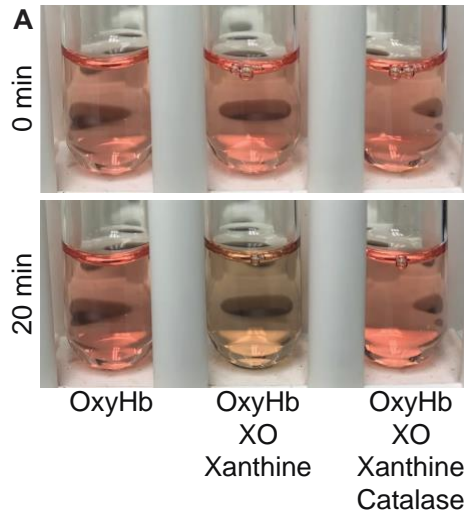


Figure 25. XO activity facilitates oxyhemoglobin degradation.

Oxyhemoglobin (17 μM) was incubated with XO (50 mU/mL) and xanthine (400 μM) for 20 minutes. Degradation of oxyhemoglobin and loss of iron was evaluated by eye A) and spectrophotometer B-C). D) EPR was used to follow the production of the ascorbyl radical for assessing free iron and oxidant production. Oxyhemoglobin (17 μM) was incubated with ascorbate for 20 minutes prior to EPR measurement. E) Oxyhemoglobin (17 μM) was incubated with combinations of XO (50 mU/mL), and xanthine (400 μM) for 20 minutes. DETA NONOate was used to create a continuous flow of 40 μM NO. Each reaction was added to the Sievers Nitric Oxide Analyzer sparger and NO consumption was quantified as F) area under the curve. Min, minute; OxyHb, oxyhemoglobin; XO, xanthine oxidase; DTPA, Diethylenetriamine pentaacetate; EPR, electron paramagnetic resonance; DETA NONOate, (Z)-1-[2-(2-Aminoethyl)-N-(2-ammonioethyl)amino]diazene-1,1,2-diolate; NO, nitric oxide.

3.5 Discussion

It has been well established that XO activity is elevated in numerous hemolytic conditions; however, the role of XO during heme crisis has not previously been established. Hemolytic conditions, such as SCD, affect ~300,000 new patients each year¹⁰, yet treatment options remain limited and there are currently no SCD treatments designed specifically to target hemolysis during heme crisis. XO has traditionally been considered a harmful enzyme when elevated during pathological conditions; however, we hypothesized that the robust increase in XO activity associated with hemolytic disease has an important and protective role.

Healthy RBC lifespan is ~115 days¹³⁷, at which time the cells undergo hemolysis and release their hemoglobin and heme into circulation⁹⁰. Haptoglobin and hemopexin bind hemoglobin and heme, respectively, and target them to macrophages or the liver for catabolism and clearance^{31,32}. Healthy subjects have a large enough pool of haptoglobin and hemopexin to mitigate circulating free hemoglobin and heme levels caused by the turnover of RBCs. In SCD

patients, RBC lifespan is reduced to 2-21 days, dramatically increasing the degree of hemolysis compared to their healthy counterparts¹³⁸. This results in depletion and saturation of canonical degradation pathways and an increase in free hemoglobin and heme levels. The Cooperative Study of Sickle Cell Disease reported that SCD patients have cell free hemoglobin concentrations of 3.6 g/dL and heme concentrations of 2.23 mM during a hemolytic crisis event¹²⁵. This far exceeds the normal circulating levels of 0.0006-0.0034 g/dL hemoglobin¹³⁹ and heme in healthy humans.

To investigate the role of XO during a hemolytic crisis event in SCD, we generated transgenic AA control and SS sickle mice by transplanting AA or SS Townes bone marrow into C57BL/6J mice. The WT AA and WT SS mice were challenged with 40 μ mol/kg of hemin and evaluated 24 hours post-hemin injection (Figure 17A). The WT SS mice experienced a greater degree of hemolysis compared to the WT AA mice as evidenced by a significantly greater decrease in hematocrit and hemoglobin (Figure 17C-D). Because the WT SS sickle mice have depleted hemopexin concentrations¹²⁹, it is not surprising to observe greater rates of hemolysis and heme toxicity (WT SS survival rate 75%, compared to WT AA survival rate 100%; Figure 18B). However, a possible caveat of these results is that the increase in hemolysis observed in the WT SS mice could be due to disease progression, rather than a greater extent of hemolysis in response to hemin challenge. The elevated levels of hemolysis in the WT SS sickle mice corresponded to a significant elevation in plasma XO activity in response to heme challenge (Figure 17E) and demonstrated a clear link between free heme and release of XO into circulation.

The liver is an important site for both heme clearance and XO production. Hemopexin binds free heme and targets it to the liver for hepatic catabolism and clearance^{31,33}. Additionally, the majority of XO is transcribed and translated in the liver and hepatic derived XO accounts for more than 50% of XO found in circulation⁹³. Despite the established connection between

hemolytic disease and elevated XO activity, the mechanism of hepatic XO release was not previously established. To investigate the mechanism of hepatic XO release, we treated primary murine hepatocytes or AML12 cells with 10 μ M hemin. The cellular release of XO was measured by evaluating the XO activity in the media of treated cells. Hemin treatment resulted in a significant increase in XO release from primary murine hepatocytes and AML12 cells (Figure 19A-B). AML12 cells were used to investigate the mechanism of XO release due to the difficulty and short-term culture duration of primary murine hepatocytes. Heme is a known agonist of TLR4; therefore, we used siRNA knockdown and pharmacologic inhibition of TLR4 to assess the impact on XO release. Both methods completely blunted the release of XO into the media (Figure 19C-D). We have demonstrated for the first time, a direct link between heme-TLR4 signaling and hepatic release of XO. Additionally, the release of XO is heme specific as oxyhemoglobin did not cause a release of XO from AML12 cells (Figure 19E). Heme-TLR4 signaling not only releases the XO contained in hepatocytes, but also increases the transcription and translation of XOR as shown by an increase in mRNA and protein levels (Figure 19F-G). We hypothesize that heme-hemopexin delivery to the liver serves as a signaling mechanism to allow heme to bind hepatic TLR4, resulting in the downstream upregulation of XOR and increase in circulating XO.

Next, we tested the effects of specifically depleting XO from the liver compartment. We transplanted SS sickle Townes bone marrow into litter mate control (*HXdh^{fl/fl}*) or hepatocyte specific XOR knockout mice (*HXdh^{-/-}*) and challenged the mice with 40 μ mol/kg of hemin (Figure 21A). Hepatocyte specific XO knockout increased death compared to the littermate controls, highlighting the importance of hepatic derived XO in managing the response to heme crisis (Figure 21B). Increased death in the knockout group suggests that XO could in fact be playing a protective role during heme crisis. To our knowledge, this is the first evidence demonstrating elevated XO

activity may not always be pathologic and it could have previously undiscovered, protective functions.

When XO is released from the liver, it enters the circulation where it can bind to distal endothelium via electrostatic interactions with GAGs, heparin sulfate (HS) and chondroitin sulfate (CS)⁶⁷. This allows for an increase in XO concentration on the endothelial surface of organs that do not typically have high XO expression. It has been demonstrated in disease states, such as lung cancer, that GAG expression can be altered¹⁰⁶. Changes in HS and CS expression may control the amount of XO binding on the endothelium and could also influence XO's ability to have a protective role during heme crisis.

We hypothesized that XO could function as a secondary mechanism of heme clearance, to help manage heme overload when canonical mechanisms such as hemopexin become saturated. Molecular modeling identified a predicted heme binding site in the FAD domain of XO (Figure 23A). XDH is converted to XO reversibly via modification of cystine residues (Cys535 and Cys992) to form a disulfide bridge or irreversibly via proteolytic cleavage at lysine 551¹⁴⁰. These modifications cause structural changes within the FAD domain that is the key structural difference between XDH and XO. This suggests XO may bind heme as a protective mechanism during heme crisis, while XDH is unable to bind heme. We confirmed heme-XO interaction with a heme-binding dot blot and determined that XO activity increases the interaction (Figure 23B). Additionally, the interaction was stronger than heme and albumin (Figure 24A) increasing the biological relevance of the XO's ability to scavenge heme.

Hemolytic diseases, including SCD, are often associated with platelet activation and it has been previously reported that there is a correlation between markers of hemolysis in SCD and platelet activation^{141,142}. Therefore, we evaluated the impact of heme-XO interaction on platelet

activation and aggregation. Pre-incubation of isolated healthy human platelets with XO and xanthine for 30 minutes prior to stimulation with hemin, inhibited hemin-induced platelet activation and aggregation. These effects were reversible with the addition of the potent XO inhibitor, febuxostat (Figure 23D-F). This suggests that an increase in XO activity in SCD could help to reduce coagulation caused by frequent hemolysis and elevated free heme.

Hemolysis releases heme and hemoglobin into circulation; therefore, we then investigated the effects of XO activity on hemoglobin degradation. When incubating oxyhemoglobin with XO and xanthine, there was a visible color change and decrease in absorbance at the 415 nm peak and the doublet peaks between 500-600 nm (Figure 25A-C). These changes in absorbance indicate degradation of oxyhemoglobin (decreased absorbance) and formation of additional hemoglobin species (presence of isosbestic points). It has been previously reported that H_2O_2 can generate ferrylhemoglobin and $O_2^{\cdot-}$ when reacting with oxyhemoglobin whereby, the $O_2^{\cdot-}$ induces the breaking apart of the porphyrin ring in a heme splitting reaction^{143,144}. To measure the release of iron from oxyhemoglobin in the presence of XO and xanthine, we performed EPR experiments to follow the ascorbyl radical and found that incubation of oxyhemoglobin with H_2O_2 or XO + xanthine resulted in a significant increase in ascorbyl radical production (Figure 25D-E). The generation of ascorbyl radicals from ascorbate can be used as a measure of oxidative stress¹⁴⁵ and in this case H_2O_2 or XO + xanthine function by causing damage to oxyhemoglobin, releasing the iron (Fe^{3+}) which reacts with ascorbate to form Fe^{2+} and ascorbyl radicals. Only the free iron can generate ascorbyl radicals as oxyhemoglobin alone did not generate an EPR signal above control (Figure 25D-E). Finally, we measured NO consumption as a functional consequence of XO-oxyhemoglobin interaction. A decrease in NO consumption, as observed by a decrease in area under the curve, suggests that XO activity prevents oxyhemoglobin from scavenging NO (Figure

25F-G). NO is an important signaling molecule in neuronal, immune, and inflammatory responses¹⁴⁶; therefore, preventing hemoglobin from scavenging NO has many implications pathologically. Decreased NO bioactivity is a major contributing factor to complications in SCD such as pulmonary hypertension, leg ulceration, priapism, and stroke²². Elevations in XO activity during hemolytic conditions such as SCD could have a protective role by increasing NO bioavailability.

We postulate that XO has a previously undescribed function in SCD, and more broadly in managing excess hemolysis. When heme is released from RBCs during hemolysis, hemopexin targets heme to the liver for clearance and degradation. Heme signals through TLR4 to increase the transcription and translation of XOR in hepatocytes and release XO into circulation. Once in circulation XO can bind distal GAGs on the surface of endothelial cells. It has previously been reported that endothelial bound XO can produce oxidants directly at the endothelial surface, resulting in damage. We have previously shown that 10 weeks of febuxostat treatment resulted in a decrease in hemolysis and an improvement in pulmonary vascular function in bone marrow transplanted WT SS sickle mice¹²⁹. However, we hypothesize that XO has dual functionality. While it may result in some degree of basal damage, during a heme crisis event, XO has important and beneficial properties to mediate damage from heme and hemoglobin. When XO binds to the endothelial surface, it creates a microenvironment specifically designed to protect against heme induced damage. XO oxidizes hypoxanthine to xanthine and xanthine to uric acid. In the process H_2O_2 is generated which can break apart the hemoglobin and cause a heme splitting reaction. This will also release iron which can be toxic to cells. However, the uric acid produced from xanthine has been shown to chelate iron and therefore XO has an additional level of protection. In summary, we hypothesize that XO creates a microenvironment on the endothelial surface designed

specifically to protect the endothelium from free hemoglobin, heme, and iron toxicity. Because XO is bound to the endothelium, rather than circulating like hemopexin, it may be more effective at protecting the endothelium than canonical degradation mechanisms.

3.6 Acknowledgements

This work was supported, in whole or in part, by National Institutes of Health Grants: F31 HL149241 (H.M. Schmidt); R25 HL128640-03 (K.C. Wood); K01 HL133331 (D.A. Vitturi); National Institutes of Health (NIH) R01 DK124510-01 and American Heart Association 19TPA34850089 (E.E. Kelley); and R01 HL133864, R01 HL128304 and American Heart Association Established Investigator Award (A.C. Straub). Graphical design was provided by Anita Impagliazzo.

4.0 General Conclusions and Future Directions

4.1 The Dual Functions of XO in Sickle Cell Disease

XO is a crucial enzyme responsible for the oxidation of hypoxanthine to xanthine and xanthine to uric acid as part of purine degradation; however, this essential function also has a downside with the production of the reactive species H_2O_2 or $\text{O}_2^{\cdot-}$. Similarly, we have uncovered a dual functionality of XO in the context of SCD, that may be extended to other hemolytic conditions. As previously described in the literature, an increase in plasma XO activity can be pathological. When we treated bone marrow transplanted SS sickle mice with febuxostat, an FDA-approved XO inhibitor, for 10 weeks we observed a decrease in hemolysis and an improvement in pulmonary vasoreactivity¹²⁹. We hypothesized that inhibition of XO activity had beneficial effects under basal conditions of SCD due to the decrease in ROS production at the endothelial surface. Patients with SCD are highly susceptible to crisis events that can be triggered by stress; however, mouse models of sickle cell disease experience fewer crisis events. Therefore, to specifically investigate the role of XO during a heme crisis event, we injected bone marrow transplanted SS sickle mice with 40 $\mu\text{mol/kg}$ hemin and observed the acute effects 24 hours post-heme challenge. The hepatocyte specific XO knockout SS sickle mice had increased death compared to the littermate controls, suggesting a protective role for hepatic derived XO during heme crisis. In these two studies we identified a pathologic and protective function for XO. We hypothesize that the role of XO in SCD is condition dependent and that XO activity is increased in chronic hemolytic conditions, such as SCD, in anticipation of a heme crisis event. This may result in some degree of

endothelial damage; however, it prepares the endothelium for a heme crisis event when canonical heme scavenging, and degradation pathways become saturated.

4.2 Is the role of XO condition and compartment specific?

Our studies suggest that XO could have a condition dependent role in SCD: harmful under basal conditions and protective during heme crisis. Additionally, we hypothesize that the role of XO could also be compartment dependent. When bone marrow transplanted mice were treated with Febuxostat for 10 weeks, we observed a decrease in hemolysis and an improvement in pulmonary vasoreactivity. However, when hemolysis and vasoreactivity was evaluated in bone marrow transplanted hepatocyte-specific XO knockout mice, there were no benefits observed compared to the littermate controls. Febuxostat treatment inhibits XO activity globally in all tissues of the mice, while hepatocyte-specific XO knockout only eliminates hepatic derived XO. The difference in response between the febuxostat treated mice and the hepatocyte-specific XO knockout mice suggests that hepatocyte derived XO is not the driver of hemolysis and pulmonary vascular dysfunction in SCD, and we hypothesized another source of XO, such as the endothelium, was responsible for these negative effects. In contrast, in our acute heme crisis SCD model, the hepatocyte-specific XO knockout mice showed increased death compared to their littermate controls. This suggests that hepatic-derived XO is at least partially responsible for the protective effects we observed in this model. When we treated bone marrow transplanted WT SS mice with febuxostat for two weeks prior to heme challenge, we observed a small increase in death compared to the untreated mice, but to a lesser extent than the hepatocyte-specific XO knockout mice (data not shown). This highlights the importance of hepatic-derived XO in the protective mechanism we

observed. Therefore, we hypothesize that endothelial-derived XO causes hemolysis leading to pulmonary vascular dysfunction and hepatocyte-derived XO protects the endothelium from heme induced damage during a crisis event.

This hypothesis requires further investigation of endothelial-derived XO in SCD. To our knowledge, we have developed the first endothelial-specific XO knockout mouse model. Future directions of our lab include characterization of these mice in the following conditions:

- 1) Endothelial-specific XO knockout mice will be bone marrow transplanted with SS sickle Townes bone marrow. After 12 weeks of engraftment, the mice will be aged an additional 10 weeks. Hemolysis and vascular function will be assessed as previously described. We hypothesize that these mice will have a decrease in hemolysis and an improvement in pulmonary vascular function, similarly to the Febuxostat treated mice.
- 2) Endothelial specific XO knockout mice will be bone marrow transplanted with SS sickle Townes bone marrow. After 12 weeks of engraftment, baseline measurements will be collected and two weeks later the mice will be challenged with 40 $\mu\text{mol/kg}$ of hemin. Hemolysis, XO activity, and survival will be evaluated 24 hours post-heme challenge. We hypothesize that endothelial specific XO knockout will not have an impact on the ability of the mice to respond to heme crisis.

The generation of cell-type specific XO knockout mice will allow for future characterization of the compartment specific roles of XO. If XO has compartment-dependent functionality, this could provide an opportunity to develop drugs that specifically target XO. Because XO has both protective and pathologic effects in SCD, the ability to use it as a drug target is limited. Inhibiting its activity during a heme crisis event could prevent it from scavenging and degrading free heme, while increasing its activity could cause additional endothelial damage under

basal conditions. However, if XO has compartment-dependent effects, it could be possible to target hepatic-derived XO while leaving endothelial derived-XO untouched or inhibited. Future directions should investigate these mechanisms and potential therapeutic applications.

4.3 Does GAG composition mediate the role of XO activity in SCD?

XO binds to the surface of endothelial cells via electrostatic interactions with HS or CS. The composition of the glycocalyx has been shown to vary throughout the vasculature and can also be modified in various disease states. For example, a comprehensive study found significant changes in GAG composition in lung cancer¹⁰⁶. We hypothesize that alterations in the glycocalyx could serve as a regulatory mechanism for XO interaction with the endothelium. It is possible that chronic hemolytic conditions could upregulate HS or CS to increase XO binding to the endothelium and thus provide a greater degree of protection against endothelial damage caused by free heme. Future directions could measure changes in the glycocalyx composition in the vasculature of the aorta, pulmonary arteries, and mesenteric arteries from mouse models of SCD or tissue samples from human patients. We could measure glycocalyx composition and structure using liquid chromatography-mass spectrometry and Western blotting and evaluate the differences between SCD and control samples. These studies would provide insight into the degree of XO binding to the endothelial surface in the context of SCD and determine whether it is increased or decreased compared to healthy subjects. We know that circulating XO activity is increased in SCD, but it would be interesting to determine whether there is also an increase in HS and CS expression in certain vascular beds to allow a greater degree of protection in heme crisis.

4.4 What mechanisms regulate hepatic XO release?

It has previously been shown that hepatic-derived XO accounts for more than 50% of XO found in circulation⁹³. For the first time, we showed mechanistic evidence of hepatic XO release through heme-TLR4 signaling. We demonstrated that primary murine hepatocytes and AML12 cells treated with 10 μ M hemin had an increase in XOR RNA and protein expression and an increase in XO release. When TLR4 was knocked down using siRNA or pharmacologically inhibited with TAK242, these effects were blunted suggesting heme signals through TLR4 to upregulate XOR expression and release XO. Additionally, unpublished data from the Kelley lab explored transcriptional regulation of Xdh. Treatment of cells with hemin will increase the production of H₂O₂; therefore, they focused on redox regulated transcription factors including p65 and Sp1. When these transcription factors were knocked down with siRNA, the hemin induced upregulation of Xdh was blunted and ChIP experiments found enrichment near the Xdh transcription start site.

While this provides the first mechanistic link to understanding heme-mediated XO release, much of the transcriptional upregulation and mechanism of release remains to be uncovered. It is unknown if traditional TLR4 pathways are involved in hepatic XO release or whether it is through a previously unreported mechanism. Another question that remains is if the effect is truly heme dependent. Unpublished work from the Kelley lab treated AML12 cells with components of hemin: a porphyrin ring and iron. While iron treatment still resulted to XO release, similar to hemin, protoporphyrin 9 and Bay58 (compound structurally similar to protoporphyrin 9) did not signal for upregulation or release of XO. This suggests that the iron within the heme molecule is critical for the transcriptional upregulation and release of XO. Additionally, heme is only one potential agonist for TLR4. Other agonists such as LPS can activate TLR4 signaling and induce

an inflammatory response. Future studies should investigate these possibilities. We also know that other hepatic stressors such as inflammation, viral infection, hypoxia, and ischemia can release hepatic XO. These mechanisms are likely not heme-TLR4 dependent which suggests there are multiple means by which XO can be released from hepatocytes. Future studies should treat primary hepatocytes or AML12 cells with alternate TLR4 agonists and measure the XO activity in the media of the cells. AML12 cells can also be used to modulate the signaling pathways downstream of TLR4 to identify how its activation causes XO release.

Finally, the Kelley lab evaluated the mechanism of transport of XO out of the cells by treating with the canonical exocytosis inhibitor Brefeldin A, which had no effects on the upregulation or release of XO; however, when the “stress-mediated” lysosomal exocytosis pathway was inhibited with vacuolin-1 XO was not released into the media and accumulated within the cell. Together, we have identified p65-Sp1 as transcriptional regulators of Xdh in the presence of free heme or iron. XO is then released from cells by lysosomal exocytosis. These studies provide the basis for a more in depth exploration of the mechanisms regulating hepatic XO release.

4.5 Are XO allelic variants disease modifiers in SCD?

As we have demonstrated, XO activity can have opposing effects depending on the conditions. Therefore, it is important to tightly regulate its expression and activity. Several human XOR allelic variants have been identified and found to enhance or reduce XO activity. We identified a human XDH variant (Ile703Val) with an allele frequency of 0.1151 in African Americans. This mutation has been shown to have elevated XO activity compared to the wildtype

allele¹⁴⁷. Because SCD primarily affects people of African descent, this common variant could impact SCD pathology. Future directions should examine the most common XDH variants and, if it is possible to gather a large enough cohort, evaluate the outcomes and disease progressions of patients who have variants with elevated or reduced XO activity. We hypothesize that SCD patients with XDH variants such as Ile703Val which increase XO activity may have fewer crisis events or improved management of hemolysis while variants that decrease activity by inhibiting electron flow for example could have worse outcomes. However, XO activity has its advantages and disadvantages. Therefore, genetic variants that increase or decrease XO activity could have negative outcomes due to the balance of activity that is required. Future studies should pay close attention to the impact of modifying XO activity in humans.

4.6 Final Conclusions

In summary we have completed two studies in which we investigated the double-edged sword known as XO. While it has been well established that XO activity is elevated in SCD and other hemolytic conditions, its role was not previously elucidated. We reported that a source of XO other than the liver, causes hemolysis and pulmonary vascular dysfunction in a mouse model of SCD. When we looked closer at the role of XO, specifically during a heme crisis event, we found that XO had a protective function as a scavenger and degrader of free heme. While we have answered several previously unanswered questions throughout the course of this project many exciting future directions remain.

Bibliography

- 1 Aslan, M. *et al.* Oxygen radical inhibition of nitric oxide-dependent vascular function in sickle cell disease. *Proceedings of the National Academy of Sciences of the United States of America* **98**, 15215-15220, doi:10.1073/pnas.221292098 (2001).
- 2 Iwalokun, B. A., Bamiro, S. B. & Ogunledun, A. Levels and interactions of plasma xanthine oxidase, catalase and liver function parameters in Nigerian children with *Plasmodium falciparum* infection. *Apmis* **114**, 842-850, doi:10.1111/j.1600-0463.2006.apm_457.x (2006).
- 3 Luchtemberg, M. N. *et al.* Xanthine oxidase activity in patients with sepsis. *Clin Biochem* **41**, 1186-1190, doi:10.1016/j.clinbiochem.2008.07.015 (2008).
- 4 Parks, D. A., Bulkley, G. B., Granger, D. N., Hamilton, S. R. & McCord, J. M. Ischemic injury in the cat small intestine: role of superoxide radicals. *Gastroenterology* **82**, 9-15 (1982).
- 5 White, C. R. *et al.* Circulating plasma xanthine oxidase contributes to vascular dysfunction in hypercholesterolemic rabbits. *Proceedings of the National Academy of Sciences of the United States of America* **93**, 8745-8749, doi:10.1073/pnas.93.16.8745 (1996).
- 6 Freeman, B. A. *et al.* Oxygen radical-nitric oxide reactions in vascular diseases. *Adv Pharmacol* **34**, 45-69, doi:10.1016/s1054-3589(08)61080-7 (1995).
- 7 Yokoyama, Y. *et al.* Circulating xanthine oxidase: potential mediator of ischemic injury. *The American journal of physiology* **258**, G564-570, doi:10.1152/ajpgi.1990.258.4.G564 (1990).
- 8 George, J. & Struthers, A. D. Role of urate, xanthine oxidase and the effects of allopurinol in vascular oxidative stress. *Vascular health and risk management* **5**, 265-272 (2009).
- 9 Cantu-Medellin, N. & Kelley, E. E. Xanthine oxidoreductase-catalyzed reduction of nitrite to nitric oxide: insights regarding where, when and how. *Nitric oxide : biology and chemistry* **34**, 19-26, doi:10.1016/j.niox.2013.02.081 (2013).
- 10 Pinto, V. M., Balocco, M., Quintino, S. & Forni, G. L. Sickle cell disease: a review for the internist. *Intern Emerg Med* **14**, 1051-1064, doi:10.1007/s11739-019-02160-x (2019).

- 11 Kato, G. J. *et al.* Sickle cell disease. *Nature reviews. Disease primers* **4**, 18010, doi:10.1038/nrdp.2018.10 (2018).
- 12 Williams, T. N. Sickle Cell Disease in Sub-Saharan Africa. *Hematol Oncol Clin North Am* **30**, 343-358, doi:10.1016/j.hoc.2015.11.005 (2016).
- 13 Piel, F. B. *et al.* Global epidemiology of sickle haemoglobin in neonates: a contemporary geostatistical model-based map and population estimates. *Lancet* **381**, 142-151, doi:10.1016/s0140-6736(12)61229-x (2013).
- 14 Sundd, P., Gladwin, M. T. & Novelli, E. M. Pathophysiology of Sickle Cell Disease. *Annu Rev Pathol* **14**, 263-292, doi:10.1146/annurev-pathmechdis-012418-012838 (2019).
- 15 Ahmed, M. H., Ghatge, M. S. & Safo, M. K. Hemoglobin: Structure, Function and Allostery. *Subcell Biochem* **94**, 345-382, doi:10.1007/978-3-030-41769-7_14 (2020).
- 16 Mburu, J. & Odame, I. Sickle cell disease: Reducing the global disease burden. *Int J Lab Hematol* **41 Suppl 1**, 82-88, doi:10.1111/ijlh.13023 (2019).
- 17 Kato, G. J., Steinberg, M. H. & Gladwin, M. T. Intravascular hemolysis and the pathophysiology of sickle cell disease. *J Clin Invest* **127**, 750-760, doi:10.1172/jci89741 (2017).
- 18 Novelli, E. M. & Gladwin, M. T. Crises in Sickle Cell Disease. *Chest* **149**, 1082-1093, doi:10.1016/j.chest.2015.12.016 (2016).
- 19 Meier, E. R. Treatment Options for Sickle Cell Disease. *Pediatric clinics of North America* **65**, 427-443, doi:10.1016/j.pcl.2018.01.005 (2018).
- 20 Nader, E., Romana, M. & Connes, P. The Red Blood Cell-Inflammation Vicious Circle in Sickle Cell Disease. *Front Immunol* **11**, 454, doi:10.3389/fimmu.2020.00454 (2020).
- 21 Aslan, M., Thornley-Brown, D. & Freeman, B. A. Reactive species in sickle cell disease. *Ann N Y Acad Sci* **899**, 375-391, doi:10.1111/j.1749-6632.2000.tb06201.x (2000).
- 22 Gladwin, M. T. & Vichinsky, E. Pulmonary complications of sickle cell disease. *The New England journal of medicine* **359**, 2254-2265, doi:10.1056/NEJMra0804411 (2008).
- 23 Charache, S. *et al.* Effect of hydroxyurea on the frequency of painful crises in sickle cell anemia. Investigators of the Multicenter Study of Hydroxyurea in Sickle Cell Anemia. *The New England journal of medicine* **332**, 1317-1322, doi:10.1056/nejm199505183322001 (1995).

- 24 Wang, W. C. *et al.* Hydroxycarbamide in very young children with sickle-cell anaemia: a multicentre, randomised, controlled trial (BABY HUG). *Lancet (London, England)* **377**, 1663-1672, doi:10.1016/s0140-6736(11)60355-3 (2011).
- 25 Lavelle, D., Engel, J. D. & Sauntharajah, Y. Fetal Hemoglobin Induction by Epigenetic Drugs. *Semin Hematol* **55**, 60-67, doi:10.1053/j.seminhematol.2018.04.008 (2018).
- 26 Niihara, Y. *et al.* A Phase 3 Trial of l-Glutamine in Sickle Cell Disease. *The New England journal of medicine* **379**, 226-235, doi:10.1056/NEJMoa1715971 (2018).
- 27 Ataga, K. I. *et al.* Crizanlizumab for the Prevention of Pain Crises in Sickle Cell Disease. *The New England journal of medicine* **376**, 429-439, doi:10.1056/NEJMoa1611770 (2017).
- 28 Howard, J. *et al.* A phase 1/2 ascending dose study and open-label extension study of voxelotor in patients with sickle cell disease. *Blood* **133**, 1865-1875, doi:10.1182/blood-2018-08-868893 (2019).
- 29 Vichinsky, E. *et al.* A Phase 3 Randomized Trial of Voxelotor in Sickle Cell Disease. *The New England journal of medicine* **381**, 509-519, doi:10.1056/NEJMoa1903212 (2019).
- 30 Vinchi, F. *et al.* Hemopexin therapy improves cardiovascular function by preventing heme-induced endothelial toxicity in mouse models of hemolytic diseases. *Circulation* **127**, 1317-1329, doi:10.1161/circulationaha.112.130179 (2013).
- 31 Vinchi, F. *et al.* Hemopexin therapy reverts heme-induced proinflammatory phenotypic switching of macrophages in a mouse model of sickle cell disease. *Blood* **127**, 473-486, doi:10.1182/blood-2015-08-663245 (2016).
- 32 Jain, M. D. *et al.* Seek and you shall find--but then what do you do? Cold agglutinins in cardiopulmonary bypass and a single-center experience with cold agglutinin screening before cardiac surgery. *Transfusion medicine reviews* **27**, 65-73, doi:10.1016/j.tmr.2012.12.001 (2013).
- 33 Smith, A. & McCulloh, R. J. Hemopexin and haptoglobin: allies against heme toxicity from hemoglobin not contenders. *Frontiers in physiology* **6**, 187, doi:10.3389/fphys.2015.00187 (2015).
- 34 Nagababu, E. & Rifkind, J. M. Heme degradation by reactive oxygen species. *Antioxidants & redox signaling* **6**, 967-978, doi:10.1089/ars.2004.6.967 (2004).

- 35 Belcher, J. D. *et al.* Haptoglobin and hemopexin inhibit vaso-occlusion and inflammation in murine sickle cell disease: Role of heme oxygenase-1 induction. *PLoS one* **13**, e0196455, doi:10.1371/journal.pone.0196455 (2018).
- 36 Nur, E., Biemond, B. J., Otten, H. M., Brandjes, D. P. & Schnog, J. J. Oxidative stress in sickle cell disease; pathophysiology and potential implications for disease management. *American journal of hematology* **86**, 484-489, doi:10.1002/ajh.22012 (2011).
- 37 Takimoto, E. & Kass, D. A. Role of oxidative stress in cardiac hypertrophy and remodeling. *Hypertension (Dallas, Tex. : 1979)* **49**, 241-248, doi:10.1161/01.HYP.0000254415.31362.a7 (2007).
- 38 Son, S. M. Reactive oxygen and nitrogen species in pathogenesis of vascular complications of diabetes. *Diabetes & metabolism journal* **36**, 190-198, doi:10.4093/dmj.2012.36.3.190 (2012).
- 39 Beckman, J. S., Beckman, T. W., Chen, J., Marshall, P. A. & Freeman, B. A. Apparent hydroxyl radical production by peroxynitrite: implications for endothelial injury from nitric oxide and superoxide. *Proceedings of the National Academy of Sciences of the United States of America* **87**, 1620-1624 (1990).
- 40 Radi, R., Beckman, J. S., Bush, K. M. & Freeman, B. A. Peroxynitrite oxidation of sulfhydryls. The cytotoxic potential of superoxide and nitric oxide. *The Journal of biological chemistry* **266**, 4244-4250 (1991).
- 41 Day, R. O. *et al.* Allopurinol: insights from studies of dose-response relationships. *Expert opinion on drug metabolism & toxicology* **13**, 449-462, doi:10.1080/17425255.2017.1269745 (2017).
- 42 Pacher, P., Nivorozhkin, A. & Szabo, C. Therapeutic effects of xanthine oxidase inhibitors: renaissance half a century after the discovery of allopurinol. *Pharmacological reviews* **58**, 87-114, doi:10.1124/pr.58.1.6 (2006).
- 43 Harrison, R. Structure and function of xanthine oxidoreductase: where are we now? *Free radical biology & medicine* **33**, 774-797 (2002).
- 44 Enroth, C. *et al.* Crystal structures of bovine milk xanthine dehydrogenase and xanthine oxidase: structure-based mechanism of conversion. *Proceedings of the National Academy of Sciences of the United States of America* **97**, 10723-10728 (2000).
- 45 Della Corte, E. & Stirpe, F. The regulation of rat-liver xanthine oxidase: Activation by proteolytic enzymes. *FEBS letters* **2**, 83-84 (1968).

- 46 Stirpe, F. & Della Corte, E. The regulation of rat liver xanthine oxidase. Conversion in vitro of the enzyme activity from dehydrogenase (type D) to oxidase (type O). *The Journal of biological chemistry* **244**, 3855-3863 (1969).
- 47 Corte, E. D. & Stirpe, F. The regulation of rat liver xanthine oxidase. Involvement of thiol groups in the conversion of the enzyme activity from dehydrogenase (type D) into oxidase (type O) and purification of the enzyme. *The Biochemical journal* **126**, 739-745 (1972).
- 48 Hewinson, J., Stevens, C. R. & Millar, T. M. Vascular physiology and pathology of circulating xanthine oxidoreductase: from nucleotide sequence to functional enzyme. *Redox report : communications in free radical research* **9**, 71-79, doi:10.1179/135100004225004797 (2004).
- 49 Battelli, M. G., Polito, L., Bortolotti, M. & Bolognesi, A. Xanthine Oxidoreductase-Derived Reactive Species: Physiological and Pathological Effects. *Oxidative medicine and cellular longevity* **2016**, 3527579, doi:10.1155/2016/3527579 (2016).
- 50 Kelley, E. E. *et al.* Moderate hypoxia induces xanthine oxidoreductase activity in arterial endothelial cells. *Free radical biology & medicine* **40**, 952-959, doi:10.1016/j.freeradbiomed.2005.11.008 (2006).
- 51 Poss, W. B., Huecksteadt, T. P., Panus, P. C., Freeman, B. A. & Hoidal, J. R. Regulation of xanthine dehydrogenase and xanthine oxidase activity by hypoxia. *The American journal of physiology* **270**, L941-946, doi:10.1152/ajplung.1996.270.6.L941 (1996).
- 52 Linder, N., Martelin, E., Lapatto, R. & Raivio, K. O. Posttranslational inactivation of human xanthine oxidoreductase by oxygen under standard cell culture conditions. *Am J Physiol Cell Physiol* **285**, C48-55, doi:10.1152/ajpcell.00561.2002 (2003).
- 53 Hassoun, P. M. *et al.* Regulation of endothelial cell xanthine dehydrogenase xanthine oxidase gene expression by oxygen tension. *The American journal of physiology* **266**, L163-171, doi:10.1152/ajplung.1994.266.2.L163 (1994).
- 54 Terada, L. S., Piermattei, D., Shibao, G. N., McManaman, J. L. & Wright, R. M. Hypoxia regulates xanthine dehydrogenase activity at pre- and posttranslational levels. *Archives of biochemistry and biophysics* **348**, 163-168, doi:10.1006/abbi.1997.0367 (1997).
- 55 Parks, D. A., Bulkley, G. B. & Granger, D. N. Role of oxygen-derived free radicals in digestive tract diseases. *Surgery* **94**, 415-422 (1983).
- 56 Sikora, J., Orlov, S. N., Furuya, K. & Grygorczyk, R. Hemolysis is a primary ATP-release mechanism in human erythrocytes. *Blood* **124**, 2150-2157, doi:10.1182/blood-2014-05-572024 (2014).

- 57 Ghosh, S. *et al.* Extracellular hemin crisis triggers acute chest syndrome in sickle mice. *J Clin Invest* **123**, 4809-4820, doi:10.1172/jci64578 (2013).
- 58 Schaer, D. J., Buehler, P. W., Alayash, A. I., Belcher, J. D. & Vercellotti, G. M. Hemolysis and free hemoglobin revisited: exploring hemoglobin and hemin scavengers as a novel class of therapeutic proteins. *Blood* **121**, 1276-1284, doi:10.1182/blood-2012-11-451229 (2013).
- 59 López-Cruz, R. I. *et al.* Plasma Hypoxanthine-Guanine Phosphoribosyl Transferase Activity in Bottlenose Dolphins Contributes to Avoiding Accumulation of Non-recyclable Purines. *Frontiers in physiology* **7**, 213, doi:10.3389/fphys.2016.00213 (2016).
- 60 Adachi, T., Fukushima, T., Usami, Y. & Hirano, K. Binding of human xanthine oxidase to sulphated glycosaminoglycans on the endothelial-cell surface. *Biochem J* **289** (Pt 2), 523-527, doi:10.1042/bj2890523 (1993).
- 61 Houston, M. *et al.* Binding of xanthine oxidase to vascular endothelium. Kinetic characterization and oxidative impairment of nitric oxide-dependent signaling. *J Biol Chem* **274**, 4985-4994, doi:10.1074/jbc.274.8.4985 (1999).
- 62 Pritsos, C. A. Cellular distribution, metabolism and regulation of the xanthine oxidoreductase enzyme system. *Chemico-biological interactions* **129**, 195-208 (2000).
- 63 Fukushima, T., Adachi, T. & Hirano, K. The heparin-binding site of human xanthine oxidase. *Biol Pharm Bull* **18**, 156-158, doi:10.1248/bpb.18.156 (1995).
- 64 Tan, S. *et al.* Xanthine oxidase activity in the circulation of rats following hemorrhagic shock. *Free radical biology & medicine* **15**, 407-414, doi:10.1016/0891-5849(93)90040-2 (1993).
- 65 Malik, U. Z. *et al.* Febuxostat inhibition of endothelial-bound XO: implications for targeting vascular ROS production. *Free radical biology & medicine* **51**, 179-184, doi:10.1016/j.freeradbiomed.2011.04.004 (2011).
- 66 Kelley, E. E. *et al.* Binding of xanthine oxidase to glycosaminoglycans limits inhibition by oxypurinol. *The Journal of biological chemistry* **279**, 37231-37234, doi:10.1074/jbc.M402077200 (2004).
- 67 Radi, R., Rubbo, H., Bush, K. & Freeman, B. A. Xanthine oxidase binding to glycosaminoglycans: kinetics and superoxide dismutase interactions of immobilized xanthine oxidase-heparin complexes. *Archives of biochemistry and biophysics* **339**, 125-135, doi:10.1006/abbi.1996.9844 (1997).

- 68 Robinson, P. C. & Dalbeth, N. Febuxostat for the treatment of hyperuricaemia in gout. *Expert opinion on pharmacotherapy*, 1-11, doi:10.1080/14656566.2018.1498842 (2018).
- 69 Seth, R., Kydd, A. S., Buchbinder, R., Bombardier, C. & Edwards, C. J. Allopurinol for chronic gout. *The Cochrane database of systematic reviews*, Cd006077, doi:10.1002/14651858.CD006077.pub3 (2014).
- 70 Knake, C., Stamp, L. & Bahn, A. Molecular mechanism of an adverse drug-drug interaction of allopurinol and furosemide in gout treatment. *Biochemical and biophysical research communications* **452**, 157-162, doi:10.1016/j.bbrc.2014.08.068 (2014).
- 71 Okamoto, K. *et al.* An extremely potent inhibitor of xanthine oxidoreductase. Crystal structure of the enzyme-inhibitor complex and mechanism of inhibition. *The Journal of biological chemistry* **278**, 1848-1855, doi:10.1074/jbc.M208307200 (2003).
- 72 Okamoto, K. & Nishino, T. Crystal structures of mammalian xanthine oxidoreductase bound with various inhibitors: allopurinol, febuxostat, and FYX-051. *Journal of Nippon Medical School = Nippon Ika Daigaku zasshi* **75**, 2-3 (2008).
- 73 Takano, Y. *et al.* Selectivity of febuxostat, a novel non-purine inhibitor of xanthine oxidase/xanthine dehydrogenase. *Life sciences* **76**, 1835-1847, doi:10.1016/j.lfs.2004.10.031 (2005).
- 74 Liu, C. T. *et al.* Risk of Febuxostat-Associated Myopathy in Patients with CKD. *Clinical journal of the American Society of Nephrology : CJASN* **12**, 744-750, doi:10.2215/cjn.08280816 (2017).
- 75 White, W. B. *et al.* Cardiovascular Safety of Febuxostat or Allopurinol in Patients with Gout. *The New England journal of medicine* **378**, 1200-1210, doi:10.1056/NEJMoa1710895 (2018).
- 76 Osarogiagbon, U. R. *et al.* Reperfusion injury pathophysiology in sickle transgenic mice. *Blood* **96**, 314-320 (2000).
- 77 Hassoun, P. M. *et al.* Upregulation of xanthine oxidase by lipopolysaccharide, interleukin-1, and hypoxia. Role in acute lung injury. *American journal of respiratory and critical care medicine* **158**, 299-305, doi:10.1164/ajrccm.158.1.9709116 (1998).
- 78 Battelli, M. G. *et al.* Serum xanthine oxidase in human liver disease. *Am J Gastroenterol* **96**, 1194-1199, doi:10.1111/j.1572-0241.2001.03700.x (2001).

- 79 Stirpe, F., Ravaioli, M., Battelli, M. G., Musiani, S. & Grazi, G. L. Xanthine oxidoreductase activity in human liver disease. *Am J Gastroenterol* **97**, 2079-2085, doi:10.1111/j.1572-0241.2002.05925.x (2002).
- 80 Chatterjee, S. *et al.* Oxidative stress induces protein and DNA radical formation in follicular dendritic cells of the germinal center and modulates its cell death patterns in late sepsis. *Free radical biology & medicine* **50**, 988-999, doi:10.1016/j.freeradbiomed.2010.12.037 (2011).
- 81 Ramos, M. F. P., Monteiro de Barros, A., Razvickas, C. V., Borges, F. T. & Schor, N. Xanthine oxidase inhibitors and sepsis. *Int J Immunopathol Pharmacol* **32**, 2058738418772210, doi:10.1177/2058738418772210 (2018).
- 82 Kim, N. H. *et al.* The xanthine oxidase-NFAT5 pathway regulates macrophage activation and TLR-induced inflammatory arthritis. *Eur J Immunol* **44**, 2721-2736, doi:10.1002/eji.201343669 (2014).
- 83 Hahl, P. *et al.* Identification of oxidative modifications of hemopexin and their predicted physiological relevance. *The Journal of biological chemistry* **292**, 13658-13671, doi:10.1074/jbc.M117.783951 (2017).
- 84 Silva, D. G., Belini Junior, E., de Almeida, E. A. & Bonini-Domingos, C. R. Oxidative stress in sickle cell disease: an overview of erythrocyte redox metabolism and current antioxidant therapeutic strategies. *Free radical biology & medicine* **65**, 1101-1109, doi:10.1016/j.freeradbiomed.2013.08.181 (2013).
- 85 Henneberg, R. *et al.* Protective effect of flavonoids against reactive oxygen species production in sickle cell anemia patients treated with hydroxyurea. *Revista brasileira de hematologia e hemoterapia* **35**, 52-55, doi:10.5581/1516-8484.20130015 (2013).
- 86 Lubeck, D. *et al.* Estimated Life Expectancy and Income of Patients With Sickle Cell Disease Compared With Those Without Sickle Cell Disease. *JAMA Netw Open* **2**, e1915374, doi:10.1001/jamanetworkopen.2019.15374 (2019).
- 87 Turpin, M. *et al.* Chronic blood exchange transfusions in the management of pre-capillary pulmonary hypertension complicating sickle cell disease. *Eur Respir J* **52**, doi:10.1183/13993003.00272-2018 (2018).
- 88 Estcourt, L. J., Hopewell, S., Trivella, M., Hambleton, I. R. & Cho, G. Regular long-term red blood cell transfusions for managing chronic chest complications in sickle cell disease. *The Cochrane database of systematic reviews* **2019**, doi:10.1002/14651858.CD008360.pub5 (2019).

- 89 Pritchard, K. A., Jr. *et al.* Hypoxia-induced acute lung injury in murine models of sickle cell disease. *Am J Physiol Lung Cell Mol Physiol* **286**, L705-714, doi:10.1152/ajplung.00288.2002 (2004).
- 90 Schmidt, H. M., Kelley, E. E. & Straub, A. C. The impact of xanthine oxidase (XO) on hemolytic diseases. *Redox biology* **21**, 101072, doi:10.1016/j.redox.2018.101072 (2019).
- 91 Parks, D. A. & Granger, D. N. Xanthine oxidase: biochemistry, distribution and physiology. *Acta Physiol Scand Suppl* **548**, 87-99 (1986).
- 92 Diederich, L. *et al.* On the Effects of Reactive Oxygen Species and Nitric Oxide on Red Blood Cell Deformability. *Frontiers in physiology* **9**, 332, doi:10.3389/fphys.2018.00332 (2018).
- 93 Harmon, D. B. *et al.* Hepatocyte-Specific Ablation or Whole-Body Inhibition of Xanthine Oxidoreductase in Mice Corrects Obesity-Induced Systemic Hyperuricemia Without Improving Metabolic Abnormalities. *Diabetes* **68**, 1221-1229, doi:10.2337/db18-1198 (2019).
- 94 O'Donnell, B. J. *et al.* Sleep phenotype in the Townes mouse model of sickle cell disease. *Sleep Breath* **23**, 333-339, doi:10.1007/s11325-018-1711-x (2019).
- 95 Ryan, T. M., Ciavatta, D. J. & Townes, T. M. Knockout-transgenic mouse model of sickle cell disease. *Science* **278**, 873-876, doi:10.1126/science.278.5339.873 (1997).
- 96 Wood, K. C. *et al.* Smooth muscle cytochrome b5 reductase 3 deficiency accelerates pulmonary hypertension development in sickle cell mice. *Blood Adv* **3**, 4104-4116, doi:10.1182/bloodadvances.2019000621 (2019).
- 97 Rutledge, C. *et al.* Commercial 4-dimensional echocardiography for murine heart volumetric evaluation after myocardial infarction. *Cardiovasc Ultrasound* **18**, 9, doi:10.1186/s12947-020-00191-5 (2020).
- 98 Potoka, K. P. *et al.* Nitric Oxide-Independent Soluble Guanylate Cyclase Activation Improves Vascular Function and Cardiac Remodeling in Sickle Cell Disease. *Am J Respir Cell Mol Biol* **58**, 636-647, doi:10.1165/rcmb.2017-0292OC (2018).
- 99 Rahaman, M. M. *et al.* Cytochrome b5 Reductase 3 Modulates Soluble Guanylate Cyclase Redox State and cGMP Signaling. *Circulation research* **121**, 137-148, doi:10.1161/circresaha.117.310705 (2017).

- 100 Oh, J. Y. *et al.* Absorbance and redox based approaches for measuring free heme and free hemoglobin in biological matrices. *Redox biology* **9**, 167-177, doi:10.1016/j.redox.2016.08.003 (2016).
- 101 DeVallance, E. *et al.* Exercise training prevents the perivascular adipose tissue-induced aortic dysfunction with metabolic syndrome. *Redox biology* **26**, 101285, doi:10.1016/j.redox.2019.101285 (2019).
- 102 Durgin, B. G. *et al.* Loss of smooth muscle CYB5R3 amplifies angiotensin II-induced hypertension by increasing sGC heme oxidation. *JCI Insight* **4**, doi:10.1172/jci.insight.129183 (2019).
- 103 Dawson, R. B., Rafal, S. & Weintraub, L. R. Absorption of hemoglobin iron: the role of xanthine oxidase in the intestinal heme-splitting reaction. *Blood* **35**, 94-103 (1970).
- 104 Donegan, R. K., Moore, C. M., Hanna, D. A. & Reddi, A. R. Handling heme: The mechanisms underlying the movement of heme within and between cells. *Free radical biology & medicine* **133**, 88-100, doi:10.1016/j.freeradbiomed.2018.08.005 (2019).
- 105 Suresh, K. & Shimoda, L. A. Lung Circulation. *Compr Physiol* **6**, 897-943, doi:10.1002/cphy.c140049 (2016).
- 106 Li, G. *et al.* Glycosaminoglycans and glycolipids as potential biomarkers in lung cancer. *Glycoconj J* **34**, 661-669, doi:10.1007/s10719-017-9790-7 (2017).
- 107 Phan, S. H., Gannon, D. E., Varani, J., Ryan, U. S. & Ward, P. A. Xanthine oxidase activity in rat pulmonary artery endothelial cells and its alteration by activated neutrophils. *Am J Pathol* **134**, 1201-1211 (1989).
- 108 Sohn, H. Y. *et al.* Differential regulation of xanthine and NAD(P)H oxidase by hypoxia in human umbilical vein endothelial cells. Role of nitric oxide and adenosine. *Cardiovasc Res* **58**, 638-646, doi:10.1016/s0008-6363(03)00262-1 (2003).
- 109 Rieger, J. M., Shah, A. R. & Gidday, J. M. Ischemia-reperfusion injury of retinal endothelium by cyclooxygenase- and xanthine oxidase-derived superoxide. *Exp Eye Res* **74**, 493-501, doi:10.1006/exer.2001.1156 (2002).
- 110 Kast, R. E. *et al.* Augmentation of 5-Aminolevulinic Acid Treatment of Glioblastoma by Adding Ciprofloxacin, Deferiprone, 5-Fluorouracil and Febuxostat: The CAALA Regimen. *Brain Sci* **8**, doi:10.3390/brainsci8120203 (2018).

- 111 Miyata, H. *et al.* Identification of Febuxostat as a New Strong ABCG2 Inhibitor: Potential Applications and Risks in Clinical Situations. *Front Pharmacol* **7**, 518, doi:10.3389/fphar.2016.00518 (2016).
- 112 Sachar, M., Anderson, K. E. & Ma, X. Protoporphyrin IX: the Good, the Bad, and the Ugly. *J Pharmacol Exp Ther* **356**, 267-275, doi:10.1124/jpet.115.228130 (2016).
- 113 Boakye, M. D. S., Owek, C. J., Oluoch, E., Wachira, J. & Afrane, Y. A. Challenges of achieving sustainable community health services for community case management of malaria. *BMC Public Health* **18**, 1150, doi:10.1186/s12889-018-6040-2 (2018).
- 114 Dugani, S., Veillard, J. & Kissoon, N. Reducing the global burden of sepsis. *Cmaj* **189**, E2-e3, doi:10.1503/cmaj.160798 (2017).
- 115 Fleischmann, C. *et al.* Assessment of Global Incidence and Mortality of Hospital-treated Sepsis. Current Estimates and Limitations. *American journal of respiratory and critical care medicine* **193**, 259-272, doi:10.1164/rccm.201504-0781OC (2016).
- 116 Head, S. J., Milojevic, M., Taggart, D. P. & Puskas, J. D. Current Practice of State-of-the-Art Surgical Coronary Revascularization. *Circulation* **136**, 1331-1345, doi:10.1161/circulationaha.116.022572 (2017).
- 117 Aubert, O. *et al.* COVID-19 pandemic and worldwide organ transplantation: a population-based study. *Lancet Public Health* **6**, e709-e719, doi:10.1016/s2468-2667(21)00200-0 (2021).
- 118 Janciauskiene, S., Vijayan, V. & Immenschuh, S. TLR4 Signaling by Heme and the Role of Heme-Binding Blood Proteins. *Front Immunol* **11**, 1964, doi:10.3389/fimmu.2020.01964 (2020).
- 119 Rees, D. C., Williams, T. N. & Gladwin, M. T. Sickle-cell disease. *Lancet (London, England)* **376**, 2018-2031, doi:10.1016/s0140-6736(10)61029-x (2010).
- 120 Weatherall, D., Akinyanju, O., Fuchareon, S., Olivieri, N. & Musgrove, P. in *Disease Control Priorities in Developing Countries* (ed D.T. et al. Jamison) 663-680 (Oxford University Press, 2006).
- 121 Weatherall, D. J. The inherited diseases of hemoglobin are an emerging global health burden. *Blood* **115**, 4331-4336, doi:10.1182/blood-2010-01-251348 (2010).
- 122 Hebbel, R. P., Morgan, W. T., Eaton, J. W. & Hedlund, B. E. Accelerated autoxidation and heme loss due to instability of sickle hemoglobin. *Proceedings of the National Academy of Sciences of the United States of America* **85**, 237-241, doi:10.1073/pnas.85.1.237 (1988).

- 123 Jeney, V. *et al.* Pro-oxidant and cytotoxic effects of circulating heme. *Blood* **100**, 879-887, doi:10.1182/blood.v100.3.879 (2002).
- 124 Liu, S. C., Zhai, S. & Palek, J. Detection of hemin release during hemoglobin S denaturation. *Blood* **71**, 1755-1758 (1988).
- 125 Vichinsky, E. P. *et al.* Acute chest syndrome in sickle cell disease: clinical presentation and course. Cooperative Study of Sickle Cell Disease. *Blood* **89**, 1787-1792 (1997).
- 126 Muller-Eberhard, U., Javid, J., Liem, H. H., Hanstein, A. & Hanna, M. Plasma concentrations of hemopexin, haptoglobin and heme in patients with various hemolytic diseases. *Blood* **32**, 811-815 (1968).
- 127 Wochner, R. D., Spilberg, I., Iio, A., Liem, H. H. & Muller-Eberhard, U. Hemopexin metabolism in sickle-cell disease, porphyrias and control subjects--effects of heme injection. *The New England journal of medicine* **290**, 822-826, doi:10.1056/nejm197404112901503 (1974).
- 128 Adisa, O. A. *et al.* Association between plasma free haem and incidence of vaso-occlusive episodes and acute chest syndrome in children with sickle cell disease. *Br J Haematol* **162**, 702-705, doi:10.1111/bjh.12445 (2013).
- 129 Schmidt, H. M. *et al.* Xanthine Oxidase Drives Hemolysis and Vascular Malfunction in Sickle Cell Disease. *Arterioscler Thromb Vasc Biol* **41**, 769-782, doi:10.1161/atvbaha.120.315081 (2021).
- 130 Vickers, S. D., Saporito, D. C. & Leonardi, R. Measurement of Fatty Acid β -Oxidation in a Suspension of Freshly Isolated Mouse Hepatocytes. *J Vis Exp*, doi:10.3791/62904 (2021).
- 131 Majumder, N. *et al.* Oxidized carbon black nanoparticles induce endothelial damage through C-X-C chemokine receptor 3-mediated pathway. *Redox biology* **47**, 102161, doi:10.1016/j.redox.2021.102161 (2021).
- 132 Davies, K. J., Sevanian, A., Muakkassah-Kelly, S. F. & Hochstein, P. Uric acid-iron ion complexes. A new aspect of the antioxidant functions of uric acid. *The Biochemical journal* **235**, 747-754, doi:10.1042/bj2350747 (1986).
- 133 Kelley, E. E., Buettner, G. R. & Burns, C. P. Production of lipid-derived free radicals in L1210 murine leukemia cells is an early oxidative event in the photodynamic action of Photofrin. *Photochem Photobiol* **65**, 576-580, doi:10.1111/j.1751-1097.1997.tb08608.x (1997).

- 134 Straub, A. C. *et al.* Endothelial cell expression of haemoglobin α regulates nitric oxide signalling. *Nature* **491**, 473-477, doi:10.1038/nature11626 (2012).
- 135 Rozga, J., Piątek, T. & Małkowski, P. Human albumin: old, new, and emerging applications. *Ann Transplant* **18**, 205-217, doi:10.12659/aot.889188 (2013).
- 136 Helms, C. & Kim-Shapiro, D. B. Hemoglobin-mediated nitric oxide signaling. *Free radical biology & medicine* **61**, 464-472, doi:10.1016/j.freeradbiomed.2013.04.028 (2013).
- 137 Franco, R. S. Measurement of red cell lifespan and aging. *Transfus Med Hemother* **39**, 302-307, doi:10.1159/000342232 (2012).
- 138 Steinberg, M. H. Sick cell anemia, the first molecular disease: overview of molecular etiology, pathophysiology, and therapeutic approaches. *ScientificWorldJournal* **8**, 1295-1324, doi:10.1100/tsw.2008.157 (2008).
- 139 Hulko, M. *et al.* Cell-free plasma hemoglobin removal by dialyzers with various permeability profiles. *Sci Rep* **5**, 16367, doi:10.1038/srep16367 (2015).
- 140 Nishino, T. *et al.* Mechanism of the conversion of xanthine dehydrogenase to xanthine oxidase: identification of the two cysteine disulfide bonds and crystal structure of a non-convertible rat liver xanthine dehydrogenase mutant. *The Journal of biological chemistry* **280**, 24888-24894, doi:10.1074/jbc.M501830200 (2005).
- 141 Helms, C. C. *et al.* Mechanisms of hemolysis-associated platelet activation. *J Thromb Haemost* **11**, 2148-2154, doi:10.1111/jth.12422 (2013).
- 142 Villagra, J. *et al.* Platelet activation in patients with sickle disease, hemolysis-associated pulmonary hypertension, and nitric oxide scavenging by cell-free hemoglobin. *Blood* **110**, 2166-2172, doi:10.1182/blood-2006-12-061697 (2007).
- 143 Rifkind, J. M., Nagababu, E., Ramasamy, S. & Ravi, L. B. Hemoglobin redox reactions and oxidative stress. *Redox report : communications in free radical research* **8**, 234-237, doi:10.1179/135100003225002817 (2003).
- 144 Nagababu, E. & Rifkind, J. M. Reaction of hydrogen peroxide with ferrylhemoglobin: superoxide production and heme degradation. *Biochemistry* **39**, 12503-12511, doi:10.1021/bi992170y (2000).
- 145 Buettner, G. R. & Jurkiewicz, B. A. Ascorbate free radical as a marker of oxidative stress: an EPR study. *Free radical biology & medicine* **14**, 49-55, doi:10.1016/0891-5849(93)90508-r (1993).

- 146 Tuteja, N., Chandra, M., Tuteja, R. & Misra, M. K. Nitric Oxide as a Unique Bioactive Signaling Messenger in Physiology and Pathophysiology. *J Biomed Biotechnol* **2004**, 227-237, doi:10.1155/s1110724304402034 (2004).
- 147 Ichida, K., Amaya, Y., Okamoto, K. & Nishino, T. Mutations associated with functional disorder of xanthine oxidoreductase and hereditary xanthinuria in humans. *International journal of molecular sciences* **13**, 15475-15495, doi:10.3390/ijms131115475 (2012).